# UNDERSTANDING THE ROLE OF CARCINOEMBRYONIC ANTIGEN-RELATED CELL ADHESION MOLECULES IN GASTRIC EPITHELIAL CELLS

*By*

**DEBASHISH CHAKRABORTY**

**LIFE11201704001**

**National Institute of Science Education and Research (NISER)**
**Bhubaneswar**

***A thesis submitted to the***

***Board of Studies in Life Sciences***

***In partial fulfillment of requirements***

***for the Degree of***

**DOCTOR OF PHILOSOPHY**

***of***

**HOMI BHABHA NATIONAL INSTITUTE**

**December, 2025**

# Homi Bhabha National Institute[1]

## Recommendations of the Viva Voce Committee

As members of the Viva Voce Committee, we certify that we have read the dissertation prepared by Debashish Chakraborty entitled "Understanding the role of carcinoembryonic antigen-related cell adhesion molecules in gastric epithelial cells" and recommend that it may be accepted as fulfilling the thesis requirement for the award of Degree of Doctor of Philosophy.

| S. No. | Doctoral Committee | Name | Signature | Date | In-Person/Online |
|---|---|---|---|---|---|
| 1. | Chairman | Prof. Chandan Goswami | Chandan Goswami | 20/04/2026 | In person |
| 2. | Guide/Convener | Dr. Asima Bhattacharyya | | 20/04/2026 | In person |
| 3. | Co-Guide (if any) | | | | |
| 4. | Examiner | Dr. Santanu Chattopadhyay | | 20/04/2026 | In person |
| 5. | Member - 1 | Dr. Subhasis Chattopadhyay | | 20/04/2026 | In Person |
| 6. | Member - 2 | Dr. Harapriya Mohapatra | | 20/04/2026 | In person |
| 7. | Member - 3 | Prof. Jagneshwar Dandapat | | 20/04/2026 | online |
| 8. | Technology Advisor (if any) | | | | |

---

Final approval and acceptance of this thesis is contingent upon the candidate's submission of the final copies of the thesis to HBNI.

I hereby certify that I have read this thesis prepared under my direction and recommend that it may be accepted as fulfilling the thesis requirement.

**Date:** 20.4.2026

**Place:** NISER Bhubaneswar

**Signature**

**Co-guide (if any)**

**Signature**

**Guide**

[1]This page is to be included only for final submission after successful completion of viva voce.

# STATEMENT BY AUTHOR

This dissertation has been submitted in partial fulfillment of requirements for an advanced degree at Homi Bhabha National Institute (HBNI) and is deposited in the Library to be made available to borrowers under rules of the HBNI.

Brief quotations from this dissertation are allowable without special permission, provided that accurate acknowledgement of source is made. Requests for permission for extended quotation from or reproduction of this manuscript in whole or in part may be granted by the Competent Authority of HBNI when in his or her judgment the proposed use of the material is in the interests of scholarship. In all other instances, however, permission must be obtained from the author.

Debashish Chakraborty

Debashish Chakraborty

# DECLARATION

I, hereby declare that the investigation presented in the thesis has been carried out by me. The work is original and has not been submitted earlier as a whole or in part for a degree at this or any other Institution / University.

Debashish Chakraborty

Debashish Chakraborty

# CERTIFICATION ON ACADEMIC INTEGRITY

**Undertaking by the Student:**

1. I **Debashish Chakraborty**, HBNI Enrolment No. **LIFE11201704001** hereby undertake that the Thesis, titled "**Understanding the role of carcinoembryonic antigen-related cell adhesion molecules in gastric epithelial cells**" is prepared by me and is the original work undertaken by me.
2. I also hereby undertake that this document has been duly checked through a plagiarism detection tool and the document is found to be plagiarism free as per the guidelines of the Institute/UGC.
3. I am aware and undertake that if plagiarism is detected in my thesis at any stage in the future, suitable penalty will be imposed as applicable as per the guidelines of the Institute/UGC.

Debashish Chakraborty
Signature of the Student with date

**Endorsed by the Thesis Supervisor:**

I certify that the thesis written by the Researcher is plagiarism free as mentioned above by the student.

Signature of the Thesis Supervisor with date: 20.4.2026

Name : Dr. Asima Bhattacharyya

Designation : Associate Professor

Department/Centre: School of Biological Sciences

Name of the OCC : National Institute of Science Education and Research (NISER) Bhubaneswar

# LIST OF PUBLICATIONS ARISING FROM THE THESIS

1. #CEACAM6-positive extracellular vesicles promote gastric tumor aggression initiated by *Helicobacter pylori* infection.***Chakraborty D**, *Samal S, Banerjee S, Pal A, Poirah I, Nath G, Bhattacharyya A. *Biochemical and Biophysical Research Communications.* 2026 Mar 19:805:153379.
2. #Protumorigenic responses of CEACAM6 in *Helicobacter pylori*-infected gastric cancer cells. **Chakraborty D**, Poirah I, Samal S, Banerjee S, Pal A, Mahish C, Chattopadhyay S, Kanungo GN, Samantasinghar P, Nath G, Rout N, Singh SP, Bhattacharyya A. *Journal of Cellular and Molecular Medicine.* 2026 Jan;30 (2):e70869.
3. RHOA-dependent regulation of mitochondrial remodeling and cell motility in hypoxia-exposed gastric epithelial cells. Pal A, Bawali P, Brahma A, Rana SR, Mohapatra R, **Chakraborty D**, Poirah I, Samal S, Banerjee S, Smoot DT, Ashktorab H, and Bhattacharyya A. *Journal of Cell Science.* 2025 Jul 15;138 (14): jcs263690.
4. Hypoxia and Hypoxia-Reoxygenation Potentiate *Helicobacter pylori* Infection and Gastric Epithelial Cell Proliferation. Poirah I, Chakraborty S, Padhan PK, Mishra AK, **Chakraborty D**, Dixit P, Samal S, Rout N, Singh SP, Nath G, Smoot DT and Bhattacharyya, A. *Cancer Medicine*. 2025 May;14(9):e70860.
5. The influence of hypoxia-mediated CEACAM6 upregulation on epithelial cell and macrophage response in the context of gastric cancer. Poirah I, **Chakraborty D**, Dixit P, Samal S, Banerjee S, Mukherjee T, Chattopadhyay S, Nath G and Bhattacharyya A. *European Journal of Clinical Investigation*. 2024 Dec;54 Suppl 2(Suppl 2):e14352.
6. Siah2-GRP78 interaction regulates ROS and provides a proliferative advantage to *Helicobacter pylori*-infected gastric epithelial cancer cells. Dixit P, Suratkal SS, Kokate SB, **Chakraborty D**, Poirah I, Samal S, Rout N, Singh SP, Sarkar A, Bhattacharyya A. *Cellular and Molecular Life Sciences.* 2022 Jul 11;79(8):414.
7. *Helicobacter pylori*-induced gastric cancer is orchestrated by MRCKβ-mediated Siah2 phosphorylation. Dixit P, Kokate SB, Poirah I, **Chakraborty D**, Smoot DT, Ashktorab H, Rout N, Singh SP, Bhattacharyya A. *Journal of Biomedical Science.* 2021 Feb 3;28(1):12.
8. Testin and Filamin-C downregulation by acetylated Siah2 increases invasiveness of *Helicobacter pylori*-infected gastric cancer cells. Kokate SB, Dixit P, Poirah I, Roy AD, **Chakraborty D**, Rout N, Singh, SP, Ashktorab H, Smoot DT, Bhattacharyya A. *The International Journal of Biochemistry & Cell Biology.* 2018 Oct:103:14-24.
9. Acetylation-mediated Siah2 stabilization enhances PHD3 degradation in *Helicobacter pylori*-infected gastric epithelial cancer cells. Kokate SB, Dixit P, Das L, Rath S, Roy AD, Poirah I, **Chakraborty D**, Rout N, Singh SP, Bhattacharyya A. *The FASEB Journal.* 2018 Oct;32(10):5378-5389.

#Pertaining to the thesis. *Co-first author.

**Review articles and book chapters**

1. Methods to Evaluate the Effects of HAT/KAT Inhibition on SIAH2-Driven Reactive Oxygen Species Generation in *Helicobacter pylori*-infected Gastric Epithelial Cells. Dixit P, Kokate

SB, Rath S, Das L, **Chakraborty D**, Bhattacharyya A. In HDAC/HAT Function Assessment and Inhibitor Development: *Methods in Molecular Biology.* 2023:2589:317-335.

2. Hypoxia-driven metabolic heterogeneity and immune evasive behaviour of gastrointestinal cancers: elements of a recipe for disaster. Mishra AK, Singh SK, Dayanandan S, Banerjee S; Chakraborty S, Gopal AB, Samal S, Poirah I, **Chakraborty D**, Bhattacharyya A. *Cytokine.* 2022 Aug:156:155917.
3. Silent hypoxia in COVID-19: a gut microbiota connection. Gopal AB, Chakraborty S, Padhan PK, Barik A, Dixit P, **Chakraborty D**, Poirah I, Samal S, Sarkar A, Bhattacharyya A. *Current Opinion in Physiology.* 2021 Oct:23:100456.

**Conferences**

1. A novel potential biomarker in gastric cancer. **Chakraborty D**[$], Samal S, Banerjee S, Pal A, Poirah I, Nath G, Bhattacharyya A. PHYSICON 2025, XXXVI Annual Conference of Physiological Society of India, "Innovations in Physiology: From Cell to Systems", AIIMS, Bhubaneswar, 21st-23rd November.
2. CEACAM6: a key player in gastric cancer progression. **Chakraborty D**, Poirah I, Samal S, Banerjee S, Pal A, Mahish C, Chattopadhyay S, Kanungo GN, Samantasinghar P, Nath G, Rout N, Singh SP, Bhattacharyya A. 33rdAnnual International CEACAM/PSG Symposium (virtual). Department of Surgery, Division of Liver and Pancreas at the University of California, Los Angeles, USA, 12th September, 2025.
3. Investigating the role of Rho GTPases in extracellular vesicle-mediated gastric cancer (GC) progression. Banerjee S, Samal S, Pal A, Mohanty P, **Chakraborty D**, Dash S, Rout N, Singh SP, Nath G, Bhattacharyya A. 9th Annual Meeting of the Society for Molecular Signalling, School of Life Sciences University of Hyderabad, India, 1st-3rd February 2024.
4. CEACAM dynamics in hypoxia determines gastric carcinogenesis. Poirah I, **Chakraborty D**, Dixit P, Samal S, Chakraborty S, Singh SP, Singer BB, Bhattacharyya A. 91st Annual Meeting of Society of Biological Chemists (India) on "Life at the Confluence of Biology and Chemistry", Society of Biological Chemists (I) Kolkata Chapter, 8th-11th December, 2022.
5. Study of extracellular vesicles released from *Helicobacter pylori*-infected gastric epithelial cells and determining their protein content. Samal S, Dixit P, Banerjee S, Poirah I, **Chakraborty D**, Bhattacharyya A. 7th Warsaw Conference on Perspectives of Molecular Oncology (virtual), Maria Skłodowska-Curie National Research Institute of Oncology, Warsaw, Poland, 6th -7th October, 2022.
6. Determination of the characteristics and protein signature of extracellular vesicles released by *Helicobacter pylori*-infected gastric epithelial cells. Samal S, Dixit P, Banerjee S, Poirah I, **Chakraborty D**, Bhattacharyya A. HBNI Theme Meeting on Life Sciences, Raja Ramanna Centre for Advanced Technology, Indore, 7th -10th September 2022.
7. SIAH2 regulates expression of CEACAMs in *Helicobacter pylori*-infected gastric epithelial cells. **Chakraborty D**, Dixit P, Poirah I, Samal S, Singer B B, Rout N, Singh S P, Bhattacharyya A. International Conference on Recent Trends in Biotechnology 2022, Centurion. University of Technology & Management, Bhubaneswar, 22nd -23rd of June 2022.
8. Association between CEACAMs and hypoxia defines gastric cancer progression". Poirah I, **Chakraborty D**, Dixit P, Samal S, Padhan PK, Barik A, Singh SP,

Singer BB and Bhattacharyya A. AACR Annual Meeting 2021 (virtual); April 10-15, 2021 and May 17-21, 2021; Philadelphia, USA.

9. *Helicobacter pylori*-mediated gastric cancer: at the crossroads between hypoxia and inflammation. Roy AD, Poirah I, **Chakraborty D**, Dixit P, Singh A, Singh SP and Bhattacharyya A. 17th International Congress of Immunology, Beijing, China,19th - 23rd Oct 2019.
10. *Helicobacter pylori* increases reactive oxygen species burden of infected gastric epithelial cells via involvement of Siah proteins. Dixit P, Kokate SB, Poirah I, Roy AD, **Chakraborty D**, Rout N, Singh SP and Bhattacharyya A. 14th Indo Australian Biotechnology Conference, ACTREC, Navi Mumbai, India, 22nd -23rd Oct, 2018.
11. Generation of reactive oxygen species in *Helicobacter pylori*-infected gastric epithelial cells is associated with Siah proteins. Dixit P, Kokate SB, Poirah I, Roy AD, **Chakraborty D**, Rout N, Singh SP and Bhattacharyya A. 4th International Conference on Translational Research, Goa, India, 11-13 Oct 2018.
12. SIAH2 acetylation regulates invasiveness of *Helicobacter pylori*-infected human gastric epithelial cells. Kokate SB, Dixit P, Das L, Rath S, Roy AD, Poirah I, **Chakraborty D**, Rout N, Singh SP and Bhattacharyya A. 13th National Research Scholars Meet (13th NRSM-2017, OP01), ACTREC, Mumbai, India.
    Presenter, $awarded a prize for poster presentation.

Debashish Chakraborty

Debashish Chakraborty

# CONTENTS


| | | Page No. |
|---|---|---|
| SUMMARY | | 12-13 |
| LIST OF ABBREVIATIONS | | 14-17 |
| LIST OF FIGURES | | 18-19 |
| LIST OF TABLES | | 19 |
| Chapter 1 | Introduction | 20-47 |
| | Section A | 21-36 |
| | 1.A.1. Epidemiology | 21 |
| | 1.A.2. Risk factors | 21 |
| | 1.A.3. Classification of GC | 22-23 |
| | 1.A.4. Pathogenesis of *H. pylori* | 24-29 |
| | 1.A.4.1. CagA | 29-30 |
| | 1.A.4.2. VacA | 30-31 |
| | 1.A.5. Mechanisms of *H. pylori*-mediated GC development | 31-32 |
| | 1.A.6. CEACAMs | 32-33 |
| | 1.A.6.1. CEACAMs as pathogen receptors | 34-35 |
| | 1.A.6.2. CEACAMs in cancer | 35-36 |
| | Section B | 36-47 |
| | 1.B.1. Tumor microenvironment | 36-37 |
| | 1.B.2. Role of macrophages within the TME of *H. pylori*-mediated GC | 37-38 |

| | | |
|---|---|---|
| | 1.B.3. Soluble mediators released within the TME are critical to tumor progression | 38-39 |
| | 1.B.4.1. The timescale of EV research | 39-41 |
| | 1.B.4.2. EV biogenesis and physiological functions | 41-42 |
| | 1.B.4.3. Cargoes of EVs | 42-43 |
| | 1.B.4.4. EVs in cancer | 43 |
| | 1.B.4.5. EVs and cancer progression | 43-44 |
| | 1.B.4.6. EVs in GC | 45 |
| | 1.B.4.7. EVs as biomarkers | 46-47 |
| | 1.B.5. Unanswered questions | 47 |
| Chapter 2 | *H. pylori* upregulate CEACAM6 in GCCs | 48-55 |
| | 2.1 CEACAMs are upregulated in GC | 49-51 |
| | 2.2 CEACAM6 is specifically upregulated upon *H. pylori* infection | 51-54 |
| | 2.3 Discussion | 54-55 |
| Chapter 3 | CEACAM6 promotes tumorigenic potential in GCCs | 56-64 |
| | 3.1 CEACAM6-expression supports pro-tumorigenic responses in GCCs | 57-59 |
| | 3.2 Supernatants released from *CEACAM6*-expressing cells can promote tumorigenesis in recipient cells | 59-62 |
| | 3.3 Discussion | 62-64 |
| Chapter 4 | *CEACAM6*-expressing GCCs alter macrophage polarization | 65-73 |
| | 4.1. Metastatic GC exhibit M2 infiltration of macrophages | 66-67 |

| | | |
|---|---|---|
| | 4.2. *CEACAM6*-expressing GCCs promote M2 polarization of macrophages | 67-71 |
| | 4.3. *CEACAM6*-expressing GCCs release cytokines that promote M2 polarization of macrophages | 71-72 |
| | 4.4. Discussion | 73 |
| Chapter 5 | GC aggressiveness is amplified by *H. pylori* infection-derived EVs containing CEACAM6 | 74-84 |
| | 5.1. AGS cell–derived EVs contain CEACAM6 | 75-77 |
| | 5.2. EVs secreted by *CEACAM6*-expressing cells are CEACAM6-enriched | 77-81 |
| | 5.3. The recipient cells exposed to CEACAM6-enriched EVs acquired tumorigenic potentials | 81-82 |
| | 5.4. CEACAM6 is localised to the EV membrane and metastatic GC patients release CEACAM6-enriched EVs | 82-84 |
| | 5.5. Discussion | 84 |
| Chapter 6 | Conclusions | 85-87 |
| | Key findings | 86-87 |
| Chapter 7 | Materials and methods | 88-106 |
| | 7.1. GCCs | 89 |
| | 7.2. Cell passaging | 89 |
| | 7.3. Cell freezing and revival | 89-90 |
| | 7.4. *H. pylori* maintenance and infection | 90 |
| | 7.5. *H. pylori* freezing and revival | 90-91 |

7.6. Transformation 91

7.7. Transfection 91-92

7.8. Supernatant collection 92

7.9. EV isolation 92-93

7.10. Bioinformatic analysis 93

7.11. Biopsy and sera collection 93

7.12. EV isolation from sera 93-94

7.13. Tissue sectioning 94

7.14. Cell and EV lysate preparation 94

7.15. Sonication of EVs 95

7.16. SDS PAGE 95-97

7.17. Western blotting 97-98

7.17.1 Reprobing of immunoblots 98

7.18. Flow cytometry of GCCs 98-99

7.19. PBMC isolation and macrophage generation 99

7.20. Macrophage-epithelial cell co-culture 99-100

7.21. Flow cytometry of macrophages 100

7.22. Immunofluorescence and confocal microscopy 100-101

7.23. Cytokine array analysis 101

7.24. Treatment with EVs 101

7.25. Wound healing assay 101-102

7.26. Clonogenic assay 102

7.27. Population doubling assay 102-103

7.28. Invasion assay 103-104

7.29. Nanoparticle tracking analysis 104

| | | |
|---|---|---|
| | 7.30. Transmission electron microscopy | 104 |
| | 7.31. Dynamic light scattering | 104 |
| | 7.32. Statistical analysis | 104-105 |
| Bibliography | | 106-115 |
| Appendix I | LIST OF PLASMIDS USED | 116 |
| Appendix II | LIST OF PRIMARY ANTIBODIES USED | 116-117 |
| Appendix III | LIST OF SECONDARY ANTIBODIES USED | 118 |

# SUMMARY

*Helicobacter pylori* colonizes the gastric epithelium by interacting with carcinoembryonic antigen-related cell adhesion molecules (CEACAMs), notably CEACAM1, CEACAM5 and CEACAM6, expressed on the gastric epithelial cells. Colonization may give rise to gastritis, occasionally advancing to gastric cancer (GC). This work explored alterations in CEACAM expression triggered by *H. pylori* infection. Results demonstrated a significant upregulation of CEACAM6 after infection which promoted gastric cancer cell (GCC) proliferation, migration and invasion. The tumor microenvironment (TME) promotes tumorigenesis through released mediators. Therefore, the paracrine effects of the *CEACAM6*-expressing GCCs were also studied on surrounding non-aggressive GCCs. Supernatants from *H. pylori*-infected CEACAM6-transfected GCCs further enhanced tumorigenic traits in neighboring cells. Within the TME, macrophages are key drivers of tumor progression. Co-culture experiments revealed that epithelial-CEACAM6 facilitated *H. pylori*-driven M2 macrophage polarization as confirmed by flow cytometry and immunofluorescence microscopy. Cytokine signatures linked to macrophage polarization were identified through antibody array analysis of the *CEACAM6*-expressing cell supernatants.

Extracellular vesicles (EVs) are key secretory modulators that contribute substantially to tumor development and progression. Significantly elevated levels of CEACAM6 were found to be present in the EVs secreted by *H. pylori*-infected gastric cancer cells (GCCs). To study the impact of CEACAM6-containing EVs, on tumor inducing capabilities, EVs were isolated from *CEACAM6*-expressing cells. Those were thoroughly characterised. Functional assays revealed that CEACAM6-positive EVs enhanced proliferation, clonogenicity, migration and invasion of recipient GCCs, with infection further amplifying these effects. EV sonication and fractionation confirmed that CEACAM6 was largely confined to the vesicle membrane. Consistent with tissue findings, sera from GC patients exhibited significantly higher

CEACAM6 in EVs compared to those in healthy controls. Collectively, these findings suggest that CEACAM6-containing EVs act as potent mediators of tumorigenesis and potential biomarkers in *H. pylori*-associated GC.

# LIST OF ABBREVIATIONS USED

AlpA/B: Adherence associated lipoprotein A/B

ANOVA: Analysis of variance

Akt: Protein Kinase B

APS: Ammonium persulfate

ATCC: American type culture collection

ARG1: Arginase1

BabA: Blood group antigen-binding adhesin A

BSA: Bovine serum albumin

*cag* PAI: Cytotoxin-associated gene pathogenicity island

BMDCs: Bone marrow derived dendritic cells

CAF: Cancer-associated fibroblast

CD: Cluster of differentiation

CEACAMs: Carcinoembryonic antigen-related cell adhesion molecules

COX2: Cyclooxygenase-2

cPD: Cumulative population doubling

circRNA: Circular RNA

DAPI: 4', 6-diamidino-2-phenylindole

DEG: Differential expression of genes

DMSO: Dimethyl sulfoxide

DupA: Duodenal ulcer promoting gene A

EDTA: Ethylenediamine tetraacetic acid 4

EMT: Epithelial-mesenchymal transition

EPIYA: Glutamate-proline-isoleucine-tyrosine-alanine

ERK: Extracellular signal-regulated kinase

ECM: Extracellular matrix

EVs: Extracellular vesicles

FAK: Focal adhesion kinase

FBS: Fetal bovine serum

FACS: Fluorescence-activated cell sorting

GC: Gastric cancer

GCCs: Gastric cancer cells

GECs: Gastric epithelial cells

GPI: Glycosylphosphatidylinositol

GSH: Glutathione

*H. pylori*: *Helicobacter pylori*

HomB: *Helicobacter* outer membrane B

Hop: *H. pylori* outer membrane protein

HRP: Horse-radish peroxidase

Hsp: Heat shock proteins

IL: Interleukin

iNOS: Inducible nitric oxide synthase

JNK: c-Jun N-terminal Kinase

KRAS: Kirsten rat sarcoma viral oncogene homolog

lncRNA: Long non-coding RNA

LPS: Lipopolysaccharide

M-CSF: Macrophage colony stimulating factor

MDSCs: Myeloid-derived suppressor cells

MFI: Mean fluorescence intensity

MMPs: Matrix metalloproteinases

miRNA: microRNA

MOI: Multiplicities of infection

mRNA: messenger RNA

MSCs: Mesenchymal stem cells

MVBs: Multivesicular bodies

NapA: Neutrophil-activating protein A

NTA: Nanoparticle tracking analysis

NFDM: Non-fat-dried milk

NF-κB: Nuclear Factor kappa-light-chain-enhancer of activated B cells

NKG2D: Natural killer group 2, member D

NK cell: Natural killer cell

OD: Optical density

OipA: Outer inflammatory protein A

OMPs: Outer membrane proteins

OMVs: Outer membrane vesicles

PBMCs: Peripheral blood mononuclear cells

PBS: Phosphate buffered saline

PD-L1: Programmed cell death protein

PFA: Paraformaldehyde

PI3K: Phosphatidylinositol 3-kinase

PVDF: Polyvinylidene fluoride

ROS: Reactive oxygen species

RNS: Reactive nitrogen species

RPMI: Roswell-park memorial institute

RT: Room temperature

SabA: Sialic acid-binding adhesin A

SDS-PAGE: Sodium dodecyl sulphate–polyacrylamide gel electrophoresis

SEM: Standard error of mean

SFM: Serum free media

SGC: Sporadic gastric cancer

SHP2: Src homology-2 domain-containing protein tyrosine phosphatase 2

STAD: Stomach adenocarcinoma

STAT3: Signal Transducer and Activator of Transcription 3

T4SS: Type IV secretion system

TAM: Tumor associated macrophages

TCGA: The cancer genome atlas

TEMED: N,N,N',N'-tetramethylethylenediamine

TILs: Tumor-infiltrating lymphocytes

TNF: Tumor necrosis factor

TME: Tumor microenvironment

UALCAN: University of alabama at birmingham cancer data analysis portal

VacA: Vacuolating cytotoxin A

VEGF: Vascular endothelial growth factor

WHO: World health organization

# LIST OF FIGURES


| Figure No | Figure legends |
|---|---|
| Figure 1 | Risk factors for GC development |
| Figure 2 | Correa's cascade shows *H. pylori*-mediated disease progression |
| Figure 3 | CEACAM family proteins |
| Figure 4 | Immune cells in TME of *H. pylori*-mediated GC |
| Figure 5 | Timeline of key advances in EV biology |
| Figure 6 | Distinct types of EVs synthesised within cells |
| Figure 7 | EVs as biomarkers |
| Figure 8 | CEACAMs are upregulated in GC patients |
| Figure 9 | *H. pylori* infection upregulates CEACAM1, CEACAM5 and CEACAM6 in AGS |
| Figure 10 | *H. pylori* infection upregulates CEACAM6 in MKN45 cells |
| Figure 11 | Surface CEACAM6 is upregulated following *H. pylori* infection in GCCs |
| Figure 12 | CEACAM6 enhances aggressive phenotype in GCCs |
| Figure 13 | Supernatants from *CEACAM6*-overexpressing cells promote aggressive phenotype in GCCs |
| Figure 14 | M2 polarized macrophages infiltrate GC tumor |
| Figure 15 | Epithelial-CEACAM6 promotes M2 polarization of macrophages |
| Figure 16 | Immunofluorescence analysis of macrophage polarization in response to *CEACAM6*-expressing GCCs |
| Figure 17 | Supernatants from *CEACAM6*-expressing cells skew macrophage polarization toward M2 phenotype |

Figure 18 EVs from GCCs contain CEACAM6

Figure 19 EVs released from *CEACAM6*-overexpressing cells are enriched in CEACAM6

Figure 20 CEACAM6-loaded EVs enhance tumorigenic properties in the recipient GCCs

Figure 21 CEACAM6 is present on the EV membranes and metastatic GC patients release CEACAM6-enriched EVs in blood

Figure 22 A summary figure recapitulating the findings of this thesis work.

# LIST OF TABLES

**Table No.** **Legend**

Table 1 List of the important virulence factors of *H. pylori*

Table 2 List of components for a 10% resolving gel

Table 3 List of components for a stacking gel

# Chapter 1

# Introduction

## Section A

### 1.A.1. Epidemiology

Gastric cancer (GC) poses a persistent clinical challenge, with late detection and limited therapeutic options resulting in poor survival outcomes. GC remains one of the foremost global health challenges among malignant diseases, occupying the fifth position in both incidence and cancer-related deaths worldwide (1). China, India and Japan collectively comprised 61.5% of global incidence in 2019, with 58.6% of deaths arising from these countries, and disability-adjusted life years (DALYs) (2). The geographical discrepancy can be attributed to food habits, environmental factors, socio-economic status and genetic makeup of the population. If the current management strategies remain unaltered, India is projected to record more than 1.6 million cases among individuals born between 2008 and 2017, positioning the country among the "category A" burden areas (3). Gastrointestinal cancers in India occur more frequently in men, with Northeastern India showing the highest rates (4). Among the Indian population, esophageal and stomach cancers are most common in men, whereas more often women suffer from esophageal and gallbladder cancers.

### 1.A.2. Risk factors

GC development can be ascribed to modifiable and non-modifiable risk factors (5) (Figure 1). Modifiable risks involve lifestyle choices such as diet, smoking and alcohol. Non-modifiable risks include age, genetics and medical conditions. Addressing lifestyle factors may lower susceptibility, though genetic predispositions remain beyond individual control.

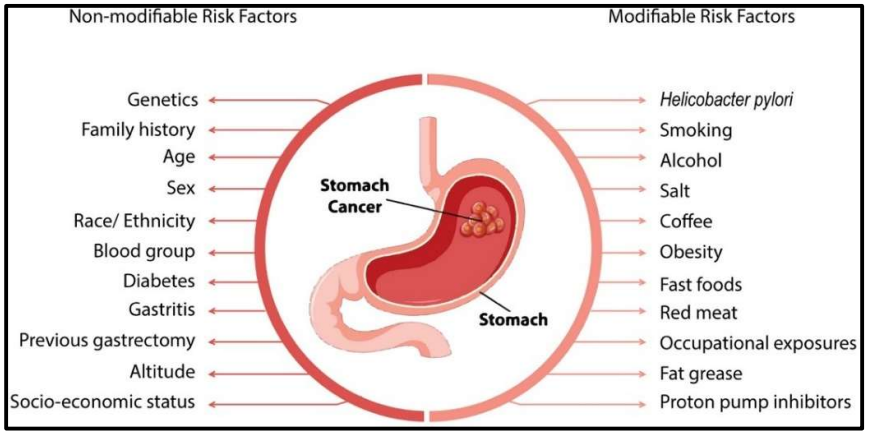


**Figure 1:** Risk factors for GC development. Figure courtesy: (5).

### 1.A.3. Classification of GC

World Health Organization (WHO) classifies GC into adenocarcinoma, signet ring-cell carcinoma and undifferentiated carcinoma. Though the Lauren system of classification remains more widely adopted, dividing GC into intestinal and diffuse types (6). GC may also arise sporadically; such cases are referred to as "sporadic gastric cancers" (SGCs) (7) and predominantly affect individuals in the age group of 45 or above. These GCs commonly arise from the interaction of several environmental determinants and are frequently diagnosed between the ages of 60 and 80.

The Cancer Genome Atlas (TCGA) defined the following subtypes of GC in 2014 (8):

1. **Epstein Barr virus (EBV)-associated (8.8%)**: Found in the proximal stomach, marked by DNA hypermethylation, Programmed Cell Death Protein-Ligand 1/Ligand 2 (PD-L1/PD-L2) overexpression and CDKN2A silencing.
2. **Microsatellite instability (MSI)-associated (21.7%)**: Linked to MutL Homolog 1 (hMLH1) promoter mutations and deficient DNA repair; associated with Lynch syndrome and distal intestinal-type cancers.
3. **Chromosomal instability (CIN)-associated (49.8%)**: Characterized by chromosomal instability and CpG island methylation; commonly arises in the gastric cardia and gastro-esophageal junction.

4. **Genomically stable (GS) (19.7%)**: Associated with diffuse GC (DGC).

In 1982, Marshall and Warren discovered that *H. pylori* infection was responsible for gastritis (9). In 1994, the International Agency for Research on Cancer (IARC) identified *H. pylori* as a Group I carcinogen (10). While *H. pylori* is frequently linked to various gastrointestinal conditions, only about 10–15% of affected individuals develop peptic ulcers and a smaller proportion (1–3%) advance to GC (11). Close to 89% of non-cardia GC incidence has been attributed to *H. pylori* infection, while 9% are linked to EBV. *H. pylori*-dependent GC progression is described by Correa's cascade which outlines a multistep progression of intestinal-type GC, beginning with chronic active gastritis then progressing through multifocal atrophic gastritis (AG), intestinal metaplasia (IM), dysplasia (low- or high-grade) and ultimately gastric adenocarcinoma (12). The modified Sydney system, introduced in 1994, employs both targeted and non-targeted biopsies from the gastric mucosa, including the antrum, incisura and corpus (13). This approach improves the detection of IM, AG and dysplasia (14). A study predicted that among 15.6 million future GC cases worldwide, 76% will stem from *H. pylori* infection, with Asia bearing 67% of the burden, followed by the Americas (13%) and Africa (12%) (3). These estimates underscore the urgent need to elucidate *H. pylori*-mediated GC pathogenesis and to develop strategies for early diagnosis, which will be critical for reducing GC-related mortality.

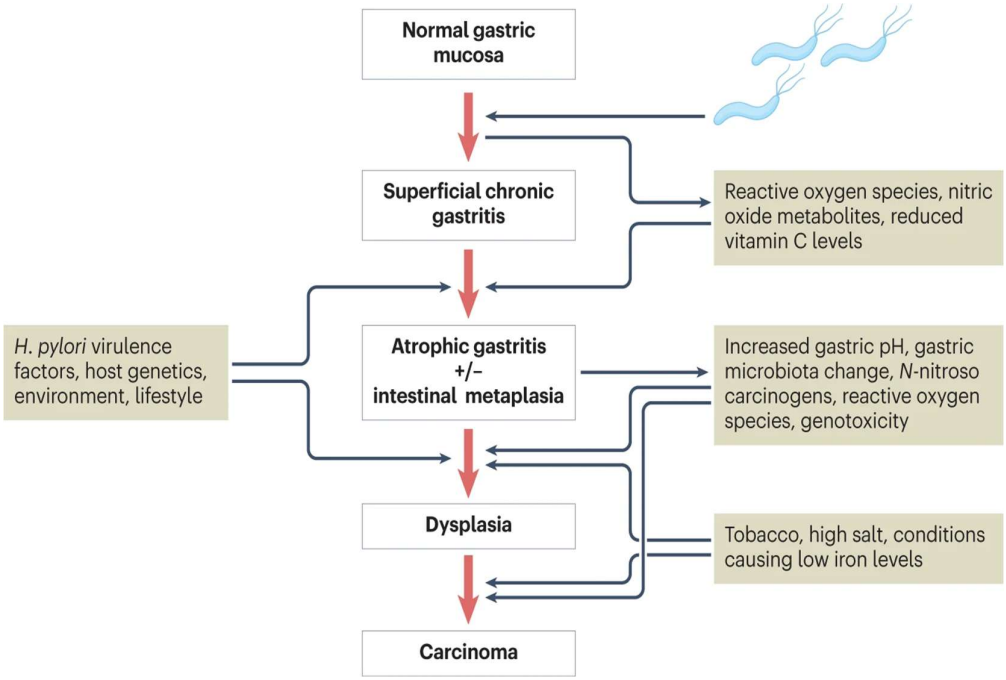


**Figure 2:** Correa's cascade shows *H. pylori*-mediated disease progression. Figure courtesy: (15).

### 1.A.4. Pathogenesis of *H. pylori*

Human gastric epithelial cells (GECs) form a protective barrier against pathogens, but *H. pylori* disrupts it by producing cytotoxins and binding with receptors. Infection involves survival inside the acidic human stomach, barrier penetration, receptor attachment and tissue damage. Key virulence factors include BabA, OipA, OMP, OMV, VacA, CagA, HtrA, NepA and SabA (16). *H. pylori* survives gastric acidity through urease-mediated acid acclimation. The urease gene cluster (*ureA/B*, *ureI*, *ureE-H*) regulates urea metabolism, with nickel insertion aided by metallochaperones UreE (17). UreI channels open under acidic pH that enables urea entry and ammonium production resulting in proton neutralisation. Extracellular urease further buffers acidity and modulates macrophage interactions.

Adhesins such as BabA, SabA, OipA and OMP bind to mucins and epithelial receptors, anchoring the bacterium. BabA binds Lewis b and ABO antigens, facilitating VacA and CagA delivery via T4SS (18). SabA targets sialylated antigens, aiding in colonization. The attachment

shields *H. pylori* from clearance mechanisms like peristalsis, mucus turnover and fluid flow. The outer membrane proteins (HOP family) of *H. pylori*, including HopQ, HopZ and Adherence associated lipoprotein A/B (AlpA), mediate adhesion to host epithelial receptors (19). OipA, linked to the *cagA* expression, induces Interleukin-8 (IL-8) secretion, inflammation and apoptosis inhibition. HopQ transports CagA into host cells, enhancing virulence, whereas Hom promotes IL-8 release and adhesion. Table 1 provides a list of virulence factors and their roles in *H. pylori* mediated pathogenesis. The subsequent sections elaborate CagA and VacA, two well-studied virulence factors responsible for *H. pylori* mediated gastritis and carcinogenesis.

**Table 1:** List of the important virulence factors of *H. pylori*

| Virulence Factor | Full Name | Mechanism of Action | Role in Pathogenesis & Disease |
|---|---|---|---|
| BabA | Blood group antigen-binding adhesin | Binds to fucosylated Lewis b ($Le^b$) blood group antigens on the gastric epithelium. | Strains expressing BabA are associated with higher bacterial loads, severe inflammation and increased cancer risk (20). |
| CagA | Cytotoxin-associated gene A | Injected into host cells via the Type IV Secretion System (T4SS). It is phosphorylated by host kinases (Src/Abl) and binds Src homology-2 domain-containing protein | Disrupts cell polarity and signaling (hummingbird phenotype). Designated as a bacterial oncoprotein, it drives proliferation and is strongly linked to GC (21). |

| | | | |
|---|---|---|---|
| | | tyrosine phosphatase 2 (SHP2). | |
| DupA | Duodenal ulcer promoting gene A | Component of a T4SS-like apparatus distinct from the Cag-T4SS. Specifically induces IL-12 and IL-8 production from immune cells. | Strongly associated with duodenal ulcers but often negatively associated with GC (22). |
| Flagella | Flagella (FlaA/FlaB) | Provides motility to move through the viscous gastric mucus. | Essential for colonization; allows the bacteria to navigate away from the acidic lumen toward the neutral pH of the epithelial surface (23). |
| GGT | γ-Glutamyl Transpeptidase | Hydrolyzes glutamine and glutathione from the host environment. | Depletes host antioxidants (causing oxidative stress) and generates ammonia. It also specifically inhibits T-cell proliferation, thereby preventing bacterial clearance (24). |
| HcpA | *Helicobacter* Cysteine-rich Protein A | A secreted protein that specifically triggers a strong Th1 (inflammatory) | The inflammatory response leads to chronic infection and is associated with diseases such as |

| | | | |
|---|---|---|---|
| | | immune response and IFN-γ production. | gastritis, peptic ulcers and GC (25). |
| HomB | *Helicobacter* Outer Membrane B | Binds to host cells and strongly induces IL-8 secretion. | Recent clinical studies correlate HomB presence specifically with peptic ulcer disease and GC in children and adults (26). |
| HopQ | *Helicobacter* Outer Membrane Protein Q | Binds to CEACAM receptors (CEACAM1, 3, 5, 6) on the host cell surface. | It acts stabilizes the T4SS needle against the host cell, ensuring efficient injection of the CagA oncoprotein (27). |
| HtrA | High Temperature Requirement A | A secreted serine protease that cleaves E-cadherin and other junctional proteins. | Opens the paracellular space (between cells), allowing bacteria to penetrate deeper tissues and facilitating epithelial-mesenchymal transition (EMT) (28). |
| OipA | Outer inflammatory protein A | Promotes adhesion and activates the STAT1 signaling pathway. | Increases the pro-inflammatory cytokine IL-8 release. Its presence correlates with high mucosal inflammation and duodenal ulcers (29). |

| | | | |
|---|---|---|---|
| NapA | Neutrophil-activating protein A | Attracts and activates neutrophils and monocytes. | Triggers an oxidative burst of reactive oxygen species (ROS) in immune cells, causing tissue damage that releases nutrients for the bacteria to feed on (30). |
| OMVs | Outer Membrane Vesicles | Spherical buds from the bacterial membrane that carry CagA, VacA and Pepsinogen to host cells. | They allow *H. pylori* to deliver virulence factors to cells *deep* in the tissue or bloodstream without direct contact, potentially explaining extra-gastric diseases (e.g., cardiovascular issues) (31,32). |
| SabA | Sialic acid-binding adhesin | Binds to sialyl-Lewis x ($sLe^x$) antigens, which are upregulated on inflamed gastric tissue. | Enables inflammation-dependent adhesion, allowing the bacteria to persist even when the tissue is chronically inflamed and the normal receptors are lost (33). |
| Tip-α | TNF-α Inducing Protein | Enters host cells and activates the NF-κB pathway. | Induces the release of TNF-α and chemokines, creating a tumor-promoting inflammatory microenvironment (34). |
| TlpD | TlpA-D Family | TlpD is a cytosolic sensor that detects | TlpD allows the bacteria to sense inflammation, ROS and flee from it to safer niches (like |

| | | | |
|---|---|---|---|
| | | ROS and cellular energy levels. | the gastric glands). It is crucial for survival in the inflamed antrum (35). |
| Urease | Urease Enzyme | Hydrolyses urea into ammonia ($NH_3$) and carbon dioxide ($CO_2$). | Raises the pH around the bacterium, allowing it to survive in the acidic stomach. Ammonia is also directly toxic to epithelial cells (36). |
| VacA | Vacuolating cytotoxin A | A secreted pore-forming toxin that enters cells via endocytosis, causing massive vacuolization and mitochondrial damage. | Induces apoptosis and inhibits T-cell activation, aiding immune evasion. Found in all strains but varies in activity (s1/m1 is most toxic) (37). |

### 1.A.4.1. CagA

CagA is one among the many proteins translated from the *cag* pathogenicity island (*cag*PAI) present in *H. pylori* genome. This protein is delivered into host GECs by a type IV secretion system (T4SS). Several *cag*PAI components are critical for the function of the T4SS and CagA translocation. CagT is important for CagA delivery into epithelial cells, while CagY modulates immune responses to support bacterial persistence and influence T4SS activity. CagL is a pilin-like surface protein that interacts with host integrin α5β1, which is required for efficient CagA translocation (38,39). CagA activity is dependent upon the Glu-Pro-Ile-Tyr-Ala (EPIYA) motifs present at the C-terminal of the protein. *H. pylori* isolated from Western

countries differs from the East Asian countries due to the presence of either the EPIYA-C or the EPIYA-D motifs, respectively (40). After translocation, CagA undergoes phosphorylation at the tyrosine residue of EPIYA motifs by various host kinases. Phosphorylated CagA interacts with SHP2 or Grb2 leading to impaired cell adhesion, altered proliferation increased IL-8 production and changes in cell elongation through Ras-ERK and Wnt-β signaling pathways (41). The resulting cytoskeletal changes and morphological alteration causes the humming bird phenotype visible in AGS cells under *in vitro* conditions. EPIYA-D containing CagA proteins exhibit stronger binding affinity towards SHP2 kinases relative to EPIYA-C containing proteins (42). This essentially translates into higher virulence of EPIYA-D carrying CagA proteins. The levels of interleukin secretion during *H pylori* infection are closely linked to both the number and specific variants of EPIYA motifs. Notably, strains harboring the EPIYA-D motif tend to produce significantly higher IL-8 compared to other motif types (43).

CagA is strongly linked to the initiation and progression of epithelial–mesenchymal transition (EMT) in the gastric mucosa. This transition is driven by multiple CagA-mediated mechanisms, including suppression of programmed cell death protein 4 (PDCD4), promotion of cancer stem cell-like traits and activation of fibroblasts (44-47). CagA inhibits Par1b activity, disrupting tight junctions and cellular polarity, causing loss of epithelial integrity (48). CagA downregulates host heat shock proteins, specifically HSPH1 (HSP105), HSPA1A (HSP72) and HSPD1 (HSP60), contributing to impaired cellular stress responses (49). HSP1 downregulation by CagA also results in the host immune suppression. The presence of CagA-positive *H. pylori* enhances susceptibility to gastritis and contributes to poor clinical outcomes in GC.

**1.A.4.2. VacA**

VacA creates pores in host cells and induces vacuolation. Its p33 subunit creates anion channels, while the p55 subunit promotes apoptosis. VacA suppresses immune responses by

inhibiting T cell function, impairs mitochondrial activity and alters cell polarity. VacA sequences exhibit diversity in three primary regions: the signal (s) region, the intermediate (i) region and the middle (m) region (50). These regions exhibit genetic polymorphism due to multiple allelic variants. Strains of *H. pylori* with VacA types s1, i1 or m1 are linked to a higher risk of GC and peptic ulcers compared to strains with s2, i2 or m2 (51). Strains with the s1 allele often carry the *cag*PAI and the adhesin BabA, while s2 strains typically lack these elements. Vacuolation process begins when VacA binds to the plasma membrane, forms oligomers and traffics to late endosomes (LEs), where it creates anion-selective channels. VacA induces autophagy in GECs by forming membrane channels through a process distinct from its vacuole-forming activity (52). This autophagy depends on VacA binding to LRP1 and may serve as a host defence to degrade the toxin (53). VacA compromises mitochondrial membrane potential, causing release of Cytochrome C followed by apoptotic pathway activation. VacA rapidly alters cell signaling by activating mitogen-activating protein (MAP) kinases (p38, ERK1/2), Cyclooxygenase-2 (COX-2) and Vascular Endothelial Growth Factor (VEGF) (54-56).

**1.A.5. Mechanisms of *H. pylori*-mediated GC development**

*H. pylori* infection impacts all three major MAPK pathways extracellular signal-regulated kinase (ERK), c-jun N-terminal kinase (JNK) and p38 which are among the key contributors to the GC development. ERK triggers nuclear factor kappa-light-chain-enhancer of activated B cells **(**NF-κB) activation, while JNK can boost the signal transducer and activator of transcription 3 (STAT3) activity (57). *H. pylori* infection-induced YAP1 activation has been associated with the progression from chronic gastritis to GC (58). The phosphatidylinositol 3-kinase/protein kinase B (PI3K/Akt) pathway promotes cell proliferation, cell survival and apoptosis inhibition (59), while also triggering EMT through activation of Snail and Twist (50). CagA also promotes stem cell-like traits via the PI3K/Akt/FOXO3a pathway (45).

*H. pylori* induces oxidative stress by generating excess ROS and reactive nitrogen species (RNS) through its metabolism and virulence factors. Upregulation of nicotinamide adenine dinucleotide phosphate (NADPH) oxidase and inducible nitric oxide synthase (iNOS) in immune cells, further exacerbates the oxidative stress. *H. pylori* disrupts expression activity of antioxidants such as glutathione (GSH) (60). It also reduces availability of antioxidant such as vitamins C, weakening the host's protection against oxidative stress (61). *H. pylori* infection contributes to genomic instability by causing gene mutations, copy number variations and chromosomal alterations. Additionally, *H. pylori* impairs the tumor suppressor p53, further enhancing cell proliferation and genomic instability (62). These changes disrupt tumor suppressors and oncogenes, promoting carcinogenesis. Chronic inflammation can create an environment that helps tumors grow. Inflammatory molecules are involved in several important steps in the development of GC. Inflammatory cytokines such as IL-6 and TNF-α can activate STAT3 and NF-κB contributing to the neoplastic transformation (63). Immune cells also produce large amounts of ROS and RNS further damaging DNA and causing genomic instability (64). Oxidative stress increases the production of inflammatory molecules such as IL-8, as well. In addition, tumor-aassociated macrophages (TAMs) release enzymes called matrix metalloproteinases that help cancer cells invade nearby tissues (65). *H. pylori* drives GC through a combination of signaling dysregulation, oxidative stress, genomic instability and chronic inflammation. A key complementary mechanism involves its engagement with CEACAM receptors on GECs, which not only facilitate bacterial colonization but also contribute to tumor progression**.**

**1.A.6. CEACAMs**

Nearly five decades ago, Dr. Phil Gold and Dr. Samuel Freedman began investigating tumor-specific antigens in colorectal carcinoma. Their work identified a marker present in both cancerous tissue and fetal organs, which they named carcinoembryonic antigen

(CEA/CEACAM5) (66). Eventually elevated CEACAM5 levels after surgery became a reliable indicator of recurrence or metastasis. Advances in molecular biology later allowed cloning of CEACAM5 cDNA and related proteins, including NCA (renamed CEACAM6) (67-69) and biliary glycoprotein (renamed CEACAM1) (70). These findings established the carcinoembryonic antigen-related cell adhesion molecule (CEACAM) family, comprising 22 genes grouped into CEACAM and pregnancy-specific glycoproteins (PSGs), located on chromosome 19q13.1–13.2 (71).

CEACAMs are widely distributed molecules present in epithelial cells, endothelial cells and immune cells (Figure 3). These are members of the immunoglobulin supergene family, typically containing an N domain resembling a variable Ig domain, followed by up to six constant C2-like domains. CEACAM5 and CEACAM6 are anchored to the membrane via glycosylphosphatidylinositol (GPI) linkage, derived from a 26-amino-acid hydrophobic region (72). Notably, GPI-linked CEACAMs are absent in the mouse genome, highlighting their relatively recent evolutionary emergence in humans (73). Six CEACAM proteins, including CEACAM1, are attached to the cell membrane through their transmembrane domains (74). CEACAM1 undergoes extensive alternative splicing, producing 12 distinct isoforms characterized by differences in the number of C2-like domains and in their cytoplasmic tails. The two main variants are the long (L) and short (S) forms, determined by exon 7 inclusion or exclusion (75). Although CEACAM proteins share similar N domains, membrane attachments and glycosylation sites, they differ in the number of C2-like domains. CEACAM5 contains six, CEACAM6 has two and CEACAM1 typically presents two or three due to alternative splicing. CEACAMs also engage in homophilic as well as heterophilic interactions (76).

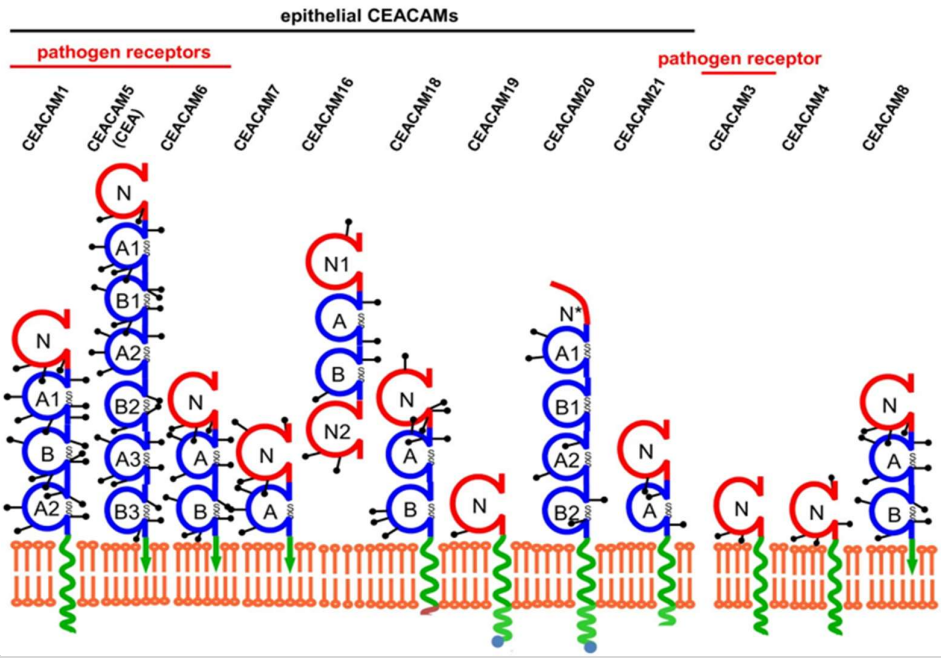


**Figure 3:** CEACAM family proteins. Figure courtesy: (77).

### 1.A.6.1. CEACAMs as pathogen receptors

The CEACAM family functions as binding receptors for numerous microbial pathogens. providing sites for infection while simultaneously enabling these microorganisms to bypass or suppress host immune defences. CEACAM1 is upregulated on activated T cells and interaction with extracellular ligands or microbial pathogens can suppress T cell activity (78). A wide range of bacteria exploit CEACAMs, including *Neisseria* species (79), *Haemophilus influenzae* (80), *H. pylori* (81), *Moraxella catarrhalis* (82), *Fusobacterium nucleatum* (83), *Escherichia coli* (84,85) and *Salmonella* species (84). For example, *Neisseria* use their opacity-associated proteins (Opa) to bind CEACAM1 on immune cells, suppressing immune function without undergoing phagocytosis (86). Enterotoxigenic *E. coli* releases heat-labile toxin in the colon, resulting in CEACAM6 upregulation. This elevated CEACAM6 then binds to the pathogen, suggesting a potential role in the enteropathy that follows infection.

In the case of *H. pylori*, the surface adhesin HopQ enables binding to multiple CEACAM family members, including CEACAM1, 3, 5 and 6 (27). This interaction provides a route for

delivery of the CagA into host cells, allowing bacterial colonization of gastric tissue and driving disease progression (81). *H. pylori* exploit human CEACAMs (CEACAM1, 5 and 6) to inject CagA into GECs via the type IV secretion system (T4SS) (21). Once inside, CagA interferes with intracellular signaling, promoting oncogenic transformation. Evidence from CEACAM-humanized mouse models shows that CagA phosphorylation and translocation depend on CEACAM engagement, underscoring its role in neoplastic changes (87).

**1.A.6.2. CEACAMs in cancer**

The long isoform of **CEACAM1** contains immunoreceptor tyrosine-based inhibitory motifs (ITIMs), which act as a platform for SHP-1/2 phosphatases. The phosphatase activity inhibits T-cell receptor signaling, thereby contributing to immune evasion. In early carcinogenesis, CEACAM1 downregulation has been associated with loss of epithelial polarity and increased proliferation, suggesting a tumor-suppressive role (88). Contrastingly, in advanced melanoma, colorectal and hepatocellular carcinomas, CEACAM1 is upregulated and promotes angiogenesis, invasion and metastatic dissemination through VEGF and integrin-mediated pathways (89). This duality of CEACAM1 is due to the distinct isoform lengths. The balance between the long cytoplasmic tail isoform (CEACAM1-L) and the short isoform (CEACAM1-S) determines whether CEACAM1 acts as a suppressor or promoter.

**CEACAM5** is widely used as a clinical biomarker in colorectal and gastrointestinal cancers (90). Mechanistically, CEACAM5 enhances homotypic and heterotypic adhesion, facilitating metastatic spread (91). Elevated CEACAM5 levels correlate with poor prognosis and chemoresistance (90). Beyond its diagnostic utility, the potential of CEACAM5 as a therapeutic target is being explored, with anti-CEA antibodies and CEA-directed CAR-T cells (92,93).

**CEACAM6** is frequently overexpressed in pancreatic, gastric, breast and lung cancers. Functionally, CEACAM6 inhibits anoikis by activating PI3K/Akt and FAK signaling, thereby

supporting survival of detached tumor cells and enhancing metastatic potential (94) CEACAM6 also modulates the tumor immune microenvironment: recent studies demonstrate its role in skewing macrophage polarization toward an M2 phenotype, fostering immunosuppressive conditions (accepted in JCMM; doi:10.1111/jcmm.70869). Clinically, CEACAM6 expression correlates with poor overall survival and resistance to EGFR-targeted therapies (95,96).

Collectively, CEACAM1, CEACAM5 and CEACAM6 exemplify how adhesion molecules are co-opted in cancer to regulate proliferation, invasion, immune escape and therapy resistance. Beyond serving as biomarkers, their active participation in tumor biology underscores the translational promise of targeting CEACAM-driven pathways in precision oncology. Importantly, given the intimate interaction of *H. pylori* with gastric epithelial CEACAMs, dissecting their roles in gastric carcinogenesis is critical to unravel how chronic infection accelerates malignant transformation and to identify novel intervention strategies in *H. pylori*-dependent GC.

**Section B**

**1.B.1. Tumor microenvironment**

The tumor microenvironment (TME) in GC contains a wide range of immune-related cells, such as macrophages, dendritic cells (DCs), myeloid-derived suppressor cells (MDSCs), T cells, and natural killer (NK) cells. Together, these populations orchestrate protective responses that counter infection and modulate disease progression (97). The immune system is essential for controlling *H. pylori* infection and limiting inflammation. With its long-standing presence in humans, *H. pylori* has evolved mechanisms that balance immune activation with evasion strategies (98). By influencing stromal cells, immune checkpoints and other regulatory pathways, the bacterium establishes a supportive microenvironment that sustains chronic colonization and contributes to gastric tumor development (Figure 4).

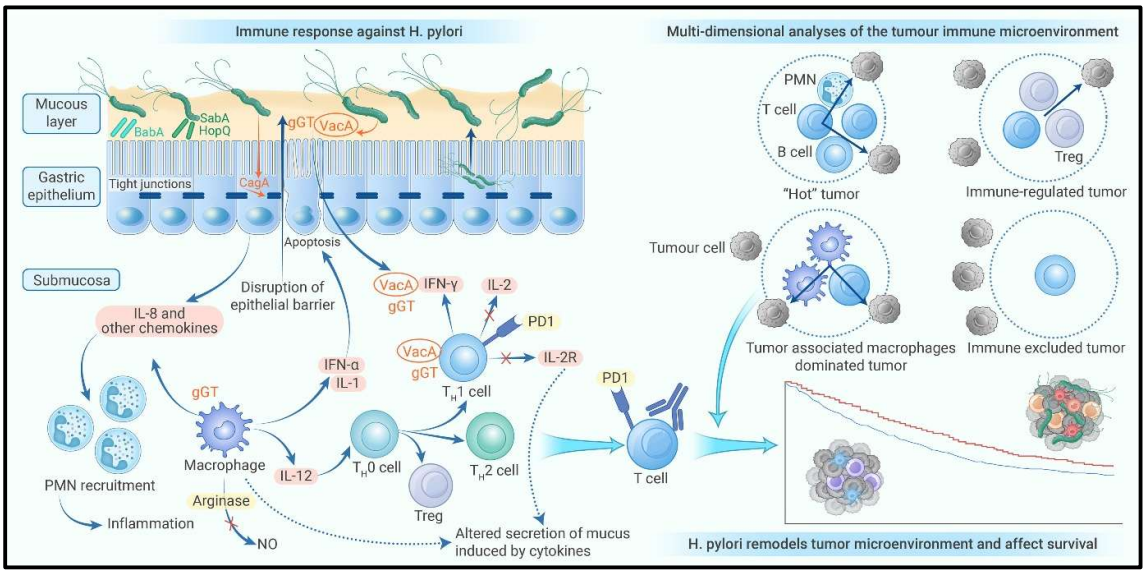


**Figure 4:** Immune cells in TME of *H. pylori*-mediated GC. Figure courtesy: (99)

### 1.B.2. Role of macrophages within the TME of *H. pylori*-mediated GC

Macrophages are highly plastic immune cells that can adopt distinct functional phenotypes depending on environmental cues. They originate from circulating peripheral blood mononuclear cells (PBMCs), which are recruited into tissues by chemokines and growth factors and subsequently differentiate in response to local signals (100). This polarization process broadly gives rise to two major subsets: classically activated M1 macrophages, which mediate antimicrobial and proinflammatory responses and alternatively activated M2 macrophages, which promote tissue repair, immune regulation and tumor progression. M1 macrophages secrete type I proinflammatory cytokines, including IL-1β, IL-12 and TNF-α (101). In contrast, alternatively activated M2 macrophages release type II cytokines such as IL-4, IL-6 and IL-10 (101). Within the TME, these polarized macrophages are referred to as TAMs. M1-like TAMs can exert anti-tumor activity through cytotoxicity and immune stimulation. The majority of TAMs in established cancers acquire an M2-like phenotype, characterized by secretion of immunosuppressive cytokines, promotion of angiogenesis and facilitation of invasion and metastasis.

Early inflammatory conditions associated with *H. pylori* infection are marked by M1

macrophage predominance, fuelling cytokine-mediated tissue injury. During *H. pylori* mediated GC development, M1 macrophage activity is gradually suppressed, shifting macrophages toward an M2-like phenotype (102). Alterations in the GC TME foster immunoediting, enabling tumor cells to evade immune surveillance by reducing immunogenicity (103). Cytokines and chemokines secreted by tumors drive the recruitment of MDSCs, regulatory T cells (Tregs), and TAMs, with elevated M2 TAM densities associated with poor overall survival (104). Compared to normal tissue, tumor samples show greater M2-TAM infiltration and poor prognosis (105). M2 TAMs, CD204-positive macrophages and their interactions with tumor-infiltrating lymphocytes (TILs) may serve as prognostic biomarkers (106). Additionally, PD-1 overexpression in M2 TAMs impairs phagocytosis and NK cell responses via TGF-β, driving tumor progression (107). Meta-analytic findings indicate that the presence of M2 macrophages and overall TAM infiltration predicts poor prognosis in GC, while M1 macrophage infiltration is associated with better survival (108). Thus, strategies aimed at reprogramming TAMs toward an M1-like phenotype or disrupting M2-associated signaling may hold therapeutic promise, while the density and phenotype of TAMs could serve as indicators of disease progression and survival outcomes in GC.

Importantly, tumor cells also secrete soluble mediators that directly induce M2 polarization. For instance in GC, tumor-derived chemokines like CCL2 and CXCL8 further recruit monocytes and condition them into M2-like macrophages (109). These findings underscore the broader role of soluble mediators within the GC microenvironment.

**1.B.3. Soluble mediators released within the TME are critical to tumor progression**

TME in GC is a rich reservoir of soluble mediators that orchestrate key steps in tumor initiation and progression. Pro-inflammatory cytokines such as IL-6, IL-8, TNF-α and TGF-β activate oncogenic pathways including STAT3, NF-κB and PI3K/Akt, driving EMT, immune evasion and resistance to apoptosis (110). Chemokines such as CCL2 and CXCL12 facilitate immune

cell recruitment, while growth factors such as VEGF, EGF and HGF promote angiogenesis and epithelial proliferation (111). Soluble enzymes, notably MMPs, degrade ECM components, enabling tumor invasion and metastatic spread. For instance, conditioned media from breast cancer cell lines induces EMT-like changes and altered glycosylation in normal MCF10A cells (112), while secreted proteins such as S100A8/A9 mediate the reprogramming of mammary epithelial cells into more malignant phenotypes (113). Similarly, conditioned media from fibroblasts has been reported to induce EMT in non-cancerous cells, underscoring the potency of tumor-secreted factors in paracrine remodeling (114). Beyond soluble proteins and metabolites, tumor cells shed extracellular vesicles (EVs) that serve as carriers of signaling molecules. EVs represent a specialized arm of the secretome with the capacity to deliver cargo directly to recipient cells, enabling long-range communication and reprogramming of non-malignant stromal and epithelial populations. EVs shed by *H. pylori*-infected gastric epithelial cells transport virulence factors and oncogenic cues that initiate EMT, immune modulation and stromal activation (115). Thus, EVs represent a critical extension of the soluble mediator network, with enhanced stability and functional precision, positioning them as key drivers of *H. pylori*-mediated gastric tumorigenesis.

### 1.B.4.1. The timescale of EV research

EVs have come a long way from being described as obscure cellular fragments to central players in biology and medicine (Figure 5). Their discovery can be traced back to the 1940s, when early experiments by Chargaff and West discovered tiny blood-derived particles with clotting activity (116). Electron microscopy later confirmed their vesicular nature, revealing lipids,

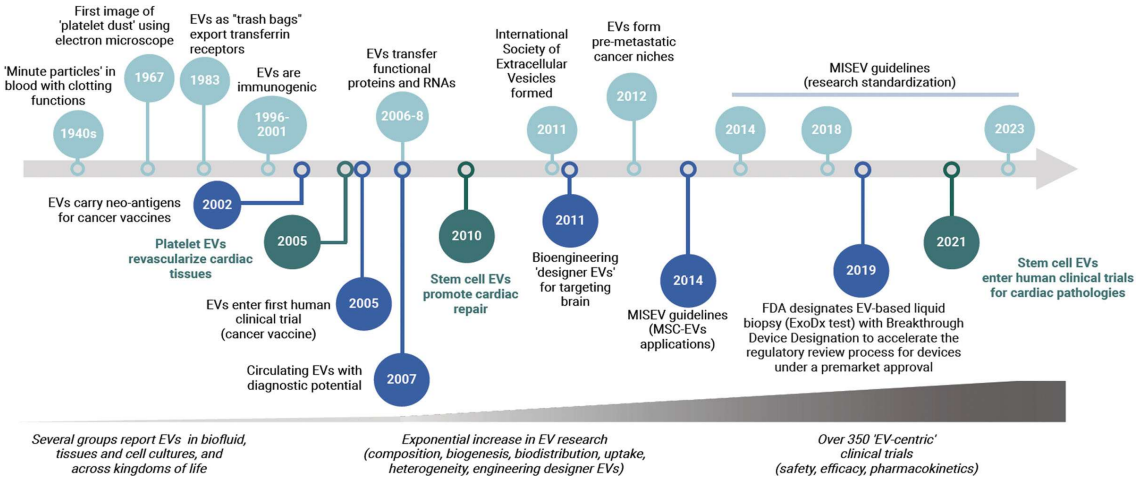


**Figure 5**: Timeline of key advances in EV biology. Figure courtesy: (117).

proteins and metabolites enclosed within (118-120). Johnstone subsequently proposed EVs as "cellular trash bags" shed by reticulocytes. By the 1990s, studies showed EVs could stimulate antigen-specific immune responses, laying the groundwork for cancer vaccine strategies (121,122). A major breakthrough followed in the mid-2000s, when EVs were found to transfer intact mRNAs and functional proteins, enabling horizontal genetic exchange and offering diagnostic potential through blood-based assays. This discovery coincided with growing interest in RNA interference, further propelling the field. Soon, therapeutic applications emerged, with EVs repairing cardiac tissue in ischemia models (123) and engineered vesicles delivering siRNA to neurons in Alzheimer's disease (124). EVs are being harnessed to deliver chemotherapeutics directly to tumors, thereby reducing systemic toxicity, as exemplified by the Phase I trial (NCT03608631) employing "iExosomes" to target metastatic pancreatic cancer (125). Hybrid vesicles, formed by fusing EVs with liposomes, unite biological function with enhanced stability for drug delivery (126). Inhalable EV-based vaccines and treatments have shown promise in mitigating inflammation and promoting tissue repair in lung diseases, including COVID-19-associated acute respiratory distress syndrome (ARDS) (127). On the technological front, Exosome Detection method via an Ultrafast isolation System (EXODUS) enables rapid, high-purity EV isolation from minimal volumes such as tears, plasma and urine

using ultrasonic nano-filtration (128).

### 1.B.4.2. EV biogenesis and physiological functions

EVs are broadly classified into exosomes (40–150 nm) and ectosomes or microvesicles (50–1000 nm) (Figure 6). Common EV markers include tetraspanins (CD9, CD63, CD81), syntenin, integrins, Alix, TSG101 and flotillin, though expression varies across cell types (129-131). Ectosomes originate from plasma membrane budding and are enriched in CD9 and CD81.

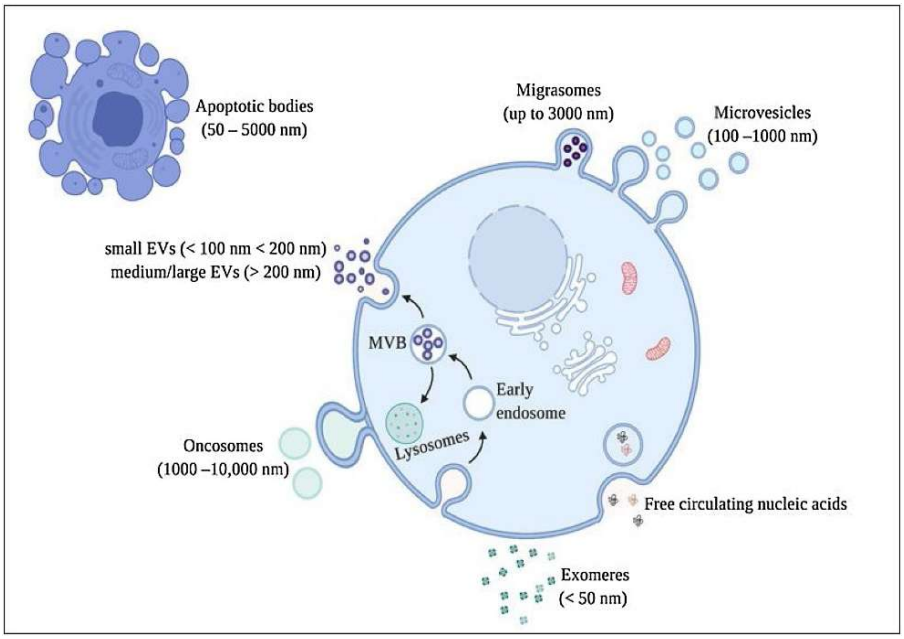


**Figure 6:** Distinct types of EVs synthesised within cells. Figure courtesy: (132).

Exosomes arise from the endocytic pathway, forming intraluminal vesicles within multivesicular bodies (MVBs) (133). MVB biogenesis can occur through the endosomal sorting complex (ESCRT) or ESCRT-independent pathway (134,135). Additionally, apoptotic bodies (1–10 μm) arise during programmed cell death (Figure 6), containing organelles and DNA to influence immunity and tissue clearance (136). Also, oncosomes (1–10 μm), released by cancer cells, drive progression, metastasis and drug resistance. These carry oncogenic cargo, serving as biomarkers and therapeutic delivery tools (137). Cells also release nonvesicular nanoparticles known as exomeres (~45 nm) and supermeres (~35 nm)(138,139). Their secretion mechanisms remain unclear and it is uncertain whether they represent aggregated

protein complexes. Exomeres display distinct proteomic signatures and unique biodistribution patterns (140). Supermeres, in contrast, are enriched with RNAs and show greater tissue accumulation than both exomeres (140).

Intercellular communication mediated through EVs is crucial for tissue patterning and development. Release of EVs supports embryonic stem cell pluripotency through activation of FAK, a mechanism also observed in cancer stem-like populations (141). Remarkably, sperm exposed to EVs from epididymal epithelial cells experiencing stress conditions gave rise to progeny with modified neurodevelopmental gene expression, suggesting transgenerational information transfer (142). EVs have been to found carry 5′-cytosine methylated DNA and histone-modifying proteins, raising the possibility of epigenetic reprogramming in recipient cells (143). Within the TME, such modifications may promote progression and therapy resistance (144,145). While EVs can act as morphogens, mechanisms restricting indiscriminate EV exchange remain poorly defined. Internalized EVs may be re-secreted or degraded, highlighting the need to clarify whether their effects are transient or long-lasting in physiology and cancer.

**1.B.4.3. Cargoes of EVs**

EVs are nanoscale, membrane-enclosed carriers containing biomolecules, shed from all types of cells. Their cargoes differ according to cell type and physiological state. Larger EVs typically harbor higher amounts of DNA along with CD9 or Annexin A1, whereas smaller EVs are preferentially enriched in CD63 and CD81 (146). EV-associated DNA has gained considerable interest (143) ; tumor-derived EVs contain genetic alterations suitable for liquid biopsy diagnostics, while mitochondrial DNA within EVs is linked to stress responses and immune signaling (147,148). EVs also carry mRNA, miRNAs, lncRNAs, piRNAs and circRNAs (149,150). miRNAs represent the predominant and functionally significant RNA species found in plasma EVs due to their implication in gene regulation and cancer progression

(151). Lipid cargo such as ceramide, cholesterol, sphingomyelin and phosphatidylserine shapes EV biogenesis and signaling, with phosphatidylserine serving as a cancer biomarker (146,152). Proteins within EVs include tetraspanins, Rab proteins, heat shock proteins, growth factors, adhesion molecules, MHC complexes, cytoskeletal components and metabolic enzymes (153,154). Notably, EVs enriched with PD-L1 and oncogenic receptors promote tumor growth and immune evasion (155). Comprehensive analysis of EV molecular contents offers significant potential for advancing diagnostics and therapeutics.

**1.B.4.4. EVs in cancer**

Early genetic events in cancer development influence the secretion of EVs, their molecular cargo and uptake mechanisms. Malignant cells generally release more EVs than non-malignant counterparts, a process thought to be regulated by calcium mobilization from the endoplasmic reticulum (156). Stress-induced activation of p53 has also been linked to enhanced EV secretion via TSAP6 (157). The activity of oncogenes reshapes EV dynamics, influencing their release, size and content (158). Mutant RAS promotes EV internalization through micropinocytosis (159,160). Oncogenic Harvey rat sarcoma viral oncogene homolog (HRAS) transformation induces the secretion of EVs containing oncogenic DNA (161). Argonaute 2 (Ago2) recruitment to multivesicular endosomes and EVs is disrupted by mutant Kirsten rat sarcoma viral oncogene homolog (KRAS), resulting in altered miRNA packaging (162). Several miRNAs with oncogenic properties have been recognized as key drivers of tumor development and progression. EVs released from breast cancer cells have been shown to generate mature miRNAs from precursors and their transfer can induce transformation in non-tumorigenic epithelial cells (163). While EVs may contribute to cancer risk, studying their role in tumor initiation is limited by the absence of precursor lesion models and specific EV markers.

**1.B.4.5. EVs and cancer progression**

Tumor progression is shaped by a multifaceted signaling network between malignant and non-malignant cells, which acts to both advance and restrain disease. Pancreatic cancer–derived EVs carry biomolecules that induce endoplasmic reticular stress in normal recipient cells, imparting tumorigenic potential (164). EVs derived from non-malignant cells can package Phosphatase and Tensin Homolog (PTEN) and transfer it to inhibit Akt pathway activity and proliferation, highlighting their tumor-suppressive role (165). This bidirectional EV transfer within the TME suggests that the relative abundance and molecular cargo of cancer cell- versus stromal cell-derived EVs may ultimately dictate disease progression.

EVs released by natural killer (NK) cells contain cytotoxic proteins capable of inducing cancer cell death, thereby potentially restraining tumor progression. EVs secreted by multiple myeloma cells carry natural killer group 2, member D (NKG2D) ligands that transiently stimulate NK activity; however, sustained exposure reduces NKG2D expression and weakens NK cell function. This showcases a dual role in which cancer cell EVs may first activate immune responses but are ultimately exploited to promote immune evasion and disease advancement. EVs contribute to the establishment of an immunosuppressive TME by inhibiting T-cell activity (166,167) and DC activity (168), while driving macrophages and MDSCs toward tumor-supportive phenotypes (169,170).

EVs actively reshape the local microenvironment to establish niches that favor tumor expansion. They influence vascular remodeling and recruit bone marrow–derived cells (BMDCs), thereby supporting metastatic colonization (171,172). In addition to the bloodstream, cancer cells exploit lymphatic routes. Interestingly, EVs also accumulate in organs where metastasis is rare, including the pancreas, the kidneys, heart, bladder and muscles (173). Mechanisms that restrict EV entry into metastatic niches have been described, highlighting the importance of reciprocal signaling between cancer cells and the surrounding stroma (174).

### 1.B.4.6. EVs in GC

Ongoing research highlights EVs as key players in the biological processes of GC (175). Distinct protein and RNA profiles have been identified in EVs isolated from GC patients and cell lines. Cancer-associated fibroblast (CAF)-derived EVs significantly stimulate migration and invasion of scirrhous-type GC cells, with CD9-positive vesicles enhancing motility (176). By delivering Apolipoprotein E (ApoE), EVs derived from M2-TAMs activate PI3K–Akt signaling in GCCs, inducing cytoskeletal reorganization and migration both *in vitro* and *in vivo* (177). Mesenchymal stem cells (MSCs) derived EVs also contribute to GC progression by promoting tumor growth, stimulating CAF differentiation and enhancing malignant properties by inducing EMT and cancer stemness via Akt activation (178). Human bone marrow-MSC EVs further drive GC growth through Hedgehog signaling, with pathway inhibition reducing tumor promotion (179). GC-derived EVs are enriched with oncogenic miRNAs (e.g., miR-217, miR-25, miR-10, let-7 family) and lncRNAs (e.g., ZFAS1), which are transferred to recipient cells to reprogram gene expression and signaling pathways (175). These RNAs suppress tumor suppressors such as CDH1, enhancing proliferation, migration and invasion.

Chronic inflammation in GC has been linked to EVs from *H. pylori* infection, which are increased in patient gastric juices and preferentially taken up by epithelial cells to drive inflammatory responses. CagA has been detected in serum-derived exosomes from cagA-positive patients, suggesting systemic transfer to distant organs (180). EV dependent mesenchymal to epithelial transition induced by *H. pylori*-infected GCCs reprogram TAMs to support cancer progression (181). Additionally, *H. pylori* OMVs modulate immunity by inducing COX-2 expression in monocytes and subsequently suppressing T cell proliferation (169). Collectively, these findings establish EVs as critical mediators of GC progression, metastasis and immune evasion.

### 1.B.4.7. EVs as biomarkers

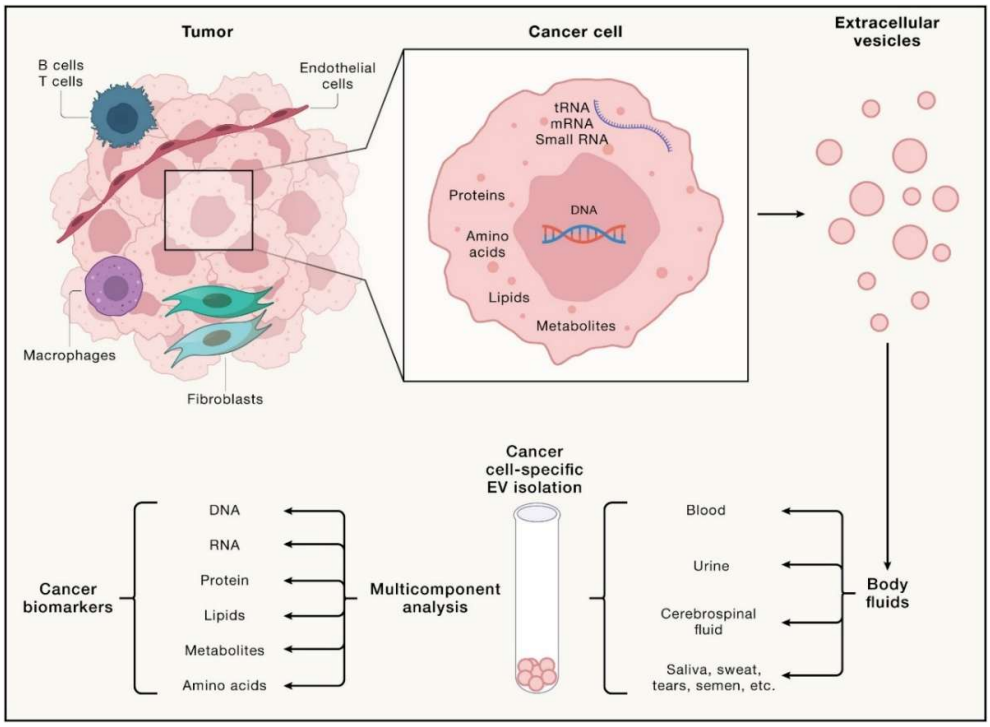


**Figure 7:** EVs as biomarkers. Figure courtesy: (182).

EVs can be detected in circulation and other body fluids, making them potential minimally invasive biomarkers for diagnostic and therapeutic assessment (Figure 7). EVs isolated from stool contain ribosomal RNA of human and bacterial origin, supporting their application in gastrointestinal cancer and microbiome surveillance (183). DNA within EVs has emerged as a cancer biomarker. In pancreatic cancer, EV-derived DNA carries mutations such as $KRAS^{G12D}$ and $TP53^{R273H}$, while $GPC1^{+}$ EVs indicate early disease (182). Although present at low levels, EV-associated DNA yields higher sequencing coverage, indicating greater diagnostic utility than circulating-free DNA. EV–associated proteins serve as valuable markers that enable selective capture and detection of cancer-derived EVs. A key advantage of EVs over conventional biomarkers, such as soluble proteins, is their composite nature (147). EVs package a wide range of biomolecules that can be profiled in parallel, strengthening diagnostic precision and monitoring of cancer.

EVs represent a unique biomarker platform in *H. pylori*-mediated GC because they encapsulate

cargo of dual origin, carrying molecules from both host cells and the pathogen. This composite signature reflects the dynamic interplay between *H. pylori* and the gastric epithelium, making EVs highly informative for distinguishing infection-driven carcinogenesis from SGC. Proteomic profiling has revealed that EVs released during infection contain distinct proteins associated with inflammation, immune modulation and oncogenic signaling which may serve as early indicators of malignant transformation (184). Beyond their diagnostic value, EVs actively contribute to pathogenesis by transferring virulence factors, miRNAs and signaling molecules that drive EMT, angiogenesis and immune evasion (115). Since EVs are readily detectable in blood, gastric juice and stool, they provide a minimally invasive means to monitor both *H. pylori* infection status and its oncogenic consequences. This feature is particularly valuable in high-incidence regions where endoscopic screening is resource-intensive.

**1.B.5. Unanswered questions**

Though *H. pylori* exploit CEACAMs as receptor to bind and infect GECs, it remains elusive how the infection itself modulates the CEACAM expression and consequently how such modulation contributes to the *H. pylori*-mediated GC. The TME plays a fundamental role in orchestrating immune cell interactions, particularly macrophages, yet the involvement of CEACAMs in directing macrophage polarization remain unknown. Given that intercellular communication often occurs through EVs that promote tumor progression, it is imperative to investigate how CEACAMs may contribute to EV-mediated promotion of *H. pylori*-dependent GC. This thesis attempts to address these questions.

# Chapter 2

# *H. pylori* upregulate CEACAM6 in GCCs

**2.1 CEACAMs are upregulated in GC**

CEACAMs are widely implicated in various types of disease pathogenesis. CEACAM1, CEACAM5 and CEACAM6 have been reported in multiple malignancies (90). To explore the relevance of CEACAM family members in GC bioinformatics analyses were undertaken (the date of accession: 22$^{nd}$ December, 2025). The differential gene expression (DEG) analysis was performed using the The cancer genome atlas-stomach adenocarcinoma (TCGA-STAD) dataset in the GEPIA2 web portal (http://gepia.cancer-pku.cn/detail.php?clicktag=degenes).) ANOVA revealed that *CEACAM5* (Log2 fold change: 6.856) and *CEACAM6* (Log2 fold change: 6.711) were the most highly ranked DEGs. *CEACAM1* (Log2 fold change: 2.925) was also notable, appearing among the top 250 genes. Further analysis of the STAD dataset confirmed that transcript levels of *CEACAM1*, *CEACAM5* and *CEACAM6* were consistently elevated in cancer patients compared to non-cancerous controls (Figure 8A-C). These results suggested strong associations of these genes with GC pathogenesis.

To confirm these observations at the protein level, biopsy samples from metastatic GC patients were analyzed by immunofluorescence microscopy. Results showed markedly higher CEACAM1, CEACAM5 and CEACAM6 in tumor tissues relative to control tissues (Figure 8D-F). Quantitative analysis further revealed a significant increase in the mean fluorescence intensity (MFI) for these CEACAMs in GC samples. Subsequently, the impact of *H. pylori* infection on CEACAM expression in STAD was assessed**,** using the University of Alabama at Birmingham Cancer Data Analysis (UALCAN) portal (https://ualcan.path.uab.edu/). GC patients harboring *H. pylori* exhibited pronounced upregulation of CEACAM5 and CEACAM6 compared to controls (Figure 8G-I). These observations highlight possible links between *H. pylori* infection and CEACAM upregulation in GC.

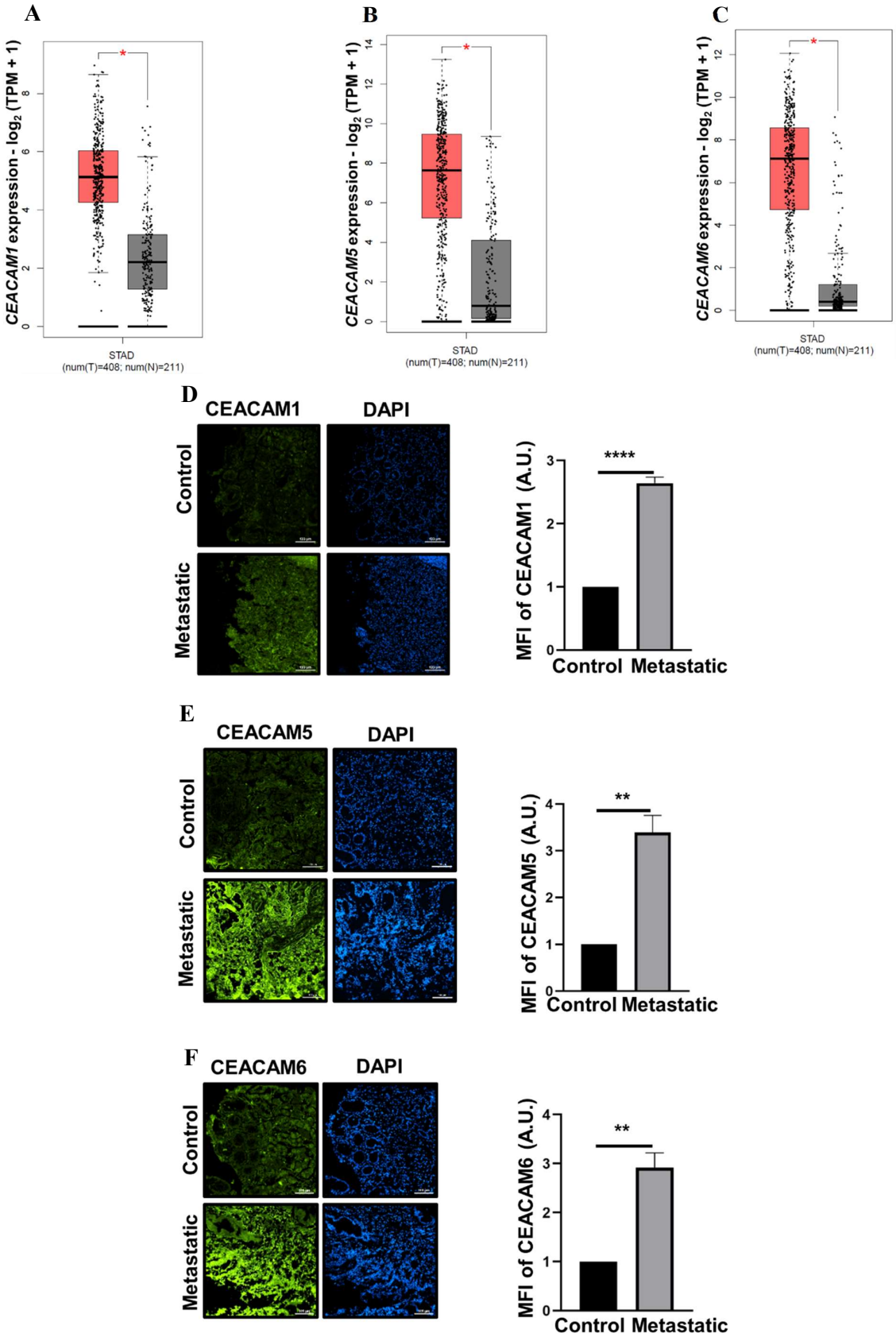
A
B
C
CEACAM1 expression - log2 (TPM + 1)
CEACAM5 expression - log2 (TPM + 1)
CEACAM6 expression - log2 (TPM + 1)
STAD
(num(T)=408; num(N)=211)
D
CEACAM1
DAPI
Control
Metastatic
MFI of CEACAM1 (A.U.)
****
Control Metastatic
E
CEACAM5
DAPI
Control
Metastatic
MFI of CEACAM5 (A.U.)
**
Control Metastatic
F
CEACAM6
DAPI
Control
Metastatic
MFI of CEACAM6 (A.U.)
**
Control Metastatic

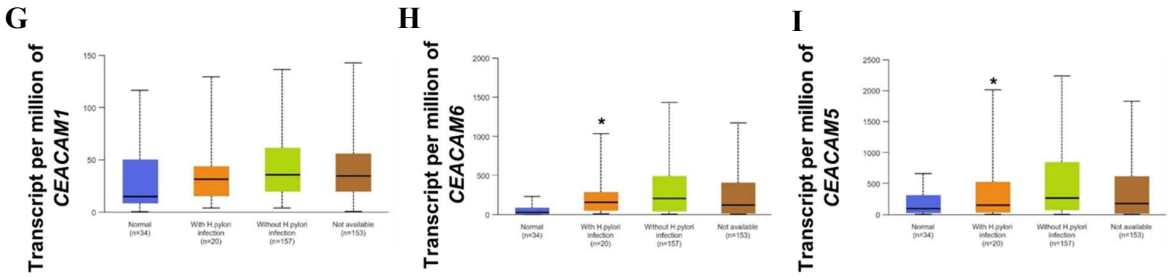


**Figure 8: CEACAMs are upregulated in GC patients. (A, B, C)** Boxplots from the GEPIA database display transcripts per million (TPM) levels of *CEACAM1*, *CEACAM5* and *CEACAM6* in normal versus stomach cancer tissues. **(D, E, F)** Representative immunofluorescence images showing CEACAM1 (green), CEACAM5 (green) and CEACAM6 (green) in metastatic vs. control GC samples compared to paired non-cancerous controls (n = 3). Nuclei are counterstained with DAPI (blue). 20× objective is used to capture the images; scale bar = 100 μm. Bar graphs depict relative fold changes in mean fluorescence intensity (MFI) of CEACAMs. Error bars expressed as mean ± SEM. Statistical significance is assessed using Student's t-test: $^{**}P < 0.01$, $^{****}P < 0.0001$. **(G, H, I)** UALCAN-based evaluation of TCGA STAD dataset depicting TPM levels of *CEACAM1*, *CEACAM5* and *CEACAM6* in normal and *H. pylori*-infected/uninfected GC patients.

### 2.2 CEACAM6 is specifically upregulated upon *H. pylori* infection

To confirm whether *H. pylori* influences CEACAM expression, AGS and MKN45 cells were subjected to infection with the *cag* (+) strain-26695. Immunoblotting of whole-cell lysates revealed increased levels of CEACAM1, CEACAM5 and CEACAM6 in AGS cells following infection (Figure 9A). Densitometry analysis identified CEACAM6 as the only protein showing statistically significant increase. Immunofluorescence microscopy data further corroborated the previous finding. The mean fluorescence intensity (MFI) analysis determined that only CEACAM6 was significantly elevated in AGS cells post-infection while CEACAM1 and CEACAM5 showed downregulation albeit statistically non-significant (Figure 9B). The lack of statistical significance and disparity in the results of CEACAM1 and CEACAM5 led

to the selection of CEACAM6 for further analysis.

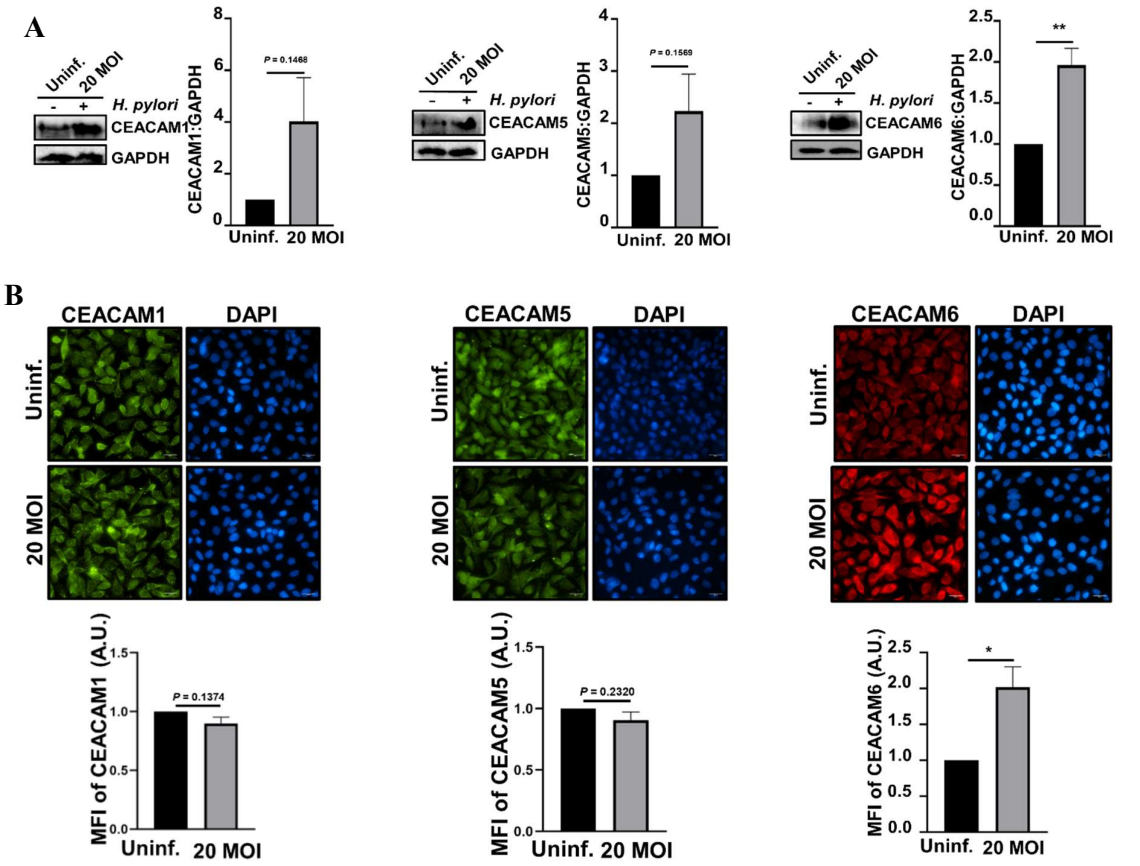


**Figure 9: *H. pylori* infection upregulates CEACAM1, CEACAM5 and CEACAM6 in AGS. (A)** Immunoblots show CEACAM1, CEACAM5 and CEACAM6 protein levels in *H. pylori*-infected AGS cells. GAPDH serves as a loading control. Accompanying bar graphs depict fold changes in CEACAM relative to GAPDH. **(B)** Confocal microscopy panels showing CEACAM1 (green), CEACAM5 (green) and CEACAM6 (red) in *H. pylori*-infected AGS cells. Nuclei are counterstained with DAPI (blue). Objective used= 63×; scale bar = 20 µm. Bar graphs represent changes in CEACAM MFI normalized to uninfected controls, displayed as arbitrary units (A.U.). Data are presented as mean ± SEM. Statistical significance is determined using Student's t-test: $*P < 0.05$, $**P < 0.01$. Uninf., uninfected.

Western blotting was performed to validate the results for CEACAM6 with MKN45 cells.

Densitometry analysis showed significant upregulation of CEACAM6 post-infection (Figure 10). MKN45 cells form multi-layered clusters that poses challenge for immunofluorescence microscopy and further quantitation. Consequently, this cell line was not used for microscopy-based validation.

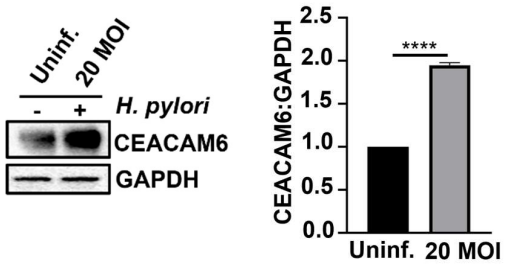


**Figure 10: *H. pylori* infection upregulates CEACAM6 in MKN45 cells.** Western blot analysis showing CEACAM6 protein levels in *H. pylori*-infected MKN45 cells. GAPDH =loading control. Bar graphs quantify the fold changes in CEACAM relative to GAPDH. Quantitative findings are expressed as mean ± SEM, with Student's t-test used to evaluate statistical significance: ****$P < 0.0001$. Uninf., uninfected.

Surface level expression of CEACAM6 in both AGS and MKN45 was then analysed by flow cytometry. *H. pylori* infection significantly elevated the CEACAM6-positive population (Figure 11A) in AGS cells. MFI values also confirmed elevated CEACAM6 levels in infected AGS cells, indicating stronger expression per cell. MKN45 cells which have high basal level of CEACAM6, showed only a modest 2% increase in CEACAM6-positive population after infection (Figure 11B). However, MFI analysis revealed that significant CEACAM6 increase in MKN45 cells occur after *H. pylori* infection.

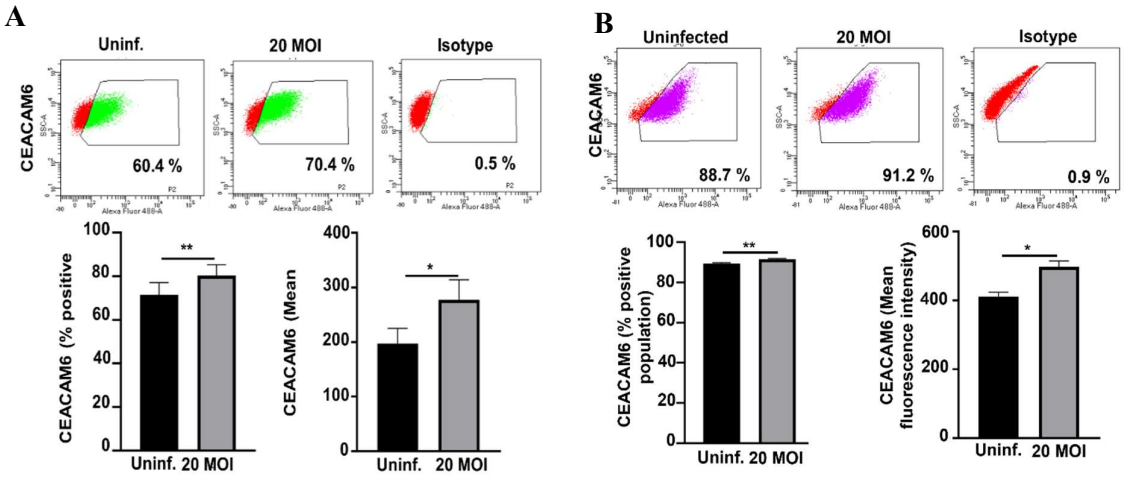


**Figure 11: Surface CEACAM6 is upregulated following *H. pylori* infection in GCCs**. Dot plots from flow cytometry depicting cell-surface levels of CEACAM6 in **(A)** AGS and **(B)** MKN45 cells infected with *H. pylori*. Bar graphs show the percentage of CEACAM6-positive cells and MFI levels of CEACAM6. Data are presented as mean ± SEM. Student's t-test determines the statistical significance.: $*P < 0.05$, $**P < 0.01$. Uninf., uninfected.

## 2.3 Discussion

The findings in the chapter provide compelling evidence that *H. pylori* infection selectively modulates CEACAM family members in GCCs, with CEACAM6 emerging as the most consistently and significantly upregulated molecule. In contrast, CEACAM1 and CEACAM5 displayed variable expression patterns and the lack of statistical significance from replicates led us to focus on CEACAM6 for downstream analyses.

Previous studies have reported strain-specific modulation of these CEACAMs, with *H. pylori* strains such as P12 and G27 showing a trend toward increased CEACAM expression, but without statistical significance (185). These observations suggest that while multiple CEACAM family members can be influenced by bacterial infection, the magnitude and consistency of modulation differ substantially.

The biological relevance of CEACAM6 in GC has been increasingly recognized in recent

literature (186). Elevated CEACAM6 expression has been linked to enhanced tumor aggressiveness, EMT and metastatic potential. These features distinguish CEACAM6 from CEACAM1 and CEACAM5, which, although upregulated in some GC contexts, do not consistently demonstrate the same breadth of functional impact. CEACAM1, for instance, may function as either a tumor suppressor or promoter, contingent on isoform balance and cellular context (187). Its dual nature complicates interpretation and CEACAM1 did not show consistent upregulation following *H. pylori* infection as revealed by this study. CEACAM5, while recognized as a classical tumor marker (CEA) in gastrointestinal malignancies, is often elevated in a broad range of cancers but lacks specificity to *H. pylori*-mediated modulation as established by this study. In contrast, CEACAM6 not only shows strong induction in response to infection but also aligns with the functional pathways directly relevant to GC progression, including the PI3K/Akt signaling, cytoskeletal remodeling and invasive behavior (188,189).

Taken together, these findings underscore the unique position of CEACAM6 in *H. pylori*-mediated GC. In the following chapter, this work is extended by assessing the tumorigenic potential of *CEACAM6*-expressing cells, thereby providing further insight into its mechanistic contribution to GC pathogenesis.

# Chapter 3

# CEACAM6 promotes tumorigenic potential in GCCs

### 3.1 CEACAM6-expression supports pro-tumorigenic responses in GCCs

CEACAM6, is frequently overexpressed in gastrointestinal malignancies and has been linked to tumor aggressiveness (186). Its role in modulating cell adhesion, invasion and apoptotic resistance suggests that CEACAM6 may act as a critical mediator of oncogenic signaling within the gastric TME. Despite these associations, its contribution to *H. pylori*-driven GC progression remains insufficiently defined. To investigate the functional impact of CEACAM6, AGS cells

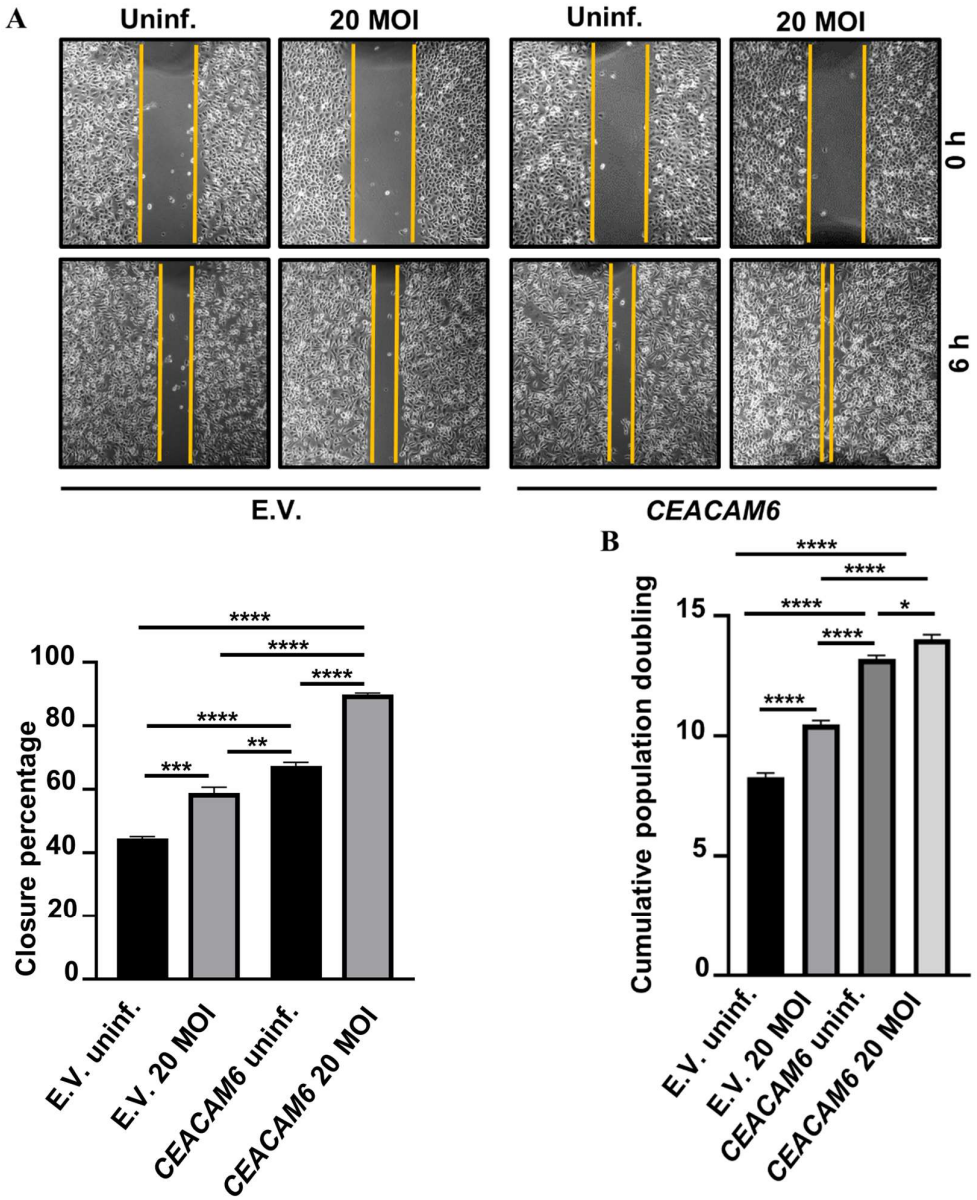

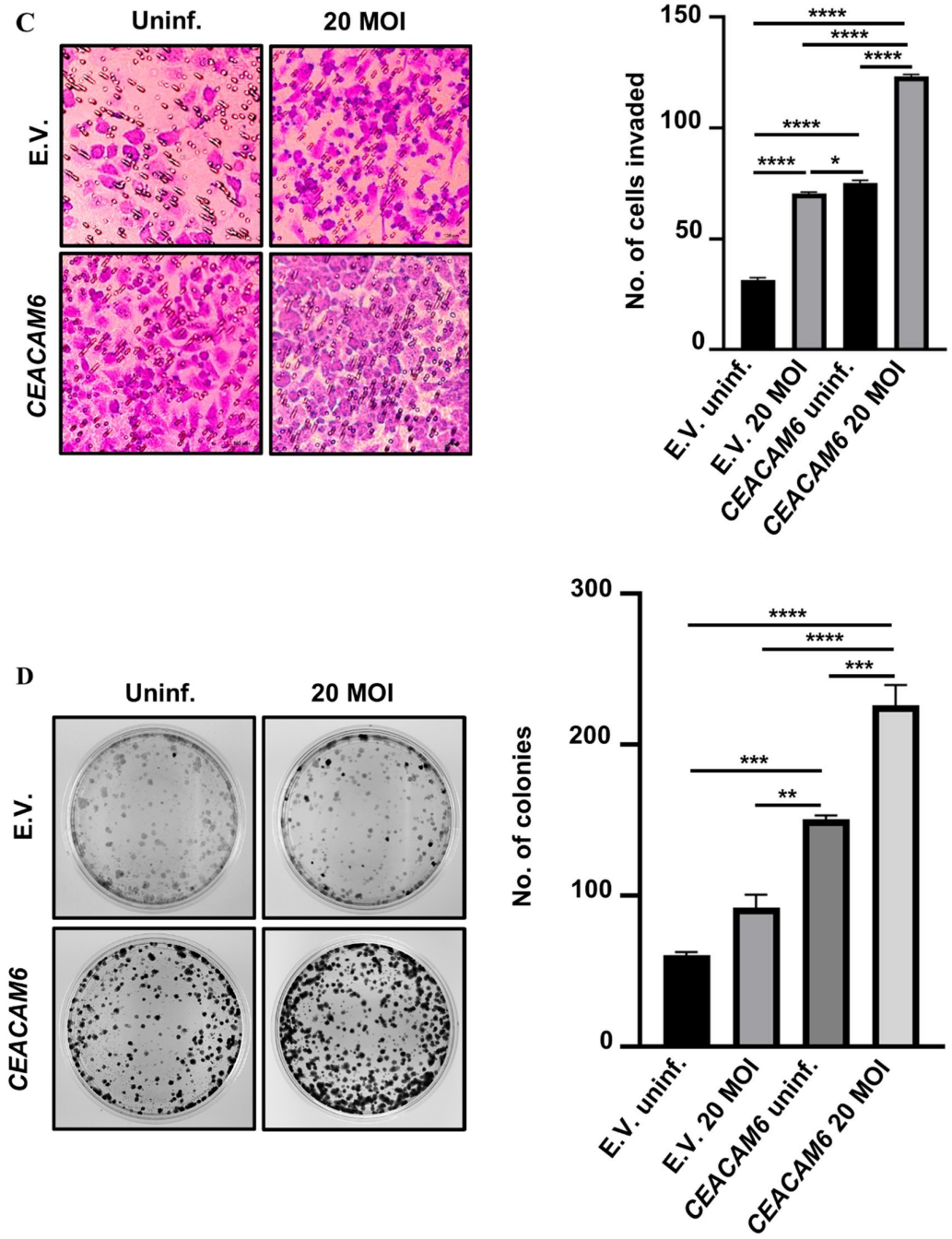


**Figure 12: CEACAM6 enhances aggressive phenotype in GCCs. (A)** Brightfield images illustrate wound closure in AGS cells stably transfected with either E.V. or CEACAM6, in the presence or the absence of *H. pylori* infection for 6 h. Objective =10× ; scale bar = 100 µm. The corresponding graph represents the wound closure. (**B**) Graph depicts cumulative population doubling in E.V. or *CEACAM6*-expressing cells. (**C**) Representative michrographs

show invasion of AGS cells expressing the empty vector or CEACAM6, with or without *H. pylori* infection. Objective =10×; scale bar = 100 μm (**D**) Representative clonogenic assay photographs demonstrating the colony-forming capacity of E.V. or *CEACAM6*-expressing AGS cells in presence or absence *H. pylori*. The graph quantifies the number of colonies formed. All the error bars represent mean ± SEM (n = 3). Two-way ANOVA followed by Tukey's post-hoc test determines the statistical significance. *$P < 0.05$, **$P < 0.01$, ***$P < 0.001$, ****$P < 0.0001$. E.V., empty vector; Uninf., uninfected.

were stably transfected with the empty vector or *CEACAM6*-expressing plasmid. Several assays were performed to measure the tumorigenesis in these cells. In wound-healing assay, CEACAM6-overexpressing cells displayed significantly greater migration ability compared with the empty vector cells. Infection with *H. pylori* further augmented the effect, showing the highest closure ability across all the conditions. (Figure 12A). In population doubling assay, *CEACAM6*-overexpressing cells infected with *H. pylori* displayed significantly higher proliferation than all other groups (Figure 12B). Invasive potential of cells was assessed through a matrigel-based Transwell invasion assay. *CEACAM6*-overexpressing cells exhibited significantly higher invasion toward a chemoattractant (RPMI 1640 supplemented with 20% FBS) with *H. pylori* infection further amplifying this effect, exhibiting the highest invasiveness across all experimental groups (Figure 12C). Colony formation capacity was significantly elevated in CEACAM6 stably expressing cells, as revealed by clonogenic assay, compared with the empty vector-expressing cells. *H. pylori* infection further promoted colony-forming ability in *CEACAM6*-expressing cells (Figure 12D).

### 3.2 Supernatants released from *CEACAM6*-expressing cells can promote tumorigenesis in recipient cells

Within the TME, malignant cells exert influence on neighboring populations either via the direct cell–cell interactions or through the secretion of soluble factors. Evidence indicates that

such communication can drive the conversion of adjacent non-malignant cells into a transformed phenotype (190). To evaluate the paracrine effects of *CEACAM6*-overexpressing GCCs, supernatants from the empty vector or CEACAM6-transfected cells, with or without *H. pylori* infection were collected and applied to recipient AGS cells. In wound-healing assay, AGS cells treated with supernatants from *CEACAM6*-expressing cells exhibited enhanced migration compared with those exposed to supernatants from the empty vector cells (Figure 13A). Cells treated with the supernatants from *H. pylori*-infected *CEACAM6*-overexpressing cells exhibited the most significant response. Transwell invasion assay demonstrated that infection enhanced the invasive potential of the empty vector cells relative to uninfected controls. AGS cells treated with supernatants from infected *CEACAM6*-expressing cells exhibited the greatest degree of invasion across all conditions (Figure 13B). The impact of the supernatants on AGS cell growth dynamics was assessed by clonogenic assay. AGS cells exposed to supernatants from

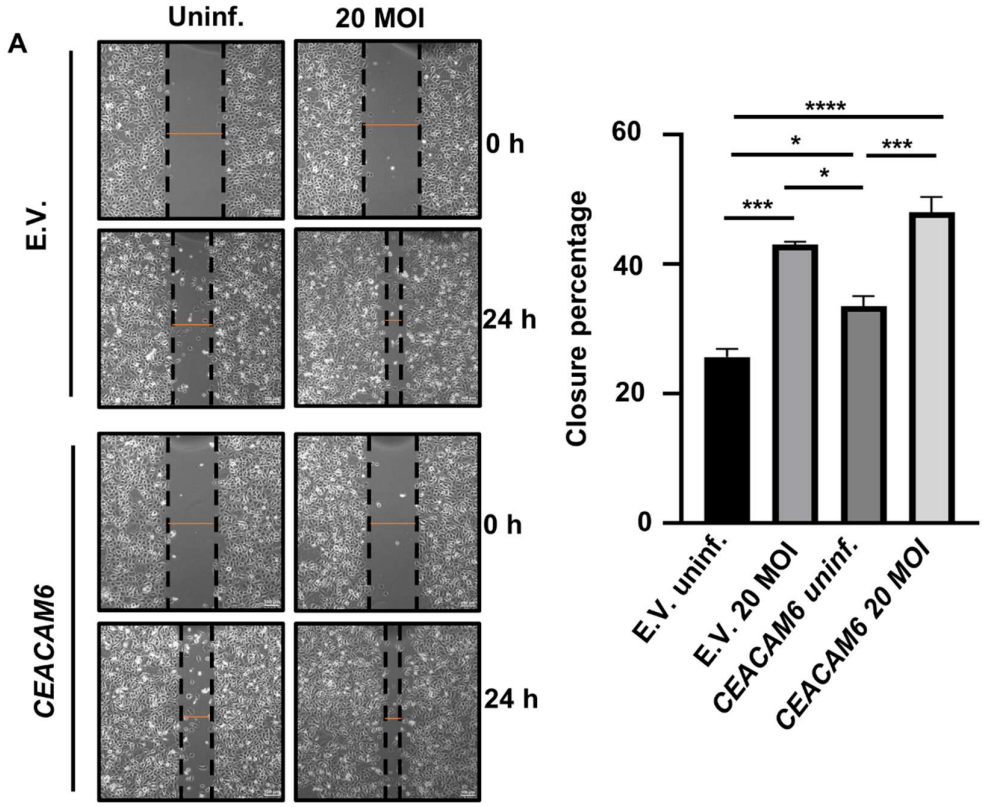

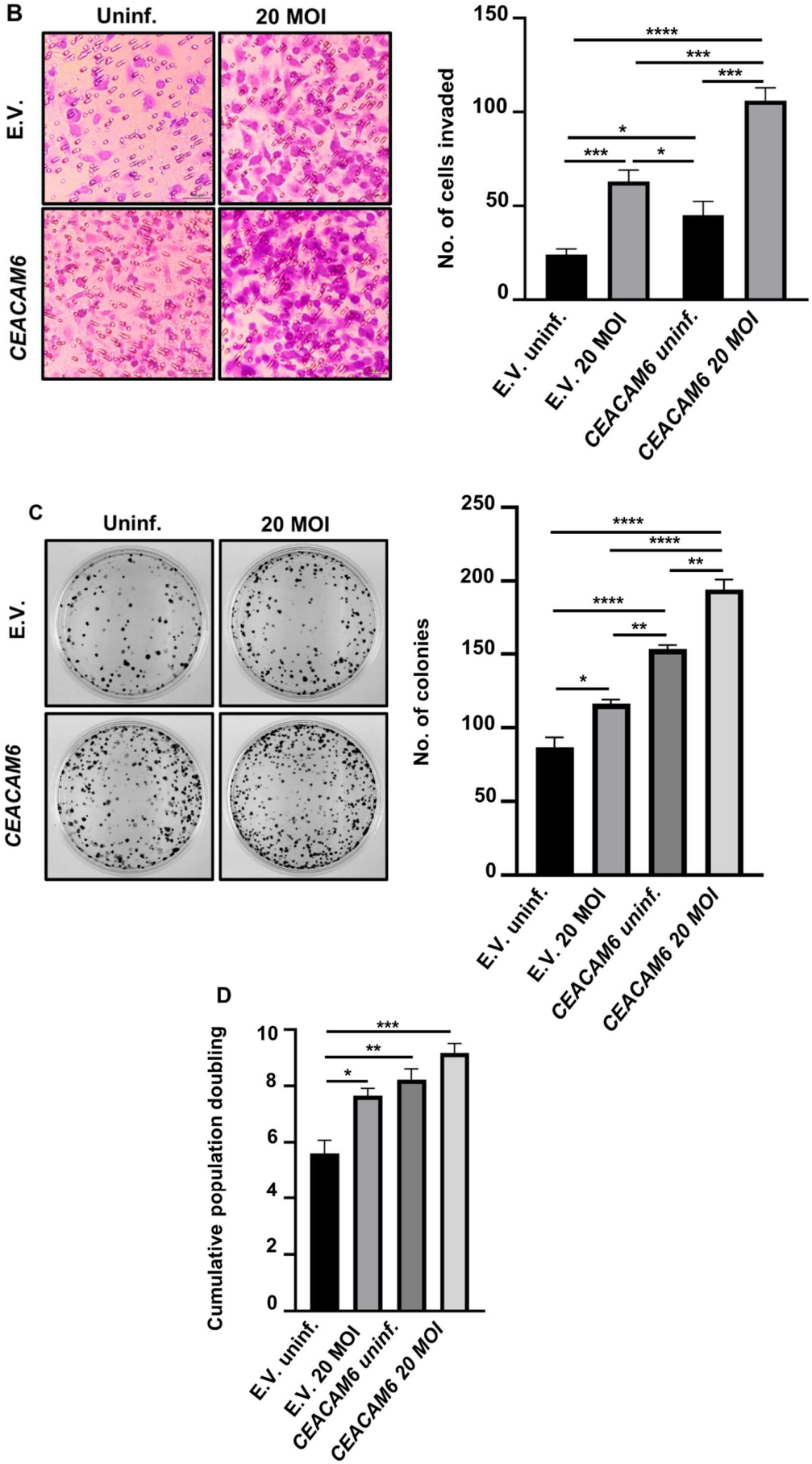
B
Uninf.
20 MOI
E.V.
CEACAM6
No. of cells invaded
150
100
50
0
****
***
***
*
***
*
E.V. uninf.
E.V. 20 MOI
CEACAM6 uninf.
CEACAM6 20 MOI
C
Uninf.
20 MOI
E.V.
CEACAM6
No. of colonies
250
200
150
100
50
0
****
****
**
****
**
*
E.V. uninf.
E.V. 20 MOI
CEACAM6 uninf.
CEACAM6 20 MOI
D
Cumulative population doubling
10
8
6
4
2
0
***
**
*
E.V. uninf.
E.V. 20 MOI
CEACAM6 uninf.
CEACAM6 20 MOI

**Figure 13: Supernatants from *CEACAM6*-overexpressing cells promote aggressive phenotypes in GCCs. (A)** Brightfield images show wound closure in AGS cells treated with supernatants from *H. pylori* infected/uninfected, E.V. or CEACAM6-transfected cells. Images are taken using a 10× objective; scale bar = 100 μm. The graph quantifies the wound closure percentage. **(B)** Matrigel invasion assay demonstrating the invasive potential of AGS cells exposed to supernatants from E.V. or CEACAM6-transfected cells. Images captured using a 20× objective; scale bar = 100 μm. The graph shows the number of invaded cells. **(C)** Clonogenic assay images depicting colony formation in AGS cells treated with supernatants from E.V. or CEACAM6-transfected cells, with or without *H. pylori* infection. The graph quantifies the colonies formed. **(D)** Cumulative population doubling of AGS cells following treatment with supernatants from E.V. or CEACAM6-transfected cells, with or without *H. pylori* infection. Statistical analysis is performed using two-way ANOVA followed by Tukey's post-hoc test. Error bars represent mean ± SEM (n = 3). $*P < 0.05$, $**P < 0.01$, $***P < 0.001$, $****P < 0.0001$. E.V., empty vector; Uninf., uninfected.

infected *CEACAM6*-expressing cells produced a markedly higher number of colonies, indicative of diminished contact inhibition (Figure 13C). Likewise, the proliferative capacity of AGS cells was assessed by population doubling assays, which showed a significant rise when cells were treated with supernatants from infected *CEACAM6*-expressing cells (Figure 13D).

### 3.3 Discussion

This study provides strong evidences that CEACAM6 is a key contributor in aggressiveness of GCCs, both in a cell-autonomous and paracrine manner. Here, it was demonstrated that CEACAM6 not only promotes proliferation, migration, invasion and clonogenicity of AGS cells but also amplifies these effects in the presence of *H. pylori* infection.

Many molecular agents may contribute to the enhance cell motility and invasiveness in

*CEACAM6*-expressing cells. In GC, CEACAM6 is negatively correlated with E-cadherin expression (188) and induces upregulation of N-cadherin, Vimentin and Slug GCCs. It was also reported that elevated MMP-9 contributed to invasiveness and migratory ability of the *CEACAM6*-expressing cells. It is also known that CEACAM6 drives EMT via the PI3K/Akt pathway (188). Data revealed that CEACAM6 expression was able to enhance the long term cell survival ability of the expressing cells. The mechanism behind this phenomenon could be ascribed to the inhibition of anoikis, a programmed cell death activated due to loss of attachment for cells to matrix. Studies have shown that overexpression of CEACAM6 induces anoikis resistance, allowing cells to survive and grow in distant sites (94). The same study also reported that the anoikis resistance was dependent on the Src-FAK pathway. Notably, *H. pylori* infection is known to activate similar PI3K/Akt and Src–FAK pathways, thereby amplifying the oncogenic effects of CEACAM6 activation. This convergence suggests that infection synergistically strengthens CEACAM6-mediated EMT magnifying tumor progression and metastatic potential in GC.

Importantly, the chapter investigates the paracrine influence of *CEACAM6*-overexpressing cells on the neighboring, less aggressive GCCs. Supernatants from *CEACAM6*-overexpressing AGS cells induced a transformation-like response in recipient cells, consistent with reports that tumor secretomes alone can trigger the EMT and long-term phenotypic reprogramming in the non-malignant epithelia. For example, conditioned medium from the malignant breast cancer cells induced an EMT-like phenotype and altered N-glycan profiles in MCF10A cells (112) Similarly, exposure to human cancer serum has been shown to transfer malignant traits to immortalized human cells (191). In another instance, conditioned medium from the primary lung cancer cells triggered EMT in A549 cells through cooperation between TGF-β1 and miR-21 (192). These studies provide direct precedent for the observation that supernatants from *CEACAM6*-expressing cells can convert recipient AGS cells towards a more aggressive state.

Together, the results position CEACAM6 as a key effector in the *H. pylori*-associated GC progression. Its dual role in promoting intrinsic tumor cell aggressiveness and modulating the TME through secreted factors, demonstrate its applicability as a potential biomarker and therapeutic target. Given this dual role, the next chapter focuses on how CEACAM6 expression in GCCs influences innate immune cells, specifically macrophage polarization.

# Chapter 4

# *CEACAM6*-expressing GCCs alter macrophage polarization

### 4.1. Metastatic GC exhibit M2 infiltration of macrophages

Macrophages are highly plastic immune cells that adapt their functional states according to microenvironmental signals. The M1 phenotype, classically activated, is defined by the pro-inflammatory and cytotoxic functions that aid in pathogen elimination and anti-tumor defense (193). In contrast, M2 macrophages are considered pro-tumorigenic due to their active participation in EMT, tissue remodelling and angiogenesis (193). Biopsy specimens and matched controls from GC patients were collected to assess macrophage polarization status. These were stained to detect macrophages in two groups. One group was stained for CD68 (pan-macrophage marker) and iNOS (M1 marker) markers to assess M1 macrophage infiltration. The immunofluorescence microscopy indicated though the GC samples exhibited high macrophage infiltration compared to control samples as denoted by CD68 staining, those were not M1 macrophages (Figure 14A). Another group of GC sample was stained for CD68 and ARG1 (M2 marker) markers to assess M2 macrophage infiltration. Here, high M2 infiltration was observed in the GC samples compared to normal samples (Figure 14B). The results confirmed that in GC, infiltration of M2 macrophages occur.

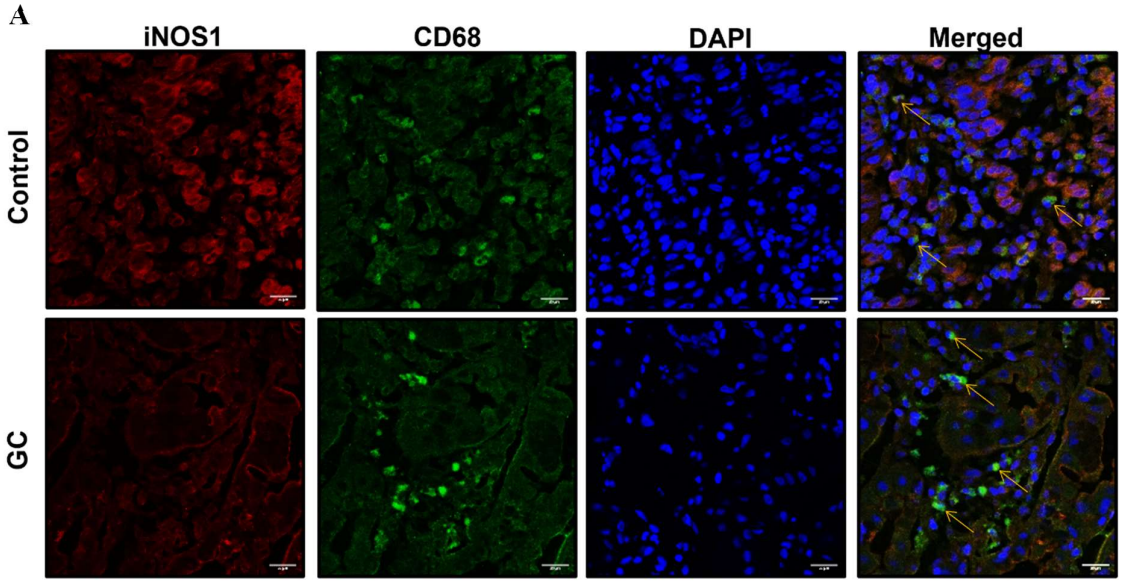

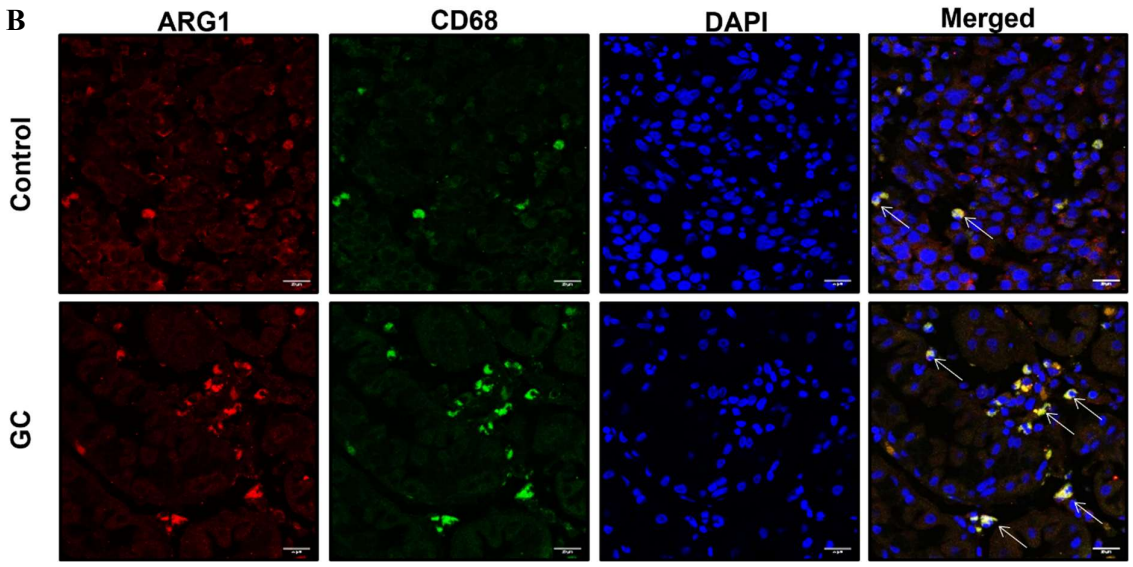


**Figure 14: M2 polarized macrophages infiltrate GC tumor.** (**A**) Confocal micrographs display CD68-positive cells (green) co-stained with either iNOS (red) or (**B**) Arginase1 (ARG1) (red) in biopsy samples from GC patients. DAPI (blue) stains the nuclei. Objective used = 63×; scale bar is 20 μm.

### 4.2. *CEACAM6*-expressing GCCs promote M2 polariation of macrophages

Previous chapters established that epithelial CEACAM6 promotes tumorigenesis. Therefore, it was important to identify whether epithelial CEACAM6 was responsible for influencing the macrophage polarization. To assess the functional impact of CEACAM6 on macrophage polarization, *in vitro* assays were performed. PBMC-derived macrophages were cocultured with *H. pylori*-infected/uninfected, the empty vector or *CEACAM6*-expressing cells. After infection, macrophages were collected and stained to assess the polarization status by flow cytometry. M1 population was identified using CD40, CD64 and CD68 markers, whereas M2 population was identified using CD68 and CD206 markers. Flow cytometry identified that coculture with the empty vector cells or CEACAM6 stably-transfected cells did not alter the $CD68^{+}CD40^{+}CD64^{+}$ macrophage population, independent of *H. pylori* exposure (Figure 15A). However, coculture with *CEACAM6*-expressing cells resulted in an increased proportion of M2 macrophages ($CD68^{+}CD206^{+}$) compared to coculture with the empty vector cells,

irrespective of infection status (Figure 15A). Moreover, M2 ($CD68^{+}CD206^{+}$) macrophage population were significantly higher when cocultured with infected *CEACAM6*-expressing cells relative to uninfected *CEACAM6*-expressing cells (Figure 15B). To further substantiate the findings, macrophages following coculture were stained for iNOS1 or ARG1 (Figure 16A). Macrophages cocultured with infected *CEACAM6*-expressing cells exhibited significantly higher ARG1 staining compared to that of all other experimental setups (Figure 16B). The presence of high iNOS staining in macrophages cocultured with the infected-empty vector or *CEACAM6*-expressing cells could indicate the LPS mediated upregulation due to *H. pylori* (Figure 16B). The results confirmed that epithelial CEACAM6 promoted M2 polarization of macrophages, with *H. pylori* infection further potentiating the effect.

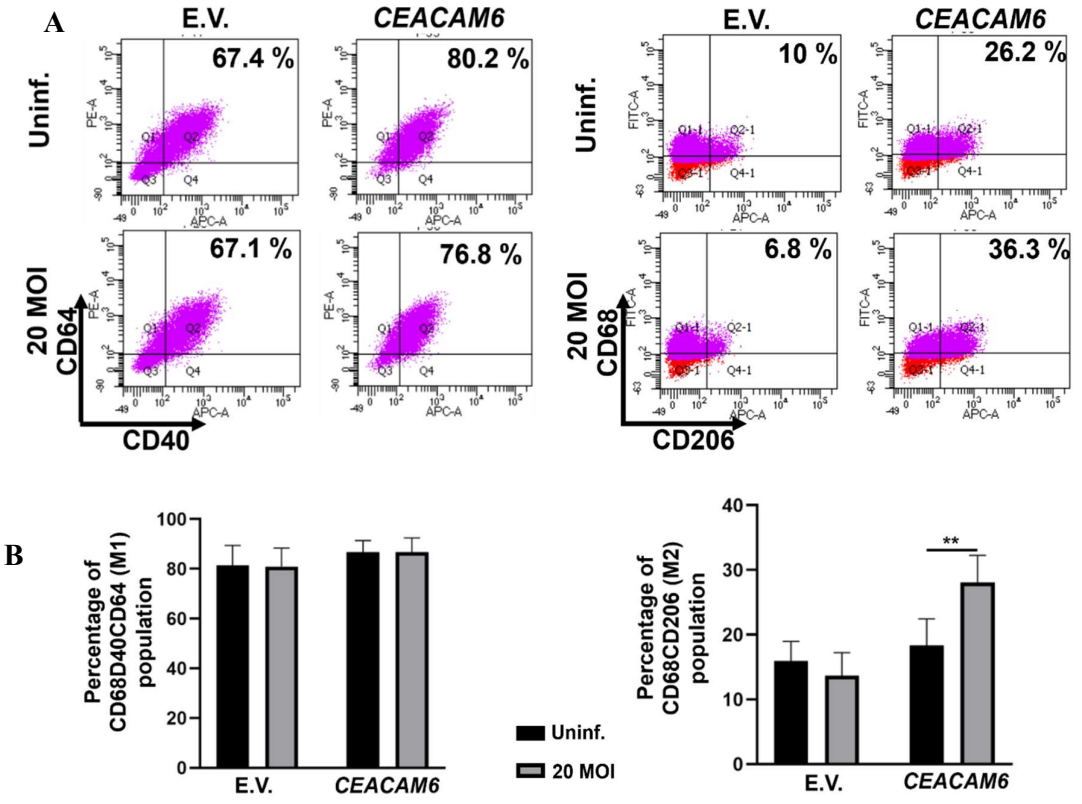

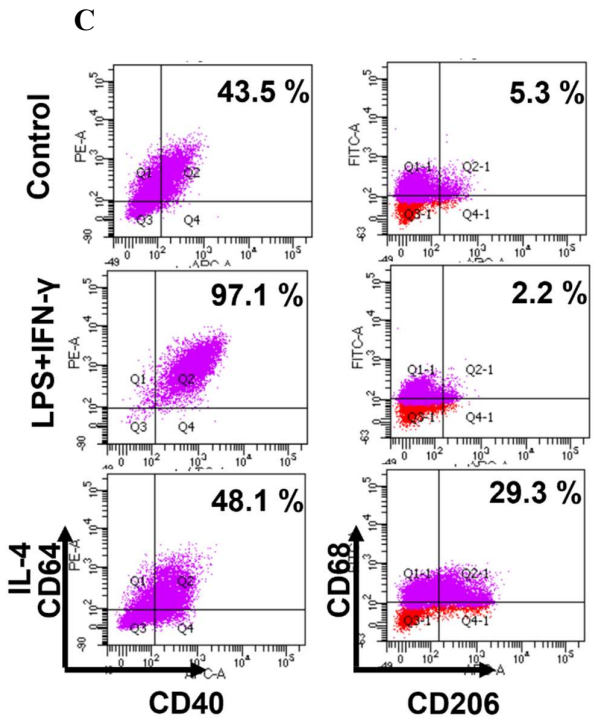


**Figure 15: Epithelial-CEACAM6 promotes M2 polarization of macrophages.** (**A**) Dot plots illustrate the distribution of $CD68^{+}CD40^{+}CDC64^{+}$ (M1) and $CD68^{+}CD206^{+}$ (M2) macrophage populations following coculture with E.V. or *CEACAM6*-overexpressing AGS cells with or without *H. pylori* infection. (**B**) Bar graphs quantify changes in M1 and M2 population. Student's t-test evaluates the statistical significance. $^{**}P < 0.01$. (**C**) Macrophages treated with LPS (100 ng/ml) and IFN-γ (20 ng/ml) or IL-4 (40 ng/ml) served as positive controls for M1 and M2 polarization, respectively. E.V.,

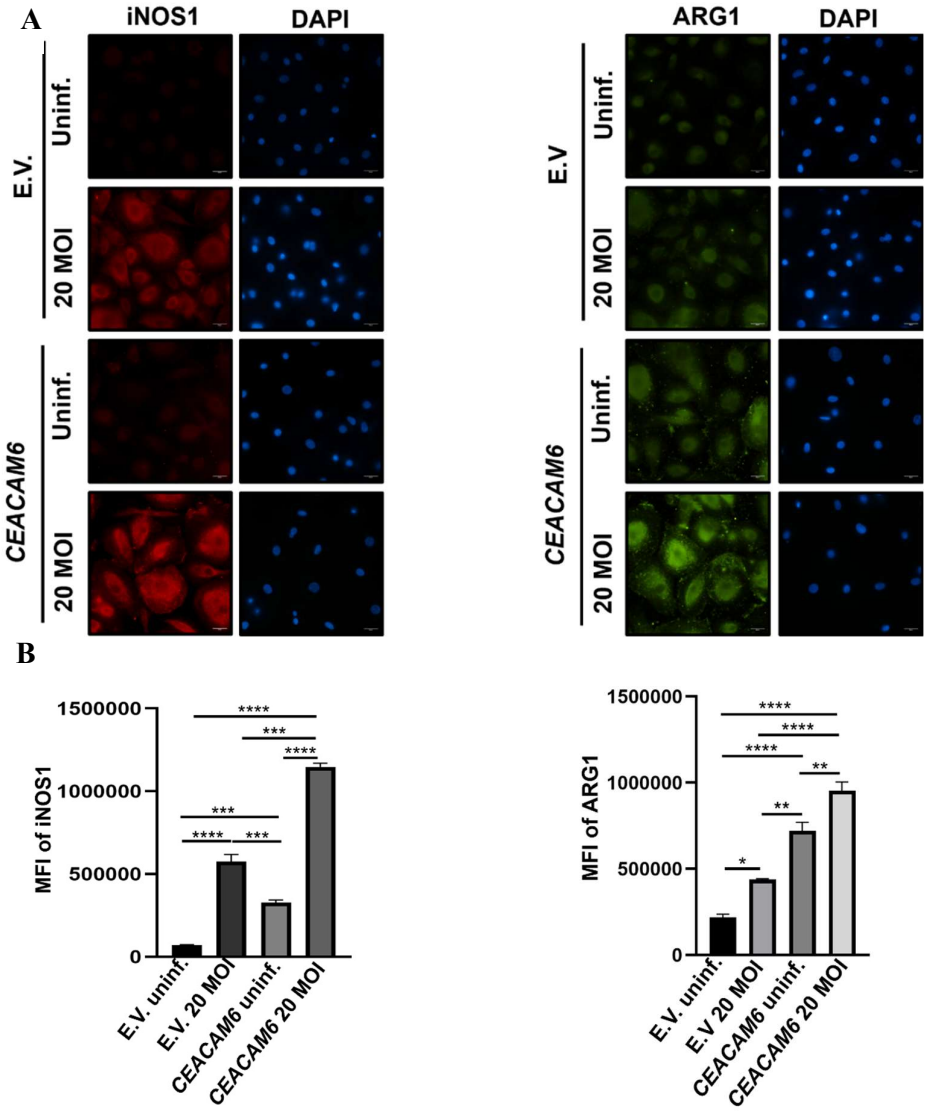
A
iNOS1
DAPI
ARG1
DAPI
E.V.
Uninf.
20 MOI
CEACAM6
Uninf.
20 MOI
E.V
Uninf.
20 MOI
CEACAM6
Uninf.
20 MOI
B
MFI of iNOS1
1500000
1000000
500000
0
E.V. uninf.
E.V. 20 MOI
CEACAM6 uninf.
CEACAM6 20 MOI
MFI of ARG1
1500000
1000000
500000
0
E.V. uninf.
E.V 20 MOI
CEACAM6 uninf.
CEACAM6 20 MOI
C
iNOS1
DAPI
ARG1
DAPI
Control
LPS+IFN-γ
IL-4
Control
LPS+IFN-γ
IL-4

**Figure 16: Immunofluorescence analysis of macrophage polarization in response to *CEACAM6*-expressing GCCs.** (**A**) Representative immunofluorescence images depict iNOS (red) and ARG1 (green) in macrophages cocultured with the empty vector or *CEACAM6*-expressing cells. DAPI (blue) is the nuclear stain. Images are taken using a 60× objective lens and scale bars correspond to 20 μm. (**B**) Bar graphs represent the MFI of iNOS and ARG1. (**C**) Macrophages stimulated with LPS (100 ng/ml) and IFN-γ (20 ng/ml) or with IL-4 (40 ng/ml) served as M1 and M2 positive controls, respectively. Error bars represent mean ± SEM (n = 3). Two-way ANOVA followed by Tukey's post-hoc test evaluate the statistical significance: $*P < 0.05$, $**P < 0.01$, $***P < 0.001$, $****P < 0.0001$. E.V., empty vector; Uninf., uninfected.

### 4.3 *CEACAM6*-expressing GCCs release cytokines that promote M2 polarization of macrophages

Macrophage polarization is strongly influenced by soluble mediators secreted from tumor cells and their microenvironment. It was critical to determine whether CEACAM6 expression and subsequent *H. pylori* infection altered the cytokine repertoire released by GCCs. Such changes may alter the balance between M1 macrophages driving inflammation and M2 macrophages facilitating tumor progression, thereby shaping the TME. For this, supernatants were collected from the empty vector or *CEACAM6*-expressing cells with or without infection. The supernatants were then analysed using inflammation antibody array kit (Figure 17A). *CEACAM6*-expressing cells infected with *H. pylori* exhibited the highest secretion levels of IL-8, soluble TNFR1 and RANTES (Figure 17B) compared to all other groups. These cytokines support M2 polarization of macrophages directly or indirectly. Moreover, infected *CEACAM6*-expressing cells displayed the lowest levels of IL-16 (Figure 17B), a cytokine associated with promoting M1 macrophage polarization.

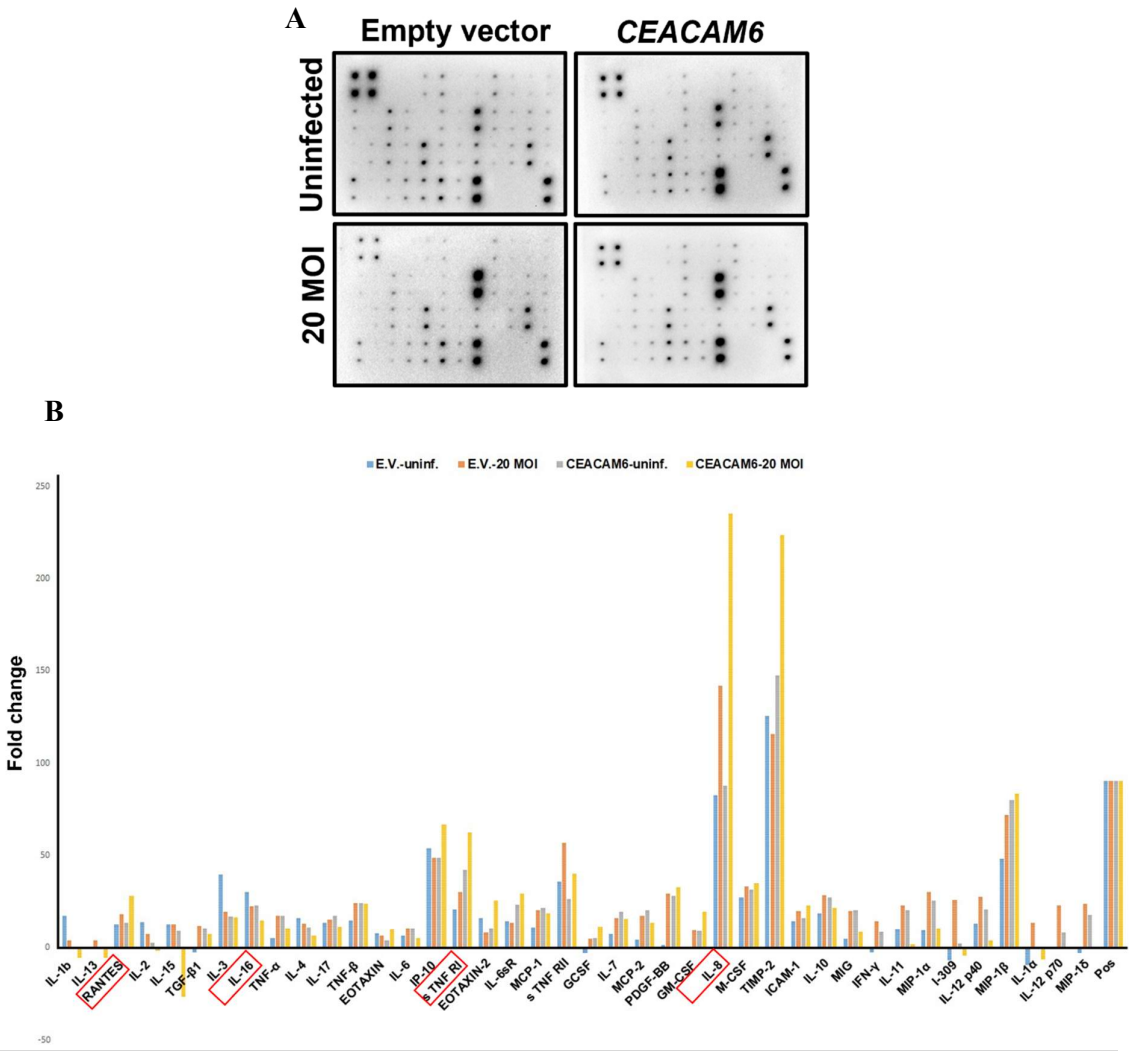


**Figure 17**: **Supernatants from *CEACAM6*-expressing cells skew macrophage polarization toward M2 phenotype.** (**A**) Representative immunoblot images illustrate cytokine profiles detected in the respective culture supernatants. The blots were generated using the human inflammation antibody array kit (Abcam), enabling simultaneous detection of multiple inflammatory mediators. (**B**) Quantitative analysis is presented as column graphs, comparing cytokine levels in supernatants collected from the empty vector controls and *CEACAM6* stably-transfected cells, with/without *H. pylori* infection. Cytokines marked in the dataset are linked to macrophage polarization in the current context.

### 4.4. Discussion

Macrophages are central regulators of the TME and their polarization into distinct functional phenotypes critically influences tumor progression. The findings from this chapter demonstrate that GC tissues exhibit high infiltration of M2 macrophages with the negligible presence of M1 macrophages. This is in agreement with earlier studies where advanced GC is characterized by a predominance of tumor-supportive macrophages (194).

Importantly, it was observed that *CEACAM6*-expressing cells promote M2 polarization of macrophages. *In vitro* coculture assays revealed that macrophages exposed to *CEACAM6*-expressing AGS cells displayed a significantly higher M2 population compared to those cocultured with the empty vector cells. This effect was further amplified when *CEACAM6*-expressing cells were infected with *H. pylori*, suggesting a synergistic role. Fluorescence microscopy confirmed elevated ARG1 staining in macrophages cocultured with infected *CEACAM6*-expressing cells, reinforcing their M2 identity.

The cytokine profiling of supernatants provided mechanistic insight into this phenomenon. M2 macrophages have been shown to facilitate EMT and metastasis in GC through secretion of matrix metalloproteinases and pro-angiogenic factors. IL-8 has been implicated in recruiting macrophages and promoting their polarization toward M2 (195-197), while RANTES enhances immunosuppressive macrophage functions and correlates with poor prognosis in gastrointestinal cancers (198,199). The role of soluble TNFR1 in dampening TNF-α–mediated inflammation has also been reported, highlighting its contributions to immune evasion (200,201). Conversely, reduced secretion of IL-16, a cytokine linked to M1 activation, was observed, thereby diminishing signals that favor antitumor macrophage responses (202). Collectively, these reports along with the results from the current study support the idea that CEACAM6 expression, particularly under *H. pylori* infection, creates a cytokine milieu that favors M2 macrophage dominance.

# Chapter 5

# GC aggressiveness is amplified by *H. pylori* infection-derived EVs containing CEACAM6

### 5.1. AGS cell–derived EVs contain CEACAM6

Previous results have established how supernatants released from *CEACAM6*-expressing cells promote tumorigenesis in the recipient naïve cells. Since EVs are amongst the main secretory factors released by cancer cells (203), it was essential to identify whether EVs released from GCCs could carry CEACAM6 or not. EVs were isolated from *H. pylori*-infected (10 or 20 MOI for 36 h) or uninfected AGS cells and characterized according to the criteria outlined in MISEV 2024 (204). The dynamic light scattering (DLS) determined the EV mean diameters as 177.1 nm (uninfected), 181.1 nm (10 MOI) and 211.2 nm (20 MOI). (Figure 18A). Particle size distribution was quantitatively assessed using the nanoparticle tracking analysis (NTA), with mode values of 142 nm in uninfected samples, 173 nm in 10 MOI-infected samples and 163 nm in 20 MOI-infected samples (Figure 18B). The morphology of EVs was visualized by transmission electron microscopy (TEM) which revealed their typical spherical shape with the size ranging between 100-200 nm. (Figure 18C). Western blotting was carried out to verify the integrity and purity of EV preparations using established EV markers. GM130, a Golgi matrix protein, served as a negative marker, while Alix and HSPA8 were used as positive EV markers, confirming the integrity of the sample preparations (Figure 18D). Importantly, western blotting also revealed the presence of CEACAM6 within the EVs. Notably, although cell lysates from infected cells showed gradual significant increase in CEACAM6 with increasing MOI as compared to the uninfected cells, only the EVs released by AGS cells infected with 20 MOI displayed significantly higher CEACAM6 (Figure 17E).

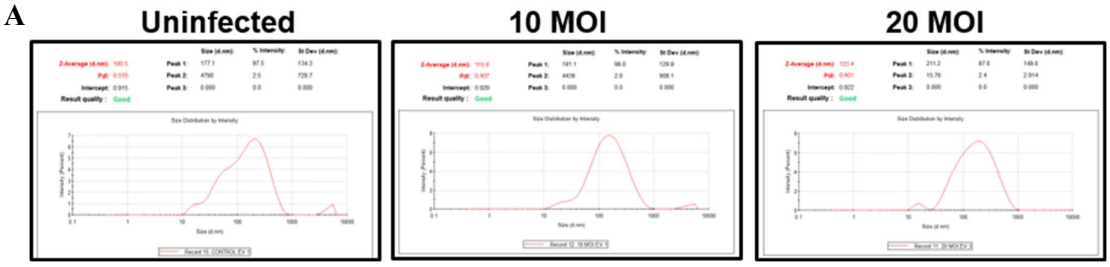

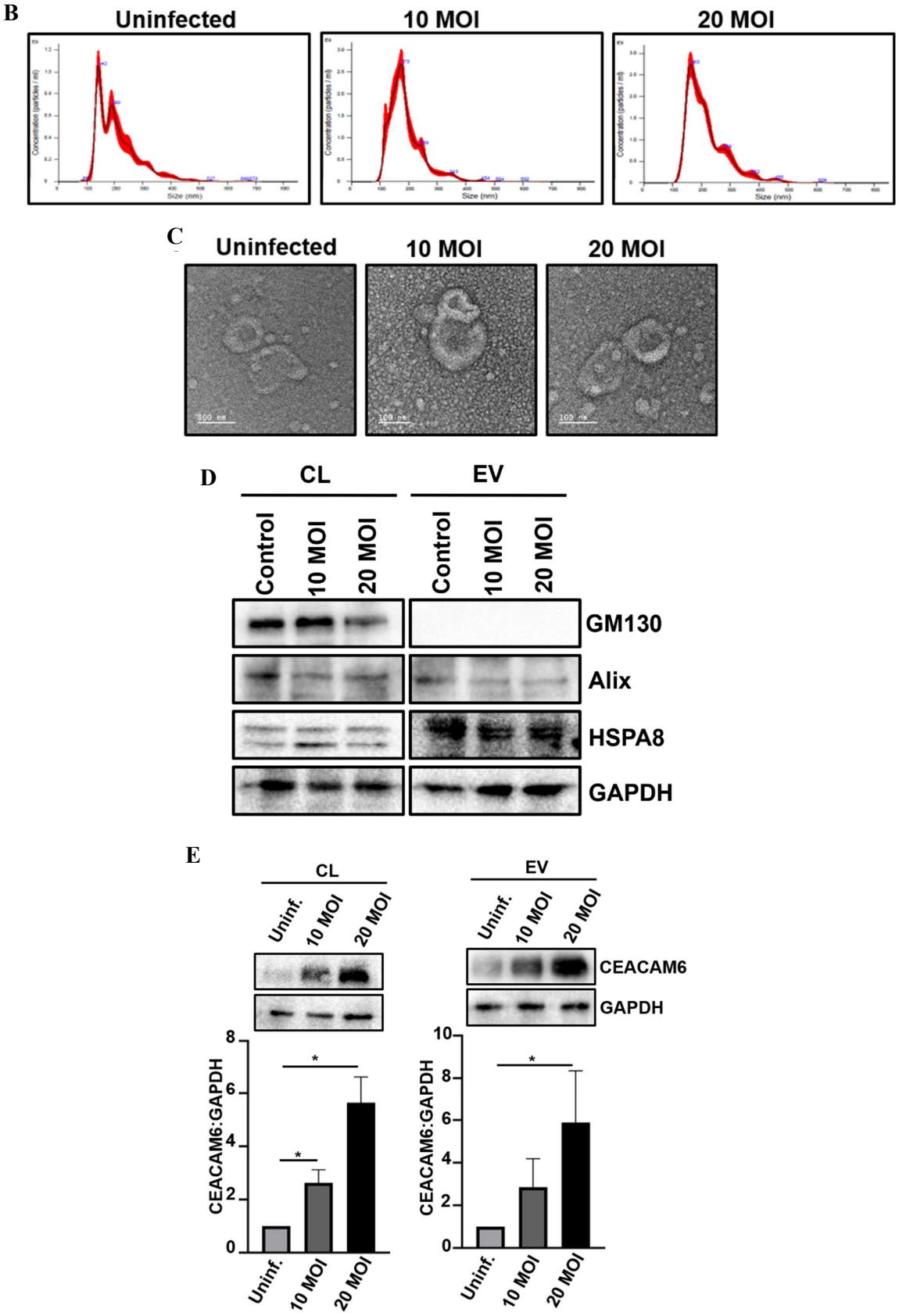
B
Uninfected
10 MOI
20 MOI
C
Uninfected
10 MOI
20 MOI
D
CL
EV
Control
10 MOI
20 MOI
Control
10 MOI
20 MOI
GM130
Alix
HSPA8
GAPDH
E
CL
EV
Uninf.
10 MOI
20 MOI
Uninf.
10 MOI
20 MOI
CEACAM6
GAPDH
CEACAM6:GAPDH
CEACAM6:GAPDH
Uninf.
10 MOI
20 MOI
Uninf.
10 MOI
20 MOI

**Figure 18: EVs from GCCs contain CEACAM6.** (**A**) DLS analysis demonstrating the size distribution profile of EVs isolated from AGS cells infected with *H. pylori* at MOI of 10 and 20. (**B**) NTA providing quantitative assessment of EV concentration and particle size distribution. (**C**) TEM images illustrating the ultrastructural morphology of EVs. Scale bar = 100 nm (D) Immunoblots show EV purity with GM130 serving as a negative control and Alix/HSPA8 as positive EV markers. (**E**) Immunoblots showing CEACAM6 protein levels in both cell lysates (CL) and EV preparations from. Bar graphs quantify the fold changes in CEACAM6. Data presented as mean ± SEM (n = 3). One-way ANOVA and subsequent Tukey's post hoc test determines statistical significance. **P* < 0.05. Uninf., Uninfected.

### 5.2. EVs secreted by *CEACAM6*-expressing cells are CEACAM6-enriched

CEACAM6 contributes to the tumorigenesis when expressed in cancer cells. Hence, when loaded in EVs, CEACAM6 may act as a transferable oncogenic factor, enhancing tumor-supportive communication across the tumor-niche. To explore its oncogenic functions, *CEACAM6* or the empty vector was ectopically expressed in AGS cells followed by *H. pylori*-infection or no infection. Thereafter, EVs were collected and systematically characterized. DLS measurements showed that EVs from the empty vector cells averaged 161.8 nm (uninfected) and 192.5 nm (infected), exceeding the sizes of EVs from the *CEACAM6*-expressing cells, which were 145.9 nm and 172 nm, respectively (Figure 19A). NTA confirmed that EVs from the empty vector cells (103 nm uninfected; 109.1 nm infected) exhibited larger modal sizes than those from the *CEACAM6*-expressing cells (96.3 nm uninfected; 100.4 nm infected) (Figure 19B). TEM revealed spherical morphology and confirmed reduction in the size of EVs from the *CEACAM6*-expressing cells in comparison to the empty vector-expressing cells (Figure 19C), supporting the DLS and NTA observations. Western blot analysis validated EV purity, showing enrichment of Alix and HSPA8 and absence of GM130. (Figure 19D).

Studies have revealed that vesicle biogenesis involves preferential inclusion or exclusion of distinct proteins, underscoring the regulated nature of EV composition (205,206). Therefore, western blotting was performed to determine whether CEACAM6-enrichment in EVs mirrored its level in the originating cells. Cell lysates from *H. pylori* infected/uninfected *CEACAM6*-expressing cells showed significantly higher CEACAM6 levels relative to the empty vector conditions (Figure 19E). EVs from *CEACAM6*-expressing infected cells showed elevated

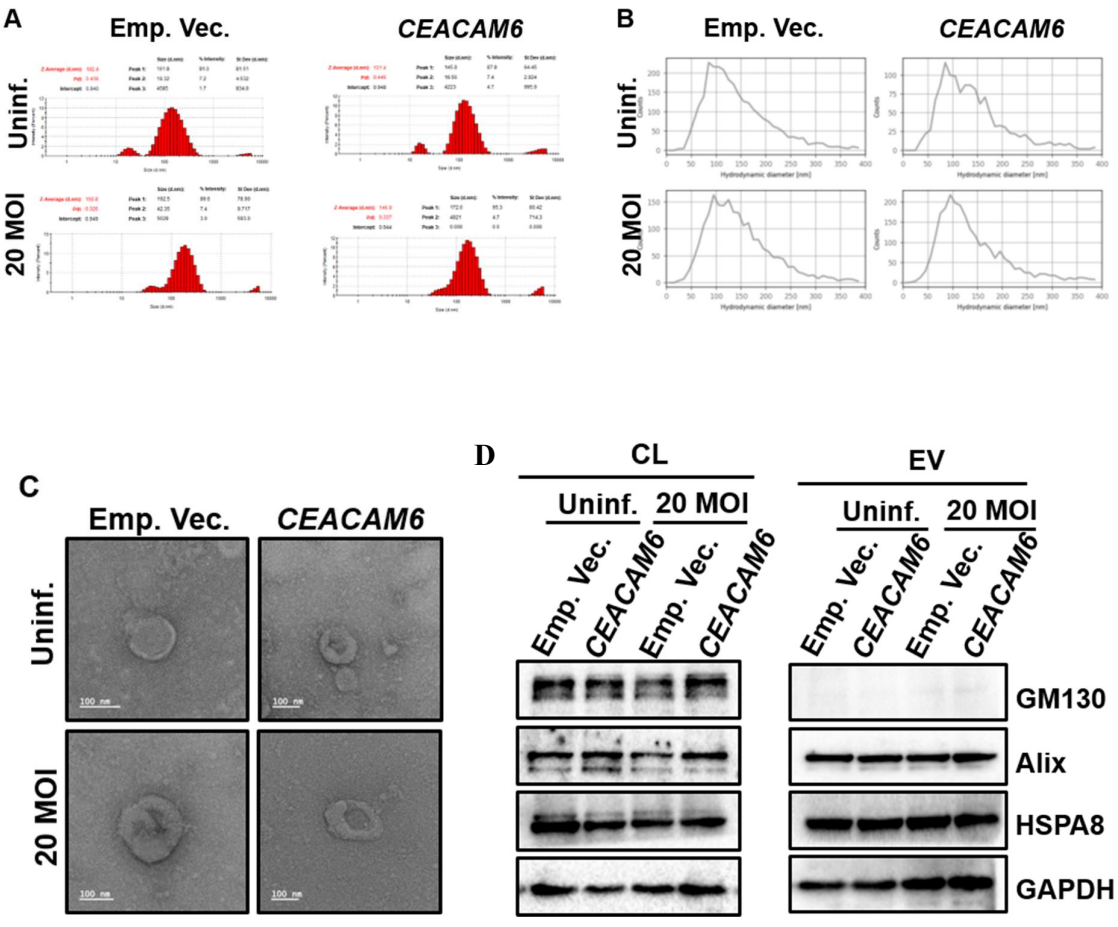

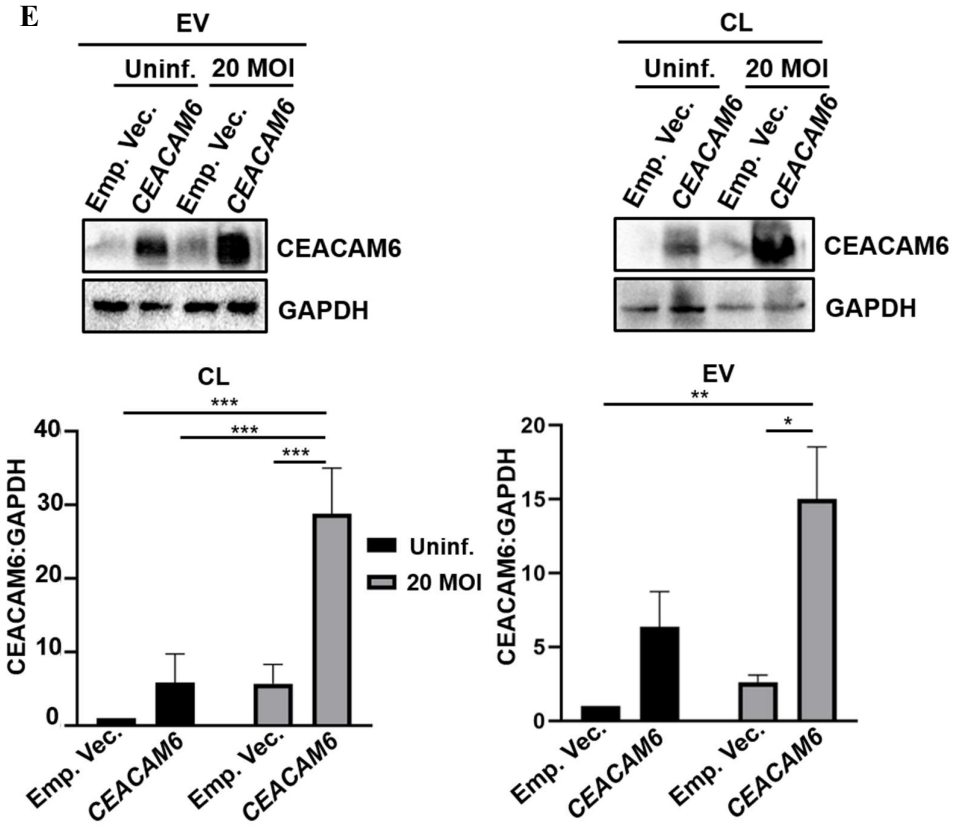


**Figure 19: EVs released from *CEACAM6*-overexpressing cells are enriched in CEACAM6.** (**A**) DLS analysis showing the particle size distribution of EVs isolated from either Emp. Vec. cells or *CEACAM6*-expressing cells, with or without *H. pylori* infection at a MOI of 20. (**B**) NTA providing quantitative measurements of EV concentration and size. (**C**) TEM images showing the shape and size of EVs. Scale bar = 100 nm (**D**) Western blot images showing EV preparations by probing for canonical EV markers, with GM130 serving as a negative marker and Alix/HSPA8 as positive markers. (**E**) Western blotting showing CEACAM6 protein levels in both cell lysates (CL) and EV fractions derived from Emp. Vec. or *CEACAM6*-expressing cells. Quantitative graphs illustrate fold changes in CEACAM6 relative to GAPDH (mean ± SEM, n = 3). One-way ANOVA with Tukey's correction establishes the statistical significance. *$P < 0.05$, **$P < 0.01$, ***$P < 0.001$. Emp.Vec., empty vector; Uninf., uninfected.

CEACAM6 relative to those from the empty vector controls with *H. pylori* infection, which

was consistent with the cellular expression pattern (Figure 19E). Together, these findings establish that CEACAM6 is robustly expressed in overexpressing GCCs and packaged into the EVs, with *H. pylori* infection further amplifying its abundance.

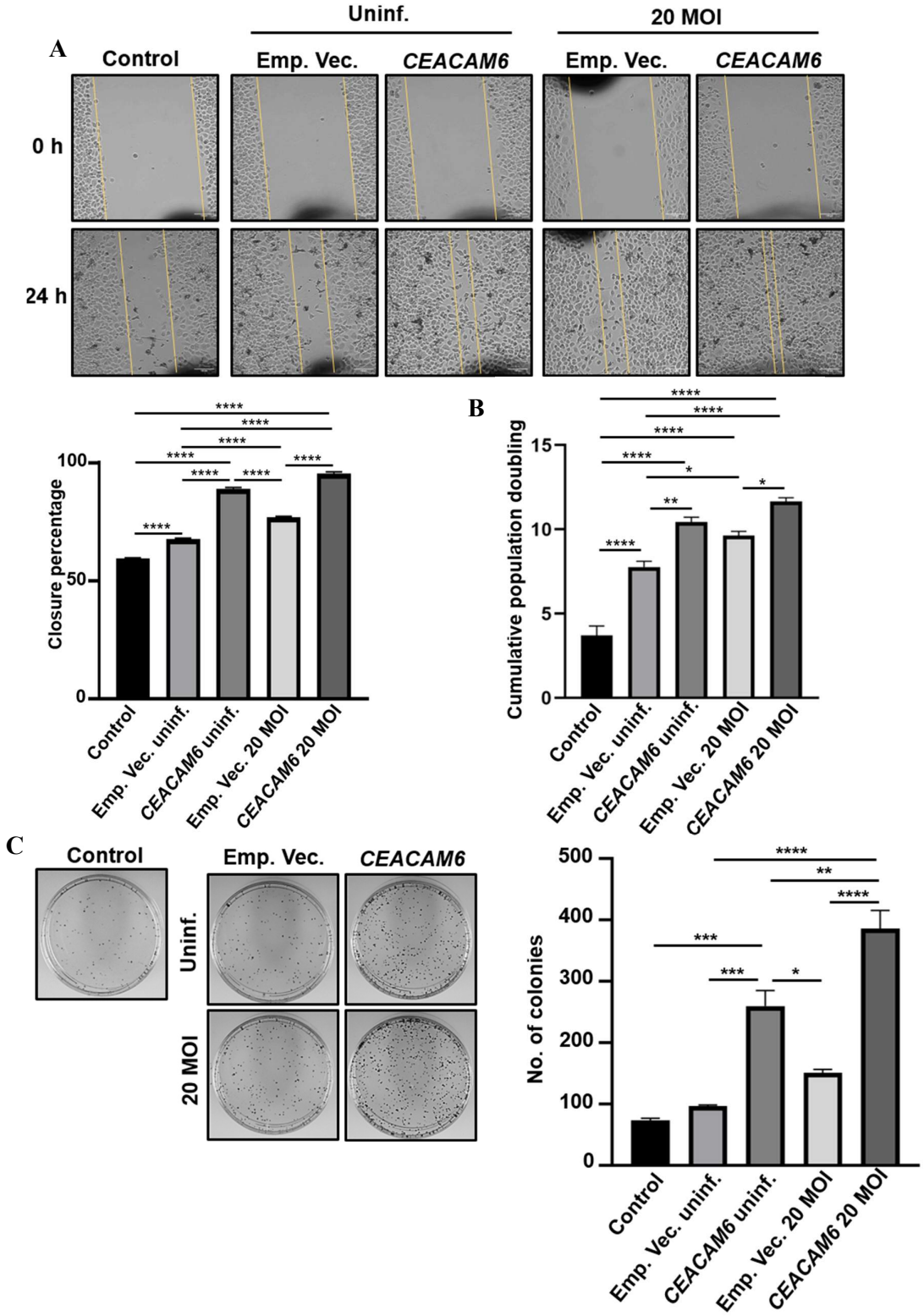

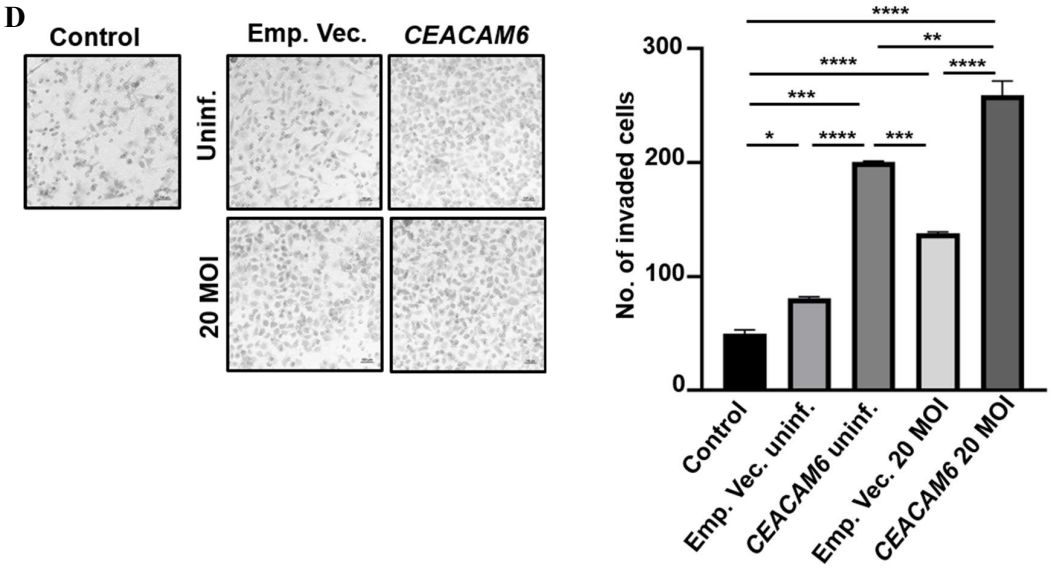


**Figure 20: CEACAM6-loaded EVs enhance tumorigenic properties in the recipient GCCs**. AGS cells are exposed to the EVs isolated from either Emp. Vec. or *CEACAM6*-expressing cells, in the presence or absence of *H. pylori* infection and subjected to a series of functional assays to assess tumorigenic potential. **(A)** Wound healing assay showing the migratory capacity of the recipient AGS cells. Objective=10×; scale bar = 100 μm. **(B)** Population doubling graph displaying proliferative ability of the cells. **(C)** Photographs showing the colony-forming ability and accompanying bar graph quantifies the same. **(D)** Micrographs showing invasive behaviour of the recipient cells. Graph shows the no. of invaded cells (mean ± SEM, n=3). ANOVA with Tukey's post hoc analysis for statistical significance determination. *$P < 0.05$, **$P < 0.01$, ***$P < 0.001$, ****$P < 0.0001$. Emp.Vec., empty vector; Uninf., uninfected.

### 5.3. The recipient cells exposed to CEACAM6-enriched EVs acquired tumorigenic potentials

To evaluate the functional impact of CEACAM6-enriched EVs, the naïve AGS cells were treated with EVs isolated from the empty vector or *CEACAM6*-expressing cells (with/without

*H. pylori*). Wound-healing analysis found that the AGS cells exposed to EVs from *CEACAM6*-expressing cells displayed significantly enhanced migration activity (Figure 20A). AGS cells treated with EVs derived from the infected counterpart exhibited the most significant migration (Figure 20A). Population doubling assay demonstrated that EVs released from infected *CEACAM6*-expressing cells significantly enhanced the proliferative potential of the recipient AGS cells relative to controls (Figure 20B).

Clonogenic assay found that the recipient cells exposed to EVs from *H. pylori*-infected *CEACAM6*-expressing cells exhibited the most significant colony formation among other experimental conditions (Figure 20C). Invasion assay exhibited increased invasive ability of the recipient AGS cells treated with the EVs from *CEACAM6*-expressing cells (Figure 20D). EVs from the *H. pylori*-infected *CEACAM6*-expressing cells imparted the most significant effect. These results collectively indicate that CEACAM6-laden EVs promote tumorigenesis with *H. pylori* infection amplifying the effect.

**5.4. CEACAM6 is localised to the EV membrane and metastatic GC patients release CEACAM6-enriched EVs**

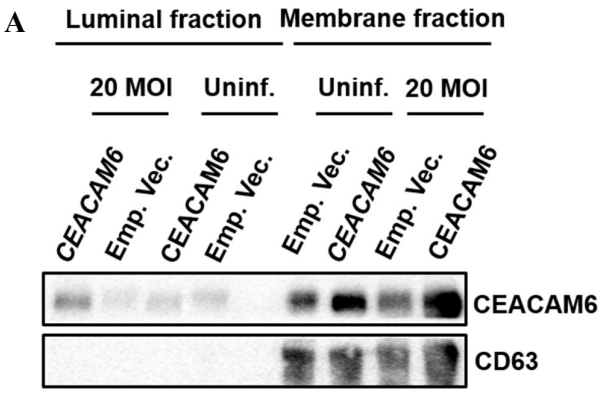

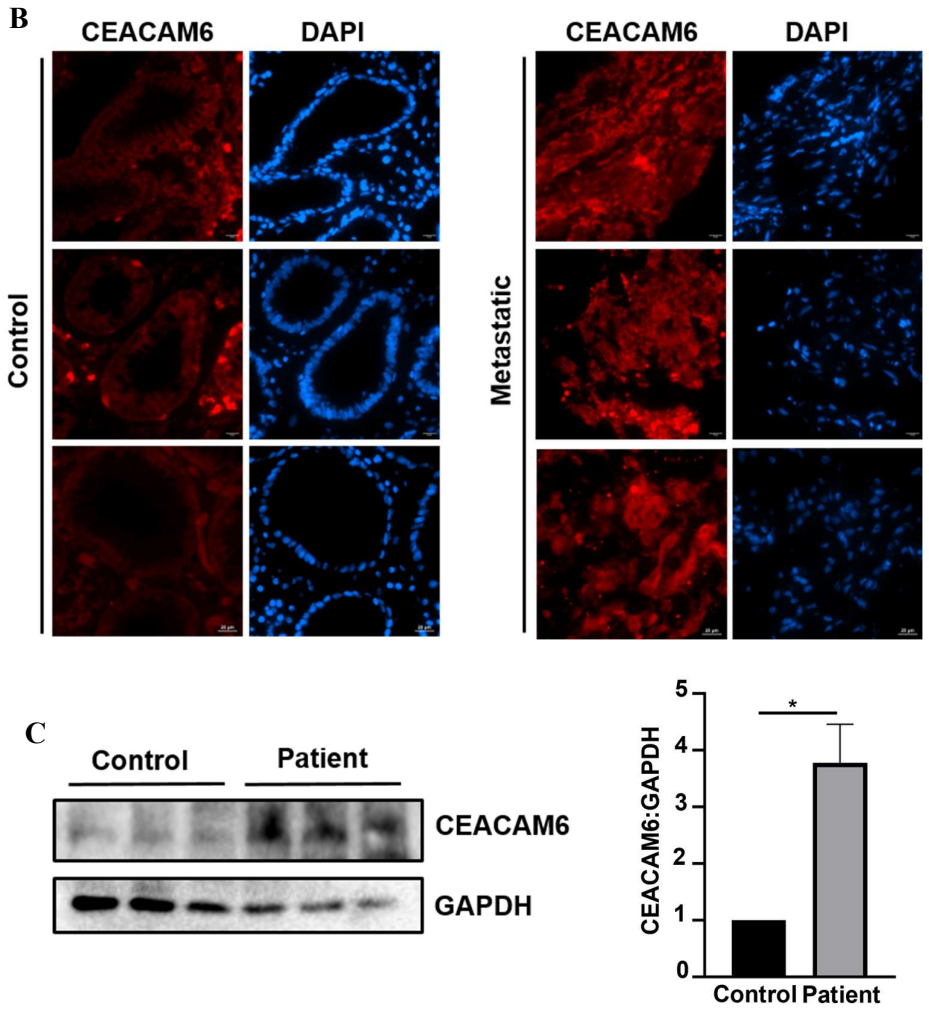


**Figure 21: CEACAM6 is present on the EV membranes and metastatic GC patients release CEACAM6-enriched EVs in blood.** (**A**) Western blotting showing the CEACAM6 in membrane and luminal fraction of the EVs from empty vector or *CEACAM6*-expressing cells. CD63 is the marker for EV membrane. (**B**) Immunofluorescence microscopy showing CEACAM6 (red) in three different GC samples and controls. DAPI (blue) is the nuclear stain. Scale bar is 20 μm. 63× objective is used. (**C**) Western blot analysis of CEACAM6 in EVs isolated from sera of GC patients and non-cancerous individuals. Graph showing CEACAM6 levels in EVs from controls versus patients, GAPDH is the loading control (mean ± SEM, n=3, Student's t-test). $*P < 0.05$.

To examine CEACAM6 distribution, EVs were fractionated into membrane and luminal

counterparts. Western blotting found CEACAM6 in membrane fraction (as denoted by CD63 bands) confirming its membrane localisation (Figure 21A). Metastatic GC tissues from three different patients exhibited high CEACAM6 as shown by immunofluorescence microscopy (Figure 21B). To ascertain whether this elevation extends to circulating vesicles, EVs were isolated from sera of GC patients and healthy controls. Western blotting demonstrated that EVs from patients contained substantially higher CEACAM6 than those from healthy individuals. (Figure 21C). These observations validate the presence of CEACAM6 in EV membranes and in circulating vesicles, underscoring its selective enrichment in the tumor-associated context. Therefore, CEACAM6 may serve as a candidate circulating biomarker for *H. pylori*-associated GC.

**5.5. Discussion**

This chapter establishes the presence of CEACAM6 in the EVs secreted by GCCs, with its levels elevated following *H. pylori* infection. Functionally, EVs derived from infected *CEACAM6*-expressing cells confer greater oncogenic activity than those released from the infected empty vector controls. CEACAM6 is also found to be predominantly EV membrane-associated. *H. pylori*-positive GC patients showed marked upregulation of CEACAM6 in both tumor tissues and circulating EVs.

The membrane localization of CEACAM6 within EVs provides a distinct diagnostic advantage, enabling direct detection in patient biofluids without the need for invasive procedures. Evidence from bladder cancer strengthens this concept, where CEACAM proteins on urinary EV membranes have been projected as non-invasive biomarkers for disease monitoring (207). CEACAM6 levels in serum-derived EVs closely parallel those observed in GC tissues, suggesting stage-specific biomarker potential. In summary, the findings from this chapter position CEACAM6-enriched EVs as facilitators of infection-driven malignant progression and promising candidate for liquid biopsy-based detection in GC.

# Chapter 6

# Conclusions

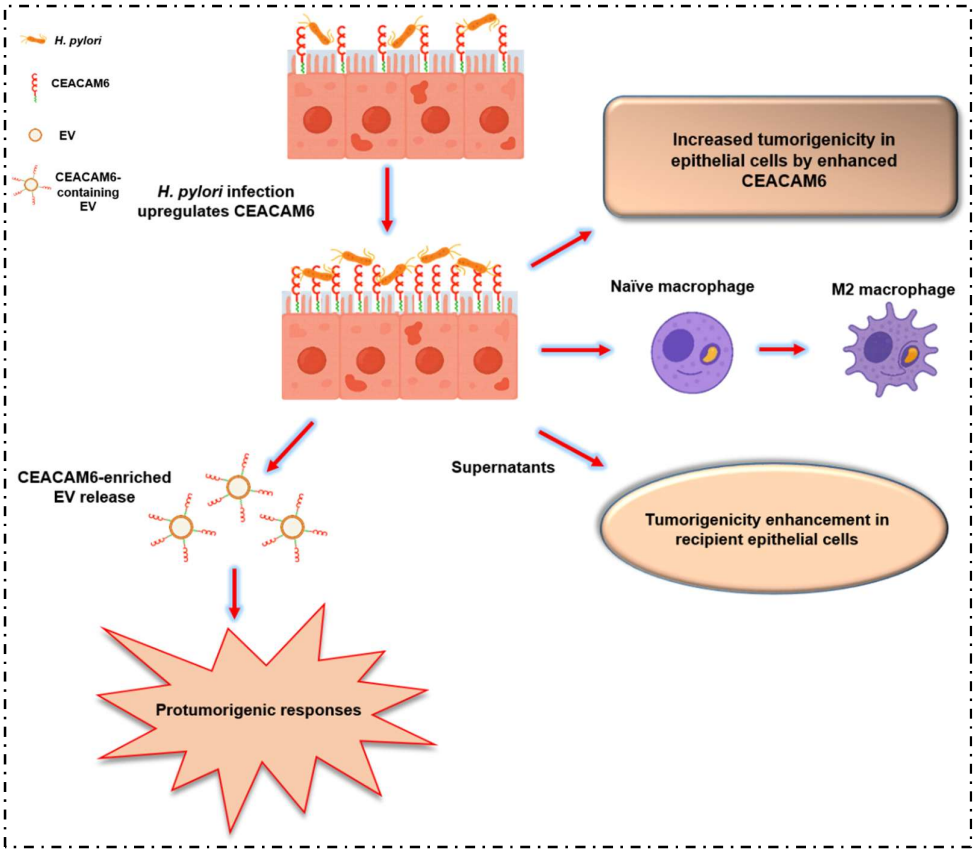


**Figure 22:** A summary figure recapitulating the findings of this thesis work.

**Key findings**

- *H. pylori* infection markedly elevates CEACAM6 expression in GCCs.
- Overexpression of CEACAM6 enhances GCC proliferation, migration and invasion, with these effects further intensified by *H. pylori* exposure.
- Supernatants from *H. pylori*-infected, *CEACAM6*-overexpressing GCCs stimulate tumorigenic activity in recipient GCCs, indicating a strong paracrine influence.
- *CEACAM6*-expressing GCCs drive macrophage polarization toward the M2 phenotype, an effect that is accentuated under *H. pylori* infection.
- *H. pylori*-infected GCCs release CEACAM6-enriched EVs which confer pro-tumorigenic properties to the recipient GCCs.
- CEACAM6 in the EVs is membrane localized.

- Metastatic GC patient-derived sera are richer with CEACAM6-enriched EVs compared to those from healthy individuals.

Based on the observations from this study, CEACAM6 emerges as a key driver of *H. pylori*-induced GC, modulating both tumorigenic behaviour and immune responses. Its enrichment on EVs further supports CEACAM6 as a promising biomarker for minimally invasive diagnostics and a potential target for therapeutic intervention in *H. pylori*-dependent GC.

# Chapter 7

# Materials and methods

### 7.1. GCCs

AGS (Cat. No. CRL1739) was purchased from American Type Cell Culture (ATCC, USA) and MKN45 was acquired from the University of Virginia under MTA.

Cells were maintained under complete media containing RPMI1640 (Cat. No. AL028A, HiMedia, India) and 10% fetal bovine serum (FBS) (Cat. No. 10270106, Thermo Fisher Scientific, USA). Before usage, FBS was subjected to heat inactivation (55 °C, 30 min). The cells were cultured under a humidified incubator (Model No. Galaxy 170R, New Brunswick, Eppendorf, Germany) at 37 °C and 5% $CO_2$. In a T-25 or T-75 flask, cells were grown in 6 mL or 18 mL of complete media.

### 7.2. Cell passaging

Cell manipulations were performed aseptically in a Class II laminar flow hood (Model No. 1300 Series A2, Thermo Fisher Scientific). For passaging or plating, cells were allowed to reach a confluency of 90%. The culture medium was discarded, and cells in T-25 or T-75 flasks were incubated with trypsin (Cat. No. TCL007-100 mL, HiMedia). After 5 min, equal volume of complete media was added the trypsinized cells. After resuspension of the cells, 10 µL of cells were added to a Neubauer haemocytometer (Cat. No. 0640010, Paul Marienfeld GmbH & Co. KG, Germany). Cells were then counted according to the following calculation:

**Number of cells=Total number of cells counted/$4\times10^4$×Volume of the suspension**

Cells centrifugation was performed (Model No. SL8R, Thermo Fisher Scientific) for 8 min at 500×g at room temperature (RT). The pellet was dispersed in a suitable volume of complete media after discarding the supernatant. Then cells were seeded or passaged as per the needs in flasks or plates.

### 7.3. Cell freezing and revival

Cells after trypsinisation were centrifuged as detailed above. The pellet was mixed in a cell freezing mix made of 90% FBS and 10% DMSO (Cat. No. TC185-100ML, HiMedia). The

suspension was then aliquoted into multiple cryovials. Cryovials were initially preserved at −80 °C for 14-16 h, after which they were moved into liquid nitrogen (−196 °C) for extended storage.

Cryovials were thawed in a 37 °C water bath and cell suspension were transferred to a 15 mL tube in 9 ml complete medium. Following centrifugation (500×g, 8 min), the pellet was dispersed in 1 ml medium. Cells were seeded into T25/T75 flasks and maintained under standard culture conditions.

### 7.4. *H. pylori* maintenance and infection

*H. pylori cagPAI* (+) strain 26695 was procured from ATCC (Cat. No. 700392). These were cultured on BD trypticase soy agar (TSA) plates supplemented with 5% defibrillated sheep blood (Cat. No. 221239; Becton, Dickinson and Company, USA). The bacteria were grown under 10% $CO_2$ and 37 °C for three days. Then the bacteria were passaged using a sterile cotton swab on a fresh TSA plate. For infection of the cell lines, an inoculum of *H. pylori* was taken from the TSA plates at 2$^{nd}$ day after passaging and added to the 8 mL of Brucella broth (Cat. No. 211088, BD) supplemented with 10% FBS within a T-25 flask. The culture was allowed to grow inside the incubator on an orbital shaker until the O.D reached 0.6-1.0. The OD was measured using a UV-VIS spectrophotometer (Model No. GENESYS 50, Thermo Fisher Scientific) at 600 nm wavelength using a cuvette.

Cultured bacteria after centrifugation (400×g, 8 min) were dispersed in appropriate media, adjusted so that 1 µl contained $1 \times 10^7$ bacteria, corresponding to multiplicities of infection (MOI) of 10 for $1 \times 10^6$ GCCs. Infections were performed with *H. pylori* at MOI 20 for 24 h in AGS and MKN45 cells, unless specified.

### 7.5. *H. pylori* freezing and revival

The freezing mixture was prepared by filtration of Brucella broth supplemented with 10% FBS and 10% glycerol (Cat. No. MB060-500ML, HiMedia). Colonies of *H. pylori* on TSA plates

were harvested at day 2nd after passaging, using an inoculation loop and suspended in 1 mL freezing mixture in 15 mL centrifuge tube. Freezing medium volume was then adjusted relative to bacterial growth. Aliquots were dispensed into cryovials and stored at -80 °C.

Frozen vials of bacteria were recovered and thawed on ice and the suspension plated onto pre-warmed TSA plates using L-shaped spreaders. Plates were incubated at 37 °C under 10% $CO_2$.

**7.6. Transformation**

Prior to transformation, XL10-Gold Ultra competent cells (Thermo Fisher Scientific) were gently thawed on ice. A mixture of 45 µL competent cells and 100 ng CEACAM6 plasmid DNA was incubated on ice for 30 min, subjected to heat shock at 42 °C for 35 s and then returned to ice for 2 min. Subsequently, 0.5 ml of SOC media (Cat. No. 15544034, Thermo Fisher Scientific) was added and the suspension was incubated at 37 °C for 1 h with shaking at 230 RPM (Model No. Innova 42R, New Brunswick, Eppendorf).

Following transformation, cells were spread onto LB agar (Cat. No. M1151, HiMedia) containing with ampicillin (100 µg/mL) (Cat. No. A022, HiMedia) using spreaders and incubated at 37 °C overnight. Colonies obtained were picked and cultured in 5 ml LB broth (Cat. No. M1245-500G, HiMedia) containing ampicillin, with incubation at 37 °C for 12–16 h under shaking conditions (230 RPM).

From these cultures, plasmid DNA was isolated with the QIAprep Spin Miniprep Kit (Cat. No. 27106, Qiagen, Germany) following the manufacturer's instructions and DNA was eluted in 30 µl of pre-warmed elution buffer. DNA concentration and purity were assessed by taking absorbance at 260/280 nm with a spectrophotometer (Model-NanoDrop 2000, Thermo Fisher Scientific).

**7.7. Transfection**

Lipofectamine 3000 (Cat. No. L3000015, Thermo Fisher Scientific) reagent was used for

transfection. 25 × $10^4$ AGS cells allowed to grow for overnight in 96-well dish. 1 h before transfection, media was replaced. As per manufacturer's protocol, two mixes were prepared in different microfuge tubes. Mix A contained plasmid, P3000 and serum free media; Mix B contained Lipofectamine 3000 and serum free media. After 5 min the two mixes were combined and incubated for 20 min at RT. Following the addition of the mixture into the wells, the plate was swirled gently to allow uniform distribution of the mixture. 48 h post transfection 200 µg/mL G418 (Cat. No. G8168, Sigma-Aldrich, USA) supplemented complete media was added. At 48 h, cells were subjected to trypsinization and subsequently seeded into 6-well plates in 300 µg/mL G418 supplemented complete media. The colonies were allowed to grow with media replacements in every 3$^{rd}$ day. Then colonies were transferred using cloning discs (Cat. No. F37847-0002, Sigma-Aldrich) into 12-well dish and gradually propagated in larger flasks. Western blotting was performed to validate the stable expression of the plasmids. The desired colonies were cultured in large scale and later cryopreserved in liquid nitrogen.

**7.8. Supernatant collection**

3 × $10^6$ stably-transfected *CEACAM6* cells and empty vector cells were seeded in 60 mm dishes. Fresh 2 mL of complete medium was added prior to infection. 24 h post infection, media were collected, centrifuged at 5000×g for 5 min and supernatants were stored in -80 °C until further usage.

**7.9. EV isolation**

20 × $10^6$ AGS cells/empty vector cells/*CEACAM6*-expressing cells were seeded in 150 mm dishes and infected with 10 or 20 MOI of *H. pylori* for 36 h. Before infection, complete media was replaced with 15 mL of RPMI1640 supplemented with 10% EV-depleted FBS (Cat. No.10270106, Thermo Fisher Scientific). After infection, media were collected and centrifuged at 2000×g for 10 min at 4 °C; the resulting supernatants were then centrifuged again at 10000×g for 30 min at 4 °C. Then supernatants were passed through a 100 kDa cut-off filters using a

centrifuge at 3000×g until retentates was around 250 µL of volume. Retentates were then resuspended with Total exosome isolation (Cat. No. 4478359, Thermo Fischer Scientific) buffer in 1:2 ratio and kept in 4 °C overnight. Next day, the suspensions were centrifuged (1 h, 10000×g, 4 °C) and the precipitated EVs were reconstituted in PBS for downstream analysis.

**7.10. Bioinformatic analysis**

The Gene Expression Profiling Interactive Analysis 2 (GEPIA2) platform (http://gepia2.cancer-pku.cn/index), a web portal for exploring gene expression in tissues from TCGA program, was employed to examine CEACAM1, CEACAM5 and CEACAM6 expression in tumor versus normal samples from STAD dataset. In addition, UALCAN (https://ualcan.path.uab.edu/) allows stratification of STAD dataset as per clinical features that include *H. pylori* infection status. Therefore, UALCAN portal was accessed to assess the expression of CEACAM1, CEACAM5 and CEACAM6 in relation to *H. pylori* infection in GC.

**7.11. Biopsy and sera collection**

Biopsy was performed on GC patients from hospital. Metastasized samples were collected from the antral region of stomachs of the patients positive for *H. pylori* infection. Alongside, paired controls were collected from an adjacent non-cancerous region from each patient. Signed consent was obtained from each patient and their identity was protected. The samples were stored in 4% PFA solution until further usage. Sera was collected from both the patients and healthy volunteer. Then the sera were processed to isolate EVs. The sample collection protocol was approved by "Institutional Ethics Committee for Human Research, National Institute of Science Education and Research" in accordance with the "Helsinki Declaration (2013), World Medical Association" guidelines.

**7.12. EV isolation from sera**

Blood from GC patients and age-matched healthy donors was drawn into EDTA tubes and

allowed to equilibrate at RT for 1 hour. Plasma was separated and clarified by centrifugation at 2000×g or 20 min, aliquoted and stored at −80 °C. For EV recovery plasma was subjected to sequential centrifugation steps (2000×g, 20 min; 10000×g, 20 min) and then ultracentrifuged at 110000×g for 70 min. The pellet was reconstituted in 200 µl PBS for downstream analyses. All steps were performed at 4 °C.

**7.13. Tissue sectioning**

The PFA from the tissue samples was removed and the tissues were incubated for 12-14 h in 30% sucrose solution. Then tissues were embedded in OCT media (Cat. No. 14020108926, Leica Biosystems, Germany) and allowed to freeze in the cryostat (Model No. CM3050S, Leica Biosystems) for 20 min. 5 µm sections were sliced from the embedded tissues and the sections were placed on glass slides. These glass slides were lysine (Cat. No. P8920-100ML, Sigma-Aldrich) coated before usage. After coating, slides were allowed to dry in an incubator at 37 °C. The slides with the tissue slices were then stored in – 20 °C until further usage.

**7.14. Cell and EV lysate preparation**

Cells were scraped into microfuge tubes after *H. pylori* infection. The samples were pelleted (250×g) for 6 min at 4 °C. Protease and phosphatase inhibitors were then added [2X protease inhibitor cocktail (Cat. No. ML051-1ML, HiMedia) + 80 mM sodium fluoride)] and mixed by vortexing twice for 15–20 seconds. Lysis buffer 2X Laemmli sample buffer (Cat. No. ML021, HiMedia) containing 5% β-mercaptoethanol (Cat. No. MB041-500ML, HiMedia) was added, followed by vortexing. The tubes were incubated at 100 °C for 8 min and briefly centrifuged for 10 s. The whole-cell lysates were either directly used for SDS-PAGE analysis or stored at -80 °C.

Protease inhibitor cocktail was added to the EV samples. Then those were mixed with 5X Laemmli buffer (Cat. No. ML121, HiMedia) containing 5% β-mercaptoethanol, vortexed, followed by dry heating for 8 min at 100 °C.

### 7.15. Sonication of EVs

EVs were disrupted by sonication (amplitude 35%, pulse of 10 s and rest of 5 s, for a total of 5 min). Then subjected to ultracentrifugation at 100000 x g for 1 h. Laemmli buffer was added to the supernatant (luminal fraction) and to the pellet (membrane fraction) separately. Those were heated at 100 °C for 8 min.

### 7.16. SDS PAGE

Materials required and the procedure for casting of the acrylamide gel:

Solution A: Stock solution of 30% acrylamide monomer and N,N'-methylene-bis-acrylamide crosslinker in a ratio of 29:1 (Cat. No. 1610156, Bio-Rad Laboratories, USA).

Solution B (resolving gel buffer): 1.5 M Tris-HCl buffer (pH 8.8) (Cat. No. 161-0798, Bio-Rad Laboratories).

Solution C (stacking gel buffer): 0.5 M Tris-HCl buffer (pH 6.8) (Cat. No. 161-0799, Bio-Rad Laboratories).

Glycerol: 50% solution of glycerol in molecular grade water (Cat. No. ML024-100ML, HiMedia).

N, N, N', N'-Tetramethyl ethylenediamine (TEMED): For gel polymerization (Cat. No. 1610800, Bio-Rad Laboratories).

Ammonium persulfate (APS): 10% APS (Cat. No. 1610700, Bio-Rad Laboratories) (prepared fresh every time). APS solution was kept away from light. The following table lists the components required for making a 10% resolving gel.

**Table 2. List of components for a 10% resolving gel**

| Components | Volume |
|---|---|
| Solution A | 1.5 mL |
| Solution B | 1.125 mL |
| Molecular grade water | 1.25 mL |

| | |
|---|---|
| 50% glycerol solution | 1.25 |
| TEMED | 2.5 µl |
| 10% APS | 35 µl |

The following table lists the components required for making a stacking gel.

**Table 3. List of components for a stacking gel**

| Components | Volume |
|---|---|
| Solution A | 0.45 mL |
| Solution C | 0.75 mL |
| Molecular grade water | 1.8 mL |
| TEMED | 3 µl |
| 10% APS | 18 µl |

The resolving and stacking gel mixtures were prepared separately in individual tubes. Immediately before casting, TEMED was added and mixed thoroughly, followed by the addition of 10% APS to initiate polymerization. Spacer (1 mm) and short plates were clamped on the casting stand. After pouring the resolving gel solution, stacking gel mixture was added without disturbing the underlying layer. A 10-well (1 mm) comb was placed into the gel, which was then allowed to polymerize at RT. Once set, gels were assembled into the electrode system and placed in the gel running tank. The electrophoresis buffer (25 mM Tris-HCl, 190 mM glycine, 0.1% SDS) was poured, comb was removed and wells were rinsed with the buffer. Protein samples, thawed from −80 °C storage on ice and equilibrated to RT, were loaded alongside a molecular weight marker (Cat. No. BM008-500, BR Biochem).

The electrode was connected to the power supply (Cat. No. 1645050, Bio-Rad Laboratories). The gel was first electrophoresed at 130 V for 15 min, followed by adjustment to 180 V to

expedite separation and continued until the tracking dye reached the bottom.

### 7.17. Western blotting

The recipe of the buffers:

- Transfer buffer: In 800 mL of distilled water 1.5 L, 4.56 g Tris-HCl and 21.63 g glycine were dissolved. After thorough mixing, 300 ml methanol was added, followed by 0.561 g SDS. The final volume was brought up to 1.5 L.
- 10X TBS: In distilled water 20 mM Tris-HCl and 500 mM NaCl was added, dissolved properly and the pH was adjusted to 7.4.
- 1X TBST: 0.1% Tween 20 (Cat. No. RM156-500G, HiMedia) was added to 1X TBS.
- Blocking buffers: 5% non-fat dried milk (NFDM) (Cat. No. RM1254, HiMedia) added in 1X TBST.

Procedure for western blotting:

After SDS-PAGE, the proteins were transferred through western blotting on a PVDF (0.45 μm, Cat No. IPVH00010, Millipore) membrane. Wet transfer was performed using Towbin's transfer buffer (208). At first, PVDF membrane was activated using chilled (4 °C) methanol for 3 min. The membrane was rinsed with deionised water to eliminate residual methanol and subsequently equilibrated in transfer buffer. A sponge was positioned on the black side of the gel cassette and Mini Trans-Blot filter paper (Cat. no. 1703932, Bio-Rad Laboratories) was layered on top. After placing the gel, the pre-activated PVDF membrane was layered directly above it. Any appearing bubbles were removed using a roller. Another filter paper was positioned on the membrane and a sponge was placed on top. The cassette was closed and inserted within the electrode for wet transfer. A cooling gel was inserted and a magnetic bead was kept within the transfer tank. Voltage was set at 40 V and run for 4 h within a 4 °C refrigerator on top of a magnetic stirrer.

After protein transfer, PVDF membranes were washed with 1× TBS and blocked for 1 h at RT.

Overnight incubation of blocked membranes with the respective primary antibodies was carried out at 4 °C in a humidified chamber. The next day, blots were washed for 10 min in 1× TBST (thrice) and subsequently exposed to HRP-conjugated secondary antibodies for 75 min at RT with gentle agitation. Membranes were washed thrice with 1× TBST (5 min each), followed by a final rinse with 1× TBS for 5 min.

Signal detection was carried out using either the SuperSignal West Femto Chemiluminescent Maximum Sensitivity Substrate (Cat. No. 34094, Thermo Fisher Scientific) or the Immobilon Western Chemiluminescent HRP Substrate (Cat. No. WBKLS-0050, Millipore). The membranes were incubated in the reagents prior to imaging. Chemiluminescent signals were captured using the ChemiDoc XRS Plus system (Cat. No. 170-8265, Bio-Rad Laboratories) and analyzed with ImageLab analysis software (Bio-Rad Laboratories).

**7.17.1 Reprobing of immunoblots**

Blots were stripped with Western Blot Stripping Buffer (Cat. No. T7135A, Takara Bio, USA) and reprobed for additional proteins. Membranes were incubated in stripping buffer for 15 min at RT with gentle agitation to remove bound primary and secondary antibodies. Following this, blots were washed thrice with 1× TBST (15 min each) and then incubated in blocking buffer for 1 h at RT with shaking. Subsequent steps were carried out as described in the section above.

**7.18. Flow cytometry of GCCs**

GCCs after infection were washed with PBS and trypsinized. Cells were then centrifuged after adding equal volume of complete media. Supernatants were discarded and cells were exposed to 50 µL of anti-CEACAM1, anti-CEACAM5 and anti-CEACAM6 antibodies prepared in fluorescence-activated cell sorting (FACS) buffer (0.1% BSA and sodium azide in PBS) for 30 min. Cells were washed once. Then cells were incubated in 50 µL of fluorophore-tagged anti-mouse secondary antibodies for 30 min at 4 °C in dark. Again, cells were washed, resuspended in FACS buffer containing 1% PFA and acquired using a flow cytometer (Model-LSRFortessa,

BD). All the washing were done by centrifugation at 1000×g for 5 min.

### 7.19. PBMC isolation and macrophage generation

Buffy coat bags were procured from blood bank. PBS was added to the buffy coat in a 1:1 ratio. 25 mL of HiSep (Cat. No. LSM1077, HiMedia) was dispensed into 50 mL centrifuge tubes, followed by slow addition of 25 mL of diluted buffy coat along the tube wall. Then, centrifugation was carried out at 400×g for 35 min at RT, with brakes turned off. A whitish PBMC ring was formed between a top layer of plasma and bottom layer of HiSep. The RBCs were pelleted at the bottom. The PBMCs were collected in a centrifuge tube and equal volume of RPMI1640 was added followed by centrifugation for 10 min. Pellets were dispersed in RPMI1640 in appropriate volume, counted and $10 \times 10^6$ PBMCs were plated in each well of 6-well dishes. After 1 h, media were removed, wells were properly rinsed with PBS and fresh RPMI1640 supplemented with 10% heat-inactivated human sera (Cat. No. RM10986, HiMedia) and 20 ng/mL M-CSF (Cat. No. CYT-308, Prospec, Israel) was added in each well. Every 2$^{nd}$ day media was replaced, till the differentiation of macrophages. Post macrophage generation, M1 or M2 phenotype of macrophages were obtained using appropriate stimulus. M1 macrophages were generated by treating naïve macrophages with 100 ng/mL of LPS (Cat. No. L4005, Sigma-Aldrich) and 20 ng/mL of IFN-Ɣ (Cat. No. CYT-206, Prospec). M2 macrophage population was differentiated from the naïve macrophages by treatment with 20 ng/mL of IL-4 (Cat. No. CYT-097, Prospec).

### 7.20. Macrophage-epithelial cell co-culture

$1.5 \times 10^6$ *CEACAM6*-expressing AGS cells along with the empty vector cells were plated on Transwells (Cat. No. TCP078, HiMedia) with 0.4 μm pore size. These Transwells were then placed in 6-well dishes containing differentiated macrophages. Prior to infection, media was replaced with RPMI1640 supplemented with 10% human serum. AGS cells were infected with

*H. pylori* for 48 h then macrophages were processed for flow cytometry analysis or immunofluorescence microscopy.

**7.21. Flow cytometry of macrophages**

After incubation, macrophages were washed with PBS and incubated with Zymefree (Cat No. TCL028-500 mL, HiMedia) for 15 min in incubator. The staining procedure was followed to stain the cell surface and then the intracellular component. Cells were pelleted at 1000×g for 5 min and then were treated with Fc binding inhibitor (Cat. No. 14-9161-73, Thermo Fisher Scientific) for 15 min. Antibodies were prepared in 50 µL FACS buffer and cells were incubated with the fluorophore-tagged antibodies (CD40, CD64, CD206) for 30 min at 4 °C under dark conditions. Cells were washed once. After fixation in PFA at RT for 10 min, cells were subjected to permeabilization buffer for 15 min. After washing, cells were blocked for 20 min. Then fluorophore-conjugated anti-CD68 antibody was added and after 30 min cells were washed. After resuspension in FACS buffer with 1% PFA, samples were stored at 4 °C in darkness until acquisition on the flow cytometer. All the washing steps were performed at 1000×g for 5 min.

**7.22. Immunofluorescence and confocal microscopy**

$0.15 \times 10^6$ AGS cells on coverslips were infected with *H. pylori* or left untreated. Following infection, coverslips were washed and fixed. Permeabilisation was done with 0.1% Triton X-100 in PBS. 5% blocking buffer was prepared by adding BSA in PBS containing 0.1% Tween 20 (PBS-T). After blocking for 1 h, overnight incubation of cells with anti-CEACAM1, anti-CEACAM5 and anti-CEACAM6 antibodies was carried out at 4 °C in a moist chamber. The next day, cells underwent three washes in PBS-T, each lasting 10 min. Cells were incubated with fluorophore-tagged secondary antibodies for 2 h at RT, under dark. After three 5 min washes in PBS-T, cells were incubated with DAPI for 20 min. After washing in PBS, coverslips were inverted and mounted onto glass slides using Fluoromount-G (Cat. No.0100-01, Southern

Biotech, USA).

Macrophages obtained after coculture were stained following the same procedure. Primary antibodies against iNOS1 and ARG1 were used.

Biopsy samples were processed using the same staining protocol, except permeabilisation was carried out with 0.5% Triton X-100 in PBS. Microscopy was performed using a confocal microscope (Model-DMi8, Leica Biosystems) or an epifluorescence microscope (Model-Eclipse Ti-U, Nikon, Japan). Quantitation of fluorescence was performed using Fiji (209).

**7.23. Cytokine array analysis**

To evaluate cytokine profiles in the collected supernatants, a Human Inflammation Antibody Array (Cat. No. ab134001, Abcam, USA) was employed. The assay was performed following the manufacturer's protocol without modification. Following incubation and processing steps, the resulting chemiluminescent signals were detected using the ChemiDoc XRS+ imaging system (Bio-Rad Laboratories) and images were captured. Subsequent intensity profiling of spots was performed using ImageLab software (Bio-Rad Laboratories). Quantification of individual cytokine spots was carried out as outlined in the manufacturer's protocol, allowing comparative assessment of cytokine expression levels across experimental groups.

**7.24. Treatment with EVs**

EV protein concentration was quantified using the Pierce BCA Protein Assay Kit (Cat. No. 23227, Thermo Fisher Scientific). AGS cells were treated with 20 µg of EVs. As an additional control, one set of AGS cells was cultured in RPMI-1640 medium supplemented with EV-depleted 10% FBS to exclude the influence of exogenous vesicles.

**7.25. Wound healing assay**

Empty vector and *CEACAM6*-expressing cells were grown till confluency in 6-well plates. Scratches were created using 200 µL pipette tips. Cells were infected with *H. pylori*. The images of wound closure were taken at 0 h and 6 h.

Similarly, scratches were created on confluent AGS cells treated with supernatants derived from the *CEACAM6*-expressing cells or empty vector cells with/without *H. pylori* infection. The images were acquired at 0 h and 24 h.

Again, AGS were treated with the EVs released from the empty vector or *CEACAM6*-expressing cells with or without infection and wound healing was performed as described earlier. The images were captured at 0 h and 24 h. Analysis for all was done by measuring the area of closure at 0 h and final time point using ImageJ.

**7.26. Clonogenic assay**

The empty vector and *CEACAM6*-expressing cells were infected for 24 h. Then cells were washed, trypsinized and 500 cells were plated in 35 mm culture dishes. The dishes were maintained for two weeks with periodic replenishment of medium. Upon visible colony formation, cells were washed followed by fixation with 4% PFA. The colonies were washed and stained for 15 min with a crystal violet (Cat. No. S012, HiMedia). Then colonies were rinsed with PBS and dried at RT.

Again, 24 h after treatment with the supernatants from the empty vector and *CEACAM6*-expressing cells, AGS cells were trypsinised and 500 cells were reseeded in 35 mm culture dishes from each setup. Rest of the procedures were performed as described above.

Similarly, AGS cells after treatment with the EVs from empty vector and *CEACAM6*-expressing cells were trypsinised and 500 cells were reseeded in 35 mm dishes. As described above, the plates were fixed and stained.

Images of all the plates were acquired using a camera and analyzed using Fiji software.

**7.27. Population doubling assay**

The proliferative capacity of GCCs was evaluated using population doubling assay. Following *H. pylori* infection for 24 h, the empty vector or *CEACAM6*-expressing cells were harvested by trypsinization. For each experimental condition, $10^4$ cells were plated in 24-well plates to

enable counting over the following three days. Cells were counted on days 2, 3 and 4 after reseeding. The following formula calculated the population doubling (210):

$$PD = \frac{\log\ N_h - \log\ N_s}{\log 2}$$

where $N_s$ = number of seeded cells and $N_h$ = number of cells counted at each time point. The population doubling values obtained for each day were summed to generate cumulative population doubling (cPD).

Similarly, AGS cells treated (24 h) with supernatants from the empty vector or *CEACAM6*-expressing cells were trypsinised and replated. Remaining procedure was followed as detailed above.

Likewise, EV treated (24 h) AGS cells were trypsinised and population doubling assay was performed.

**7.28. Invasion assay**

Invasive potential of the empty vector and *CEACAM6*-expressing cells was assessed through invasion assay. A thin layer of matrigel (Cat. No. 356230, Sigma-Aldrich) was applied to Transwell membranes with 8 µm pores (Cat. No. TCP257, HiMedia) and allowed to solidify. Designated wells of a 24-well plate were filled with 800 µl medium containing 20% FBS and Transwells were placed in those wells, ensuring no air bubbles formed. $2 \times 10^5$ cells in medium with 0.5% FBS were seeded onto the Transwells. Cells were infected with *H. pylori* or left untreated. After 24 h, the matrigel layer was gently removed using a sterile cotton swab and the inserts were fixed with 4% PFA. Inserts were rinsed twice with 1× PBS. Crystal violet (0.5 %) staining was performed for 30 min at RT, followed by washing to clear the excess stain. The membranes were then air-dried, excised and mounted onto glass slides using Fluoromount G. Brightfield microscopy was used to capture images and cells were enumerated to evaluate cell invasiveness.

Similarly, AGS cells were treated with supernatants derived from the empty vector or

*CEACAM6*-expressing cells with/ without *H. pylori* infection for 24 h. After treatment, cells were trypsinised and equal no. of AGS cells ($2 \times 10^5$) were seeded on to the top of matrigel-coated transwell inserts. Then the same procedure was followed as described above to perform the assay.

In a similar manner, after treatment of AGS cells with EVs derived from the empty vector or *CEACAM6*-expressing cells with/ without *H. pylori* infection, invasion assay was performed.

**7.29. Nanoparticle tracking analysis**

Both the size range and concentration of EVs were characterized using NTA (Model-NanoSight NS300, Malvern Instruments, UK) or (Model- ZetaView® QUATT, Particle Metrix system, Germany). EV samples were diluted in PBS before analysis.

**7.30. Transmission electron microscopy**

EV suspensions (10 µl) were loaded onto 300-mesh carbon-coated copper grids (Cat. No. CF300 Cu-50, EMS, USA) and incubated for 20 min at RT to facilitate adsorption. Excess fluid was carefully removed using blotting paper. The grids were then subjected to negative staining with 2.5% uranyl acetate (Cat. No. 22405, EMS) for 10 min, followed by a brief rinse. The step was repeated once more. After staining, the grids were vacuum-dried and examined using a TEM (Model-JEM-1230, JEOL, Japan) at 200 kV to visualize EV morphology.

**7.31. Dynamic light scattering**

EV size distribution was analysed through DLS measurements (Model- Zetasizer Nano ZS, Malvern Instruments) to assess. EV suspensions were diluted at a ratio of 1:100 in PBS prior to measurement. Data acquisition and analysis were performed with the DTS 2.0 software.

**7.32. Statistical analysis**

Statistical analyses and graphical representations were performed using GraphPad Prism software (Version 7.0; GraphPad, USA). Quantitative results, obtained from three independent experiments, were presented as mean ± SEM. Student's t-test was employed for pairwise

comparisons, whereas ANOVA was performed for experiments with more than two factors, with Tukey's post hoc test applied for multiple comparisons. Significance was established at *P* values below 0.05.

# Bibliography


1. Bray F, Laversanne M, Sung H, Ferlay J, Siegel RL, Soerjomataram I*, et al.* Global cancer statistics 2022: GLOBOCAN estimates of incidence and mortality worldwide for 36 cancers in 185 countries. *CA Cancer J Clin.* 2024.74:229-63.
2. Sharma R. Burden of Stomach Cancer Incidence, Mortality, Disability-Adjusted Life Years, and Risk Factors in 204 Countries, 1990-2019: An Examination of Global Burden of Disease 2019. *J Gastrointest Cancer.* 2024.55:787-99.
3. Park JY, Georges D, Alberts CJ, Bray F, Clifford G, Baussano I. Global lifetime estimates of expected and preventable gastric cancers across 185 countries. *Nat Med.* 2025.31:3020-7.
4. Kannan D, Venkatesh S, Kumar AM. Gastric Carcinoma - The Indian Perspective. *Gastroenterology, Hepatology and Endoscopy Practice.* 2024.4:161-5.
5. Mamun TI, Younus S, Rahman MH. Gastric cancer-Epidemiology, modifiable and non-modifiable risk factors, challenges and opportunities: An updated review. *Cancer Treat Res Commun.* 2024.41:100845.
6. Lauren P. The Two Histological Main Types of Gastric Carcinoma: Diffuse and So-Called Intestinal-Type Carcinoma. An Attempt at a Histo-Clinical Classification. *Acta Pathol Microbiol Scand.* 1965.64:31-49.
7. Sitarz R, Skierucha M, Mielko J, Offerhaus GJA, Maciejewski R, Polkowski WP. Gastric cancer: epidemiology, prevention, classification, and treatment. *Cancer Manag Res.* 2018.10:239-48.
8. Cancer Genome Atlas Research N. Comprehensive molecular characterization of gastric adenocarcinoma. *Nature.* 2014.513:202-9.
9. Warren JR, Marshall B. Unidentified curved bacilli on gastric epithelium in active chronic gastritis. *Lancet.* 1983.1:1273-5.
10. Schistosomes, liver flukes and Helicobacter pylori. *IARC Monogr Eval Carcinog Risks Hum.* 1994.61:1-241.
11. Suerbaum S, Michetti P. Helicobacter pylori infection. *N Engl J Med.* 2002.347:1175-86.
12. Correa P. Human gastric carcinogenesis: a multistep and multifactorial process--First American Cancer Society Award Lecture on Cancer Epidemiology and Prevention. *Cancer Res.* 1992.52:6735-40.
13. Eriksson NK, Farkkila MA, Voutilainen ME, Arkkila PE. The clinical value of taking routine biopsies from the incisura angularis during gastroscopy. *Endoscopy.* 2005.37:532-6.
14. Dixon MF, Genta RM, Yardley JH, Correa P. Classification and grading of gastritis. The updated Sydney System. International Workshop on the Histopathology of Gastritis, Houston 1994. *Am J Surg Pathol.* 1996.20:1161-81.
15. Malfertheiner P, Camargo MC, El-Omar E, Liou JM, Peek R, Schulz C*, et al.* Helicobacter pylori infection. *Nat Rev Dis Primers.* 2023.9:19.
16. Kao CY, Sheu BS, Wu JJ. Helicobacter pylori infection: An overview of bacterial virulence factors and pathogenesis. *Biomed J.* 2016.39:14-23.
17. Voland P, Weeks DL, Marcus EA, Prinz C, Sachs G, Scott D. Interactions among the seven Helicobacter pylori proteins encoded by the urease gene cluster. *Am J Physiol Gastrointest Liver Physiol.* 2003.284:G96-G106.
18. Ishijima N, Suzuki M, Ashida H, Ichikawa Y, Kanegae Y, Saito I*, et al.* BabA-mediated adherence is a potentiator of the Helicobacter pylori type IV secretion system activity. *J Biol Chem.* 2011.286:25256-64.
19. da Costa DM, Pereira Edos S, Rabenhorst SH. What exists beyond cagA and vacA? Helicobacter pylori genes in gastric diseases. *World J Gastroenterol.* 2015.21:10563-72.
20. Aspholm-Hurtig M, Dailide G, Lahmann M, Kalia A, Ilver D, Roche N*, et al.* Functional adaptation of BabA, the H. pylori ABO blood group antigen binding adhesin. *Science.* 2004.305:519-22.
21. Hatakeyama M. Structure and function of Helicobacter pylori CagA, the first-identified bacterial protein involved in human cancer. *Proc Jpn Acad Ser B Phys Biol Sci.* 2017.93:196-

219.
22. Hussein NR, Argent RH, Marx CK, Patel SR, Robinson K, Atherton JC. Helicobacter pylori dupA is polymorphic, and its active form induces proinflammatory cytokine secretion by mononuclear cells. *J Infect Dis.* 2010.202:261-9.
23. Gu H. Role of Flagella in the Pathogenesis of Helicobacter pylori. *Curr Microbiol.* 2017.74:863-9.
24. Ricci V, Giannouli M, Romano M, Zarrilli R. Helicobacter pylori gamma-glutamyl transpeptidase and its pathogenic role. *World J Gastroenterol.* 2014.20:630-8.
25. Deml L, Aigner M, Decker J, Eckhardt A, Schutz C, Mittl PR*, et al.* Characterization of the Helicobacter pylori cysteine-rich protein A as a T-helper cell type 1 polarizing agent. *Infect Immun.* 2005.73:4732-42.
26. Talebi Bezmin Abadi A, Rafiei A, Ajami A, Hosseini V, Taghvaei T, Jones KR*, et al.* Helicobacter pylori homB, but not cagA, is associated with gastric cancer in Iran. *J Clin Microbiol.* 2011.49:3191-7.
27. Javaheri A, Kruse T, Moonens K, Mejias-Luque R, Debraekeleer A, Asche CI*, et al.* Helicobacter pylori adhesin HopQ engages in a virulence-enhancing interaction with human CEACAMs. *Nat Microbiol.* 2016.2:16189.
28. Zarzecka U, Pu C, Posselt G, Wessler S. The multifunctional role of the protease HtrA in Helicobacter pylori pathogenesis. *FEBS Lett.* 2025.
29. Horridge DN, Begley AA, Kim J, Aravindan N, Fan K, Forsyth MH. Outer inflammatory protein a (OipA) of Helicobacter pylori is regulated by host cell contact and mediates CagA translocation and interleukin-8 response only in the presence of a functional cag pathogenicity island type IV secretion system. *Pathog Dis.* 2017.75
30. Wang G, Hong Y, Olczak A, Maier SE, Maier RJ. Dual Roles of Helicobacter pylori NapA in inducing and combating oxidative stress. *Infect Immun.* 2006.74:6839-46.
31. Wei S, Li X, Wang J, Wang Y, Zhang C, Dai S*, et al.* Outer Membrane Vesicles Secreted by Helicobacter pylori Transmitting Gastric Pathogenic Virulence Factors. *ACS Omega.* 2022.7:240-58.
32. Testerman TL, Semino-Mora C, Cann JA, Qiang B, Pena EA, Liu H*, et al.* Both diet and Helicobacter pylori infection contribute to atherosclerosis in pre- and postmenopausal cynomolgus monkeys. *PLoS One.* 2019.14:e0222001.
33. Mahdavi J, Sonden B, Hurtig M, Olfat FO, Forsberg L, Roche N*, et al.* Helicobacter pylori SabA adhesin in persistent infection and chronic inflammation. *Science.* 2002.297:573-8.
34. Tang CL, Hao B, Zhang GX, Shi RH, Cheng WF. Helicobacter pylori tumor necrosis factor-alpha inducing protein promotes cytokine expression via nuclear factor-kappaB. *World J Gastroenterol.* 2013.19:399-403.
35. Rolig AS, Shanks J, Carter JE, Ottemann KM. Helicobacter pylori requires TlpD-driven chemotaxis to proliferate in the antrum. *Infect Immun.* 2012.80:3713-20.
36. Graham DY, Miftahussurur M. Helicobacter pylori urease for diagnosis of Helicobacter pylori infection: A mini review. *J Adv Res.* 2018.13:51-7.
37. Foegeding NJ, Caston RR, McClain MS, Ohi MD, Cover TL. An Overview of Helicobacter pylori VacA Toxin Biology. *Toxins (Basel).* 2016.8
38. Backert S, Tegtmeyer N, Fischer W. Composition, structure and function of the Helicobacter pylori cag pathogenicity island encoded type IV secretion system. *Future Microbiol.* 2015.10:955-65.
39. Kaplan-Turkoz B, Jimenez-Soto LF, Dian C, Ertl C, Remaut H, Louche A*, et al.* Structural insights into Helicobacter pylori oncoprotein CagA interaction with beta1 integrin. *Proc Natl Acad Sci U S A.* 2012.109:14640-5.
40. Tissera K, Kim MA, Lai J, Angulmaduwa S, Kim A, Merrell DS*, et al.* Characterization of East-Asian Helicobacter pylori encoding Western EPIYA-ABC CagA. *J Microbiol.* 2022.60:207-14.
41. Yong X, Tang B, Li BS, Xie R, Hu CJ, Luo G*, et al.* Helicobacter pylori virulence factor CagA promotes tumorigenesis of gastric cancer via multiple signaling pathways. *Cell Commun Signal.* 2015.13:30.
42. Higashi H, Tsutsumi R, Fujita A, Yamazaki S, Asaka M, Azuma T*, et al.* Biological activity of

the Helicobacter pylori virulence factor CagA is determined by variation in the tyrosine phosphorylation sites. *Proc Natl Acad Sci U S A.* 2002.99:14428-33.
43. Bridge DR, Blum FC, Jang S, Kim J, Cha JH, Merrell DS. Creation and Initial Characterization of Isogenic Helicobacter pylori CagA EPIYA Variants Reveals Differential Activation of Host Cell Signaling Pathways. *Sci Rep.* 2017.7:11057.
44. Yu H, Zeng J, Liang X, Wang W, Zhou Y, Sun Y*, et al.* Helicobacter pylori promotes epithelial-mesenchymal transition in gastric cancer by downregulating programmed cell death protein 4 (PDCD4). *PLoS One.* 2014.9:e105306.
45. Chen ZW, Dong ZB, Xiang HT, Chen SS, Yu WM, Liang C. Helicobacter pylori CagA protein induces gastric cancer stem cell-like properties through the Akt/FOXO3a axis. *J Cell Biochem.* 2024.125:e30527.
46. Lee DG, Kim HS, Lee YS, Kim S, Cha SY, Ota I*, et al.* Helicobacter pylori CagA promotes Snail-mediated epithelial-mesenchymal transition by reducing GSK-3 activity. *Nat Commun.* 2014.5:4423.
47. Hatakeyama M. Impact of the Helicobacter pylori Oncoprotein CagA in Gastric Carcinogenesis. *Curr Top Microbiol Immunol.* 2023.444:239-57.
48. Saadat I, Higashi H, Obuse C, Umeda M, Murata-Kamiya N, Saito Y*, et al.* Helicobacter pylori CagA targets PAR1/MARK kinase to disrupt epithelial cell polarity. *Nature.* 2007.447:330-3.
49. Lang BJ, Gorrell RJ, Tafreshi M, Hatakeyama M, Kwok T, Price JT. The Helicobacter pylori cytotoxin CagA is essential for suppressing host heat shock protein expression. *Cell Stress Chaperones.* 2016.21:523-33.
50. Duan Y, Xu Y, Dou Y, Xu D. Helicobacter pylori and gastric cancer: mechanisms and new perspectives. *J Hematol Oncol.* 2025.18:10.
51. Cover TL. Helicobacter pylori Diversity and Gastric Cancer Risk. *mBio.* 2016.7:e01869-15.
52. Terebiznik MR, Raju D, Vazquez CL, Torbricki K, Kulkarni R, Blanke SR*, et al.* Effect of Helicobacter pylori's vacuolating cytotoxin on the autophagy pathway in gastric epithelial cells. *Autophagy.* 2009.5:370-9.
53. Yahiro K, Satoh M, Nakano M, Hisatsune J, Isomoto H, Sap J*, et al.* Low-density lipoprotein receptor-related protein-1 (LRP1) mediates autophagy and apoptosis caused by Helicobacter pylori VacA. *J Biol Chem.* 2012.287:31104-15.
54. Nakayama M, Kimura M, Wada A, Yahiro K, Ogushi K, Niidome T*, et al.* Helicobacter pylori VacA activates the p38/activating transcription factor 2-mediated signal pathway in AZ-521 cells. *J Biol Chem.* 2004.279:7024-8.
55. Hisatsune J, Yamasaki E, Nakayama M, Shirasaka D, Kurazono H, Katagata Y*, et al.* Helicobacter pylori VacA enhances prostaglandin E2 production through induction of cyclooxygenase 2 expression via a p38 mitogen-activated protein kinase/activating transcription factor 2 cascade in AZ-521 cells. *Infect Immun.* 2007.75:4472-81.
56. Caputo R, Tuccillo C, Manzo BA, Zarrilli R, Tortora G, Blanco Cdel V*, et al.* Helicobacter pylori VacA toxin up-regulates vascular endothelial growth factor expression in MKN 28 gastric cells through an epidermal growth factor receptor-, cyclooxygenase-2-dependent mechanism. *Clin Cancer Res.* 2003.9:2015-21.
57. Yang YJ, Lu CL, Sheu BS. Differential H. pylori-Induced MAPK Responses Regulate Lewis Antigen Expression and Colonization Density on Gastric Epithelial Cells Between Children and Adults. *Front Immunol.* 2022.13:849512.
58. Wu Y, Shen L, Liang X, Li S, Ma L, Zheng L*, et al.* Helicobacter pylori-induced YAP1 nuclear translocation promotes gastric carcinogenesis by enhancing IL-1beta expression. *Cancer Med.* 2019.8:3965-80.
59. Nagy TA, Frey MR, Yan F, Israel DA, Polk DB, Peek RM, Jr. Helicobacter pylori regulates cellular migration and apoptosis by activation of phosphatidylinositol 3-kinase signaling. *J Infect Dis.* 2009.199:641-51.
60. Shirin H, Pinto JT, Liu LU, Merzianu M, Sordillo EM, Moss SF. Helicobacter pylori decreases gastric mucosal glutathione. *Cancer Lett.* 2001.164:127-33.
61. Woodward M, Tunstall-Pedoe H, McColl K. Helicobacter pylori infection reduces systemic availability of dietary vitamin C. *Eur J Gastroenterol Hepatol.* 2001.13:233-7.
62. Murata-Kamiya N, Hatakeyama M. Helicobacter pylori-induced DNA double-stranded break

in the development of gastric cancer. *Cancer Sci.* 2022.113:1909-18.
63. De Simone V, Franze E, Ronchetti G, Colantoni A, Fantini MC, Di Fusco D*, et al.* Th17-type cytokines, IL-6 and TNF-alpha synergistically activate STAT3 and NF-kB to promote colorectal cancer cell growth. *Oncogene.* 2015.34:3493-503.
64. Kay J, Thadhani E, Samson L, Engelward B. Inflammation-induced DNA damage, mutations and cancer. *DNA Repair (Amst).* 2019.83:102673.
65. Yang Q, Guo N, Zhou Y, Chen J, Wei Q, Han M. The role of tumor-associated macrophages (TAMs) in tumor progression and relevant advance in targeted therapy. *Acta Pharm Sin B.* 2020.10:2156-70.
66. Gold P, Freedman SO. Specific carcinoembryonic antigens of the human digestive system. *J Exp Med.* 1965.122:467-81.
67. von Kleist S, Chavanel G, Burtin P. Identification of an antigen from normal human tissue that crossreacts with the carcinoembryonic antigen. *Proc Natl Acad Sci U S A.* 1972.69:2492-4.
68. Mach JP, Pusztaszeri G. Carcinoembryonic antigen (CEA): demonstration of a partial identity between CEA and a normal glycoprotein. *Immunochemistry.* 1972.9:1031-4.
69. Kuroki M, Yamanaka T, Matsuo Y, Ohtani T, Matsuo Y, Minowada J*, et al.* Characterization of a species of non-specific cross-reacting antigen (NCA) expressed by human monocytic cell lines: structure and expression during cell differentiation. *Int J Cancer.* 1994.56:886-91.
70. Kuroki M, Arakawa F, Matsuo Y, Oikawa S, Nakazato H, Matsuoka Y. Three novel molecular forms of biliary glycoprotein deduced from cDNA clones from a human leukocyte library. *Biochem Biophys Res Commun.* 1991.176:578-85.
71. Beauchemin N, Draber P, Dveksler G, Gold P, Gray-Owen S, Grunert F*, et al.* Redefined nomenclature for members of the carcinoembryonic antigen family. *Exp Cell Res.* 1999.252:243-9.
72. Hefta SA, Hefta LJ, Lee TD, Paxton RJ, Shively JE. Carcinoembryonic antigen is anchored to membranes by covalent attachment to a glycosylphosphatidylinositol moiety: identification of the ethanolamine linkage site. *Proc Natl Acad Sci U S A.* 1988.85:4648-52.
73. Kammerer R, Zimmermann W. Coevolution of activating and inhibitory receptors within mammalian carcinoembryonic antigen families. *BMC Biol.* 2010.8:12.
74. Beauchemin N, Arabzadeh A. Carcinoembryonic antigen-related cell adhesion molecules (CEACAMs) in cancer progression and metastasis. *Cancer Metastasis Rev.* 2013.32:643-71.
75. Dery KJ, Gaur S, Gencheva M, Yen Y, Shively JE, Gaur RK. Mechanistic control of carcinoembryonic antigen-related cell adhesion molecule-1 (CEACAM1) splice isoforms by the heterogeneous nuclear ribonuclear proteins hnRNP L, hnRNP A1, and hnRNP M. *J Biol Chem.* 2011.286:16039-51.
76. Khairnar V, Ngo VN. Editorial: Role of carcinoembryonic antigen-related cell adhesion molecules in pathogen responses, tumorigenicity, and immune modulation. *Front Immunol.* 2024.15:1388453.
77. Tchoupa AK, Schuhmacher T, Hauck CR. Signaling by epithelial members of the CEACAM family - mucosal docking sites for pathogenic bacteria. *Cell Commun Signal.* 2014.12:27.
78. Nakajima A, Iijima H, Neurath MF, Nagaishi T, Nieuwenhuis EE, Raychowdhury R*, et al.* Activation-induced expression of carcinoembryonic antigen-cell adhesion molecule 1 regulates mouse T lymphocyte function. *J Immunol.* 2002.168:1028-35.
79. Gu A, Zhang Z, Zhang N, Tsark W, Shively JE. Generation of human CEACAM1 transgenic mice and binding of Neisseria Opa protein to their neutrophils. *PLoS One.* 2010.5:e10067.
80. Bookwalter JE, Jurcisek JA, Gray-Owen SD, Fernandez S, McGillivary G, Bakaletz LO. A carcinoembryonic antigen-related cell adhesion molecule 1 homologue plays a pivotal role in nontypeable Haemophilus influenzae colonization of the chinchilla nasopharynx via the outer membrane protein P5-homologous adhesin. *Infect Immun.* 2008.76:48-55.
81. Koniger V, Holsten L, Harrison U, Busch B, Loell E, Zhao Q*, et al.* Helicobacter pylori exploits human CEACAMs via HopQ for adherence and translocation of CagA. *Nat Microbiol.* 2016.2:16188.
82. Hill DJ, Virji M. A novel cell-binding mechanism of Moraxella catarrhalis ubiquitous surface protein UspA: specific targeting of the N-domain of carcinoembryonic antigen-related cell adhesion molecules by UspA1. *Mol Microbiol.* 2003.48:117-29.

83. Brewer ML, Dymock D, Brady RL, Singer BB, Virji M, Hill DJ. Fusobacterium spp. target human CEACAM1 via the trimeric autotransporter adhesin CbpF. *J Oral Microbiol.* 2019.11:1565043.
84. Leusch HG, Drzeniek Z, Markos-Pusztai Z, Wagener C. Binding of Escherichia coli and Salmonella strains to members of the carcinoembryonic antigen family: differential binding inhibition by aromatic alpha-glycosides of mannose. *Infect Immun.* 1991.59:2051-7.
85. Barnich N, Carvalho FA, Glasser AL, Darcha C, Jantscheff P, Allez M*, et al.* CEACAM6 acts as a receptor for adherent-invasive E. coli, supporting ileal mucosa colonization in Crohn disease. *J Clin Invest.* 2007.117:1566-74.
86. Lee HS, Ostrowski MA, Gray-Owen SD. CEACAM1 dynamics during neisseria gonorrhoeae suppression of CD4+ T lymphocyte activation. *J Immunol.* 2008.180:6827-35.
87. Behrens IK, Busch B, Ishikawa-Ankerhold H, Palamides P, Shively JE, Stanners C*, et al.* The HopQ-CEACAM Interaction Controls CagA Translocation, Phosphorylation, and Phagocytosis of Helicobacter pylori in Neutrophils. *mBio.* 2020.11
88. Kirshner J, Schumann D, Shively JE. CEACAM1, a cell-cell adhesion molecule, directly associates with annexin II in a three-dimensional model of mammary morphogenesis. *J Biol Chem.* 2003.278:50338-45.
89. Gotz L, Rueckschloss U, Balk G, Pfeiffer V, Ergun S, Kleefeldt F. The role of carcinoembryonic antigen-related cell adhesion molecule 1 in cancer. *Front Immunol.* 2023.14:1295232.
90. Thomas J, Klebanov A, John S, Miller LS, Vegesna A, Amdur RL*, et al.* CEACAMS 1, 5, and 6 in disease and cancer: interactions with pathogens. *Genes Cancer.* 2023.14:12-29.
91. Blumenthal RD, Leon E, Hansen HJ, Goldenberg DM. Expression patterns of CEACAM5 and CEACAM6 in primary and metastatic cancers. *BMC Cancer.* 2007.7:2.
92. Shinmi D, Nakano R, Mitamura K, Suzuki-Imaizumi M, Iwano J, Isoda Y*, et al.* Novel anticarcinoembryonic antigen antibody-drug conjugate has antitumor activity in the existence of soluble antigen. *Cancer Med.* 2017.6:798-808.
93. Kim YJ, Li W, Zhelev DV, Mellors JW, Dimitrov DS, Baek DS. Chimeric antigen receptor-T cells are effective against CEACAM5 expressing non-small cell lung cancer cells resistant to antibody-drug conjugates. *Front Oncol.* 2023.13:1124039.
94. Kim EY, Cha YJ, Jeong S, Chang YS. Overexpression of CEACAM6 activates Src-FAK signaling and inhibits anoikis, through homophilic interactions in lung adenocarcinomas. *Transl Oncol.* 2022.20:101402.
95. Zhao D, Cai F, Liu X, Li T, Zhao E, Wang X*, et al.* CEACAM6 expression and function in tumor biology: a comprehensive review. *Discov Oncol.* 2024.15:186.
96. Zheng MY, Lin YT, Kuo YS, Lin YJ, Kuo MH, Huang TW*, et al.* Cytokine and epigenetic regulation of CEACAM6 mediates EGFR-driven signaling and drug response in lung adenocarcinoma. *NPJ Precis Oncol.* 2025.9:115.
97. Luster AD, Alon R, von Andrian UH. Immune cell migration in inflammation: present and future therapeutic targets. *Nat Immunol.* 2005.6:1182-90.
98. Mejias-Luque R, Gerhard M. Immune Evasion Strategies and Persistence of Helicobacter pylori. *Curr Top Microbiol Immunol.* 2017.400:53-71.
99. Mejias-Luque R, Gerhard M. Decoding the interplay: Helicobacter pylori infection, tumor immune microenvironment, and immunotherapy outcomes in gastrointestinal cancers. *Innovation (Camb).* 2025.6:100880.
100. Grage-Griebenow E, Flad HD, Ernst M. Heterogeneity of human peripheral blood monocyte subsets. *J Leukoc Biol.* 2001.69:11-20.
101. Gambardella V, Castillo J, Tarazona N, Gimeno-Valiente F, Martinez-Ciarpaglini C, Cabeza-Segura M*, et al.* The role of tumor-associated macrophages in gastric cancer development and their potential as a therapeutic target. *Cancer Treat Rev.* 2020.86:102015.
102. Hardbower DM, Asim M, Murray-Stewart T, Casero RA, Jr., Verriere T, Lewis ND*, et al.* Arginase 2 deletion leads to enhanced M1 macrophage activation and upregulated polyamine metabolism in response to Helicobacter pylori infection. *Amino Acids.* 2016.48:2375-88.
103. Schreiber RD, Old LJ, Smyth MJ. Cancer immunoediting: integrating immunity's roles in cancer suppression and promotion. *Science.* 2011.331:1565-70.

104. Liu JY, Peng CW, Yang GF, Hu WQ, Yang XJ, Huang CQ, *et al.* Distribution pattern of tumor associated macrophages predicts the prognosis of gastric cancer. *Oncotarget.* 2017.8:92757-69.
105. Yan Y, Zhang J, Li JH, Liu X, Wang JZ, Qu HY, *et al.* High tumor-associated macrophages infiltration is associated with poor prognosis and may contribute to the phenomenon of epithelial-mesenchymal transition in gastric cancer. *Onco Targets Ther.* 2016.9:3975-83.
106. Taniyama D, Taniyama K, Kuraoka K, Zaitsu J, Saito A, Nakatsuka H, *et al.* Long-term follow-up study of gastric adenoma; tumor-associated macrophages are associated to carcinoma development in gastric adenoma. *Gastric Cancer.* 2017.20:929-39.
107. Gordon SR, Maute RL, Dulken BW, Hutter G, George BM, McCracken MN, *et al.* PD-1 expression by tumour-associated macrophages inhibits phagocytosis and tumour immunity. *Nature.* 2017.545:495-9.
108. Wang XL, Jiang JT, Wu CP. Prognostic significance of tumor-associated macrophage infiltration in gastric cancer: a meta-analysis. *Genet Mol Res.* 2016.15
109. Wan C, Deng J, Zhu Y, Wan L, Xu L, Chen Q, *et al.* Targeting tumor-associated macrophages in gastric cancer progression and therapy: insights from molecular mechanisms to therapeutic applications. *Front Pharmacol.* 2025.16:1549694.
110. He Y, Hong Q, Chen S, Zhou J, Qiu S. Reprogramming tumor-associated macrophages in gastric cancer: a pathway to enhanced immunotherapy. *Front Immunol.* 2025.16:1558091.
111. Tkacz M, Tarnowski M, Poniewierska-Baran A, Serwin K, Madej-Michniewicz A, Deskur A, *et al.* Impact of Selected Serum Factors on Metastatic Potential of Gastric Cancer Cells. *Diagnostics (Basel).* 2022.12
112. Guo J, Liu C, Zhou X, Xu X, Deng L, Li X, *et al.* Conditioned Medium from Malignant Breast Cancer Cells Induces an EMT-Like Phenotype and an Altered N-Glycan Profile in Normal Epithelial MCF10A Cells. *Int J Mol Sci.* 2017.18
113. Jo SH, Heo WH, Son HY, Quan M, Hong BS, Kim JH, *et al.* S100A8/A9 mediate the reprograming of normal mammary epithelial cells induced by dynamic cell-cell interactions with adjacent breast cancer cells. *Sci Rep.* 2021.11:1337.
114. Kang M, Devarasou S, Sung NJ, Kwon TY, Shin JH. EMT induction in normal breast epithelial cells by COX2-expressing fibroblasts. *Cell Commun Signal.* 2025.23:237.
115. Wang J, Wang X, Luo H, Xie Y, Cao H, Mao L, *et al.* Extracellular vesicles in Helicobacter pylori-mediated diseases: mechanisms and therapeutic potential. *Cell Commun Signal.* 2025.23:79.
116. Chargaff E, West R. The biological significance of the thromboplastic protein of blood. *J Biol Chem.* 1946.166:189-97.
117. Rai A, Claridge B, Lozano J, Greening DW. The Discovery of Extracellular Vesicles and Their Emergence as a Next-Generation Therapy. *Circ Res.* 2024.135:198-221.
118. Wolf P. The nature and significance of platelet products in human plasma. *Br J Haematol.* 1967.13:269-88.
119. Crawford N. The presence of contractile proteins in platelet microparticles isolated from human and animal platelet-free plasma. *Br J Haematol.* 1971.21:53-69.
120. Nunez EA, Wallis J, Gershon MD. Secretory processes in follicular cells of the bat thyroid. 3. The occurrence of extracellular vesicles and colloid droplets during arousal from hibernation. *Am J Anat.* 1974.141:179-201.
121. Raposo G, Nijman HW, Stoorvogel W, Liejendekker R, Harding CV, Melief CJ, *et al.* B lymphocytes secrete antigen-presenting vesicles. *J Exp Med.* 1996.183:1161-72.
122. Wolfers J, Lozier A, Raposo G, Regnault A, Thery C, Masurier C, *et al.* Tumor-derived exosomes are a source of shared tumor rejection antigens for CTL cross-priming. *Nat Med.* 2001.7:297-303.
123. Lai RC, Arslan F, Lee MM, Sze NS, Choo A, Chen TS, *et al.* Exosome secreted by MSC reduces myocardial ischemia/reperfusion injury. *Stem Cell Res.* 2010.4:214-22.
124. Alvarez-Erviti L, Seow Y, Yin H, Betts C, Lakhal S, Wood MJ. Delivery of siRNA to the mouse brain by systemic injection of targeted exosomes. *Nat Biotechnol.* 2011.29:341-5.
125. Kalluri VS, Smaglo BG, Mahadevan KK, Kirtley ML, McAndrews KM, Mendt M, *et al.* Engineered exosomes with Kras(G12D) specific siRNA in pancreatic cancer: a phase I study with immunological correlates. *Nat Commun.* 2025.16:8696.

126. Sato Y, Zhang W, Baba T, Chung UI, Teramura Y. Extracellular vesicle-liposome hybrids via membrane fusion using cell-penetrating peptide-conjugated lipids. *Regen Ther.* 2024.26:533-40.
127. Gou J, Zhang L, Wang G, Li Z, Yin Q, Pan Y. Inhalable Exosomes in Respiratory Therapies with the Transformative Potential. *Int J Nanomedicine.* 2025.20:14219-52.
128. Chen Y, Zhu Q, Cheng L, Wang Y, Li M, Yang Q*, et al.* Exosome detection via the ultrafast-isolation system: EXODUS. *Nat Methods.* 2021.18:212-8.
129. Kugeratski FG, Hodge K, Lilla S, McAndrews KM, Zhou X, Hwang RF*, et al.* Quantitative proteomics identifies the core proteome of exosomes with syntenin-1 as the highest abundant protein and a putative universal biomarker. *Nat Cell Biol.* 2021.23:631-41.
130. Kowal J, Arras G, Colombo M, Jouve M, Morath JP, Primdal-Bengtson B*, et al.* Proteomic comparison defines novel markers to characterize heterogeneous populations of extracellular vesicle subtypes. *Proc Natl Acad Sci U S A.* 2016.113:E968-77.
131. Mathieu M, Nevo N, Jouve M, Valenzuela JI, Maurin M, Verweij FJ*, et al.* Specificities of exosome versus small ectosome secretion revealed by live intracellular tracking of CD63 and CD9. *Nat Commun.* 2021.12:4389.
132. Srivastava A, Rathore S, Munshi A, Ramesh R. Organically derived exosomes as carriers of anticancer drugs and imaging agents for cancer treatment. *Semin Cancer Biol.* 2022.86:80-100.
133. Kalluri R, LeBleu VS. The biology, function, and biomedical applications of exosomes. *Science.* 2020.367
134. Katzmann DJ, Babst M, Emr SD. Ubiquitin-dependent sorting into the multivesicular body pathway requires the function of a conserved endosomal protein sorting complex, ESCRT-I. *Cell.* 2001.106:145-55.
135. Stuffers S, Sem Wegner C, Stenmark H, Brech A. Multivesicular endosome biogenesis in the absence of ESCRTs. *Traffic.* 2009.10:925-37.
136. Bandu R, Oh JW, Kim KP. Extracellular vesicle proteins as breast cancer biomarkers: Mass spectrometry-based analysis. *Proteomics.* 2024.24:e2300062.
137. Di Vizio D, Kim J, Hager MH, Morello M, Yang W, Lafargue CJ*, et al.* Oncosome formation in prostate cancer: association with a region of frequent chromosomal deletion in metastatic disease. *Cancer Res.* 2009.69:5601-9.
138. Zhang H, Freitas D, Kim HS, Fabijanic K, Li Z, Chen H*, et al.* Identification of distinct nanoparticles and subsets of extracellular vesicles by asymmetric flow field-flow fractionation. *Nat Cell Biol.* 2018.20:332-43.
139. Zhang Q, Jeppesen DK, Higginbotham JN, Graves-Deal R, Trinh VQ, Ramirez MA*, et al.* Supermeres are functional extracellular nanoparticles replete with disease biomarkers and therapeutic targets. *Nat Cell Biol.* 2021.23:1240-54.
140. Jurj A, Paul D, Calin GA. Extracellular Vesicles in cancer: from isolation and characterization to metastasis, drug resistance, and clinical applications. *BMC Cancer.* 2025.25:1154.
141. Hur YH, Feng S, Wilson KF, Cerione RA, Antonyak MA. Embryonic Stem Cell-Derived Extracellular Vesicles Maintain ESC Stemness by Activating FAK. *Dev Cell.* 2021.56:277-91 e6.
142. Chan JC, Morgan CP, Adrian Leu N, Shetty A, Cisse YM, Nugent BM*, et al.* Reproductive tract extracellular vesicles are sufficient to transmit intergenerational stress and program neurodevelopment. *Nat Commun.* 2020.11:1499.
143. Thakur BK, Zhang H, Becker A, Matei I, Huang Y, Costa-Silva B*, et al.* Double-stranded DNA in exosomes: a novel biomarker in cancer detection. *Cell Res.* 2014.24:766-9.
144. Lee YT, Tan YJ, Falasca M, Oon CE. Cancer-Associated Fibroblasts: Epigenetic Regulation and Therapeutic Intervention in Breast Cancer. *Cancers (Basel).* 2020.12
145. Henning AN, Roychoudhuri R, Restifo NP. Epigenetic control of CD8(+) T cell differentiation. *Nat Rev Immunol.* 2018.18:340-56.
146. Yokoi A, Ochiya T. Exosomes and extracellular vesicles: Rethinking the essential values in cancer biology. *Semin Cancer Biol.* 2021.74:79-91.
147. Hoshino A, Kim HS, Bojmar L, Gyan KE, Cioffi M, Hernandez J*, et al.* Extracellular Vesicle and Particle Biomarkers Define Multiple Human Cancers. *Cell.* 2020.182:1044-61 e18.
148. Sansone P, Savini C, Kurelac I, Chang Q, Amato LB, Strillacci A*, et al.* Packaging and transfer

of mitochondrial DNA via exosomes regulate escape from dormancy in hormonal therapy-resistant breast cancer. *Proc Natl Acad Sci U S A.* 2017.114:E9066-E75.
149. Hewson C, Capraro D, Burdach J, Whitaker N, Morris KV. Extracellular vesicle associated long non-coding RNAs functionally enhance cell viability. *Noncoding RNA Res.* 2016.1:3-11.
150. Zhang J, Li S, Li L, Li M, Guo C, Yao J*, et al.* Exosome and exosomal microRNA: trafficking, sorting, and function. *Genomics Proteomics Bioinformatics.* 2015.13:17-24.
151. Mittelbrunn M, Gutierrez-Vazquez C, Villarroya-Beltri C, Gonzalez S, Sanchez-Cabo F, Gonzalez MA*, et al.* Unidirectional transfer of microRNA-loaded exosomes from T cells to antigen-presenting cells. *Nat Commun.* 2011.2:282.
152. Elsherbini A, Bieberich E. Ceramide and Exosomes: A Novel Target in Cancer Biology and Therapy. *Adv Cancer Res.* 2018.140:121-54.
153. Kumar MA, Baba SK, Sadida HQ, Marzooqi SA, Jerobin J, Altemani FH*, et al.* Extracellular vesicles as tools and targets in therapy for diseases. *Signal Transduct Target Ther.* 2024.9:27.
154. Braga-Lagache S, Buchs N, Iacovache MI, Zuber B, Jackson CB, Heller M. Robust Label-free, Quantitative Profiling of Circulating Plasma Microparticle (MP) Associated Proteins. *Mol Cell Proteomics.* 2016.15:3640-52.
155. Yang Y, Li CW, Chan LC, Wei Y, Hsu JM, Xia W*, et al.* Exosomal PD-L1 harbors active defense function to suppress T cell killing of breast cancer cells and promote tumor growth. *Cell Res.* 2018.28:862-4.
156. Taylor J, Azimi I, Monteith G, Bebawy M. Ca(2+) mediates extracellular vesicle biogenesis through alternate pathways in malignancy. *J Extracell Vesicles.* 2020.9:1734326.
157. Yu X, Harris SL, Levine AJ. The regulation of exosome secretion: a novel function of the p53 protein. *Cancer Res.* 2006.66:4795-801.
158. Kilinc S, Paisner R, Camarda R, Gupta S, Momcilovic O, Kohnz RA*, et al.* Oncogene-regulated release of extracellular vesicles. *Dev Cell.* 2021.56:1989-2006 e6.
159. Choi D, Montermini L, Meehan B, Lazaris A, Metrakos P, Rak J. Oncogenic RAS drives the CRAF-dependent extracellular vesicle uptake mechanism coupled with metastasis. *J Extracell Vesicles.* 2021.10:e12091.
160. Nakase I, Kobayashi NB, Takatani-Nakase T, Yoshida T. Active macropinocytosis induction by stimulation of epidermal growth factor receptor and oncogenic Ras expression potentiates cellular uptake efficacy of exosomes. *Sci Rep.* 2015.5:10300.
161. Lee TH, Chennakrishnaiah S, Audemard E, Montermini L, Meehan B, Rak J. Oncogenic ras-driven cancer cell vesiculation leads to emission of double-stranded DNA capable of interacting with target cells. *Biochem Biophys Res Commun.* 2014.451:295-301.
162. McKenzie AJ, Hoshino D, Hong NH, Cha DJ, Franklin JL, Coffey RJ*, et al.* KRAS-MEK Signaling Controls Ago2 Sorting into Exosomes. *Cell Rep.* 2016.15:978-87.
163. Melo SA, Sugimoto H, O'Connell JT, Kato N, Villanueva A, Vidal A*, et al.* Cancer exosomes perform cell-independent microRNA biogenesis and promote tumorigenesis. *Cancer Cell.* 2014.26:707-21.
164. Hinzman CP, Singh B, Bansal S, Li Y, Iliuk A, Girgis M*, et al.* A multi-omics approach identifies pancreatic cancer cell extracellular vesicles as mediators of the unfolded protein response in normal pancreatic epithelial cells. *J Extracell Vesicles.* 2022.11:e12232.
165. Putz U, Howitt J, Doan A, Goh CP, Low LH, Silke J*, et al.* The tumor suppressor PTEN is exported in exosomes and has phosphatase activity in recipient cells. *Sci Signal.* 2012.5:ra70.
166. Chen G, Huang AC, Zhang W, Zhang G, Wu M, Xu W*, et al.* Exosomal PD-L1 contributes to immunosuppression and is associated with anti-PD-1 response. *Nature.* 2018.560:382-6.
167. Poggio M, Hu T, Pai CC, Chu B, Belair CD, Chang A*, et al.* Suppression of Exosomal PD-L1 Induces Systemic Anti-tumor Immunity and Memory. *Cell.* 2019.177:414-27 e13.
168. Salimu J, Webber J, Gurney M, Al-Taei S, Clayton A, Tabi Z. Dominant immunosuppression of dendritic cell function by prostate-cancer-derived exosomes. *J Extracell Vesicles.* 2017.6:1368823.
169. Zeng Q, Saghafinia S, Chryplewicz A, Fournier N, Christe L, Xie YQ*, et al.* Aberrant hyperexpression of the RNA binding protein FMRP in tumors mediates immune evasion. *Science.* 2022.378:eabl7207.
170. Basso D, Gnatta E, Padoan A, Fogar P, Furlanello S, Aita A*, et al.* PDAC-derived exosomes

enrich the microenvironment in MDSCs in a SMAD4-dependent manner through a new calcium related axis. *Oncotarget.* 2017.8:84928-44.
171. Peinado H, Aleckovic M, Lavotshkin S, Matei I, Costa-Silva B, Moreno-Bueno G*, et al.* Melanoma exosomes educate bone marrow progenitor cells toward a pro-metastatic phenotype through MET. *Nat Med.* 2012.18:883-91.
172. Costa-Silva B, Aiello NM, Ocean AJ, Singh S, Zhang H, Thakur BK*, et al.* Pancreatic cancer exosomes initiate pre-metastatic niche formation in the liver. *Nat Cell Biol.* 2015.17:816-26.
173. Kang M, Jordan V, Blenkiron C, Chamley LW. Biodistribution of extracellular vesicles following administration into animals: A systematic review. *J Extracell Vesicles.* 2021.10:e12085.
174. Plebanek MP, Angeloni NL, Vinokour E, Li J, Henkin A, Martinez-Marin D*, et al.* Pre-metastatic cancer exosomes induce immune surveillance by patrolling monocytes at the metastatic niche. *Nat Commun.* 2017.8:1319.
175. Huang T, Song C, Zheng L, Xia L, Li Y, Zhou Y. The roles of extracellular vesicles in gastric cancer development, microenvironment, anti-cancer drug resistance, and therapy. *Mol Cancer.* 2019.18:62.
176. Miki Y, Yashiro M, Okuno T, Kitayama K, Masuda G, Hirakawa K*, et al.* CD9-positive exosomes from cancer-associated fibroblasts stimulate the migration ability of scirrhous-type gastric cancer cells. *Br J Cancer.* 2018.118:867-77.
177. Zheng P, Luo Q, Wang W, Li J, Wang T, Wang P*, et al.* Tumor-associated macrophages-derived exosomes promote the migration of gastric cancer cells by transfer of functional Apolipoprotein E. *Cell Death Dis.* 2018.9:434.
178. Gu J, Qian H, Shen L, Zhang X, Zhu W, Huang L*, et al.* Gastric cancer exosomes trigger differentiation of umbilical cord derived mesenchymal stem cells to carcinoma-associated fibroblasts through TGF-beta/Smad pathway. *PLoS One.* 2012.7:e52465.
179. Zhu W, Huang L, Li Y, Zhang X, Gu J, Yan Y*, et al.* Exosomes derived from human bone marrow mesenchymal stem cells promote tumor growth in vivo. *Cancer Lett.* 2012.315:28-37.
180. Choi HI, Choi JP, Seo J, Kim BJ, Rho M, Han JK*, et al.* Helicobacter pylori-derived extracellular vesicles increased in the gastric juices of gastric adenocarcinoma patients and induced inflammation mainly via specific targeting of gastric epithelial cells. *Exp Mol Med.* 2017.49:e330.
181. Che Y, Geng B, Xu Y, Miao X, Chen L, Mu X*, et al.* Helicobacter pylori-induced exosomal MET educates tumour-associated macrophages to promote gastric cancer progression. *J Cell Mol Med.* 2018.22:5708-19.
182. Kalluri R, McAndrews KM. The role of extracellular vesicles in cancer. *Cell.* 2023.186:1610-26.
183. Northrop-Albrecht EJ, Taylor WR, Huang BQ, Kisiel JB, Lucien F. Assessment of extracellular vesicle isolation methods from human stool supernatant. *J Extracell Vesicles.* 2022.11:e12208.
184. Subsomwong P, Asano K, Akada J, Matsumoto T, Nakane A, Yamaoka Y. Proteomic Profiling of Extracellular Vesicles Reveals Potential Biomarkers for Helicobacter pylori Infection and Gastric Cancer. *Helicobacter.* 2025.30:e70022.
185. Taxauer K, Hamway Y, Ralser A, Dietl A, Mink K, Vieth M*, et al.* Engagement of CEACAM1 by Helicobacterpylori HopQ Is Important for the Activation of Non-Canonical NF-kappaB in Gastric Epithelial Cells. *Microorganisms.* 2021.9
186. Wu G, Wang D, Xiong F, Wang Q, Liu W, Chen J*, et al.* The emerging roles of CEACAM6 in human cancer (Review). *Int J Oncol.* 2024.64
187. Calinescu A, Turcu G, Nedelcu RI, Brinzea A, Hodorogea A, Antohe M*, et al.* On the Dual Role of Carcinoembryonic Antigen-Related Cell Adhesion Molecule 1 (CEACAM1) in Human Malignancies. *J Immunol Res.* 2018.2018:7169081.
188. Zang M, Zhang B, Zhang Y, Li J, Su L, Zhu Z*, et al.* CEACAM6 promotes gastric cancer invasion and metastasis by inducing epithelial-mesenchymal transition via PI3K/AKT signaling pathway. *PLoS One.* 2014.9:e112908.
189. Al-Khinji A. Exploring the interactions of integrins and CEACAM6 (Review). *Exp Ther Med.* 2025.30:237.
190. Patil PU, D'Ambrosio J, Inge LJ, Mason RW, Rajasekaran AK. Carcinoma cells induce lumen

filling and EMT in epithelial cells through soluble E-cadherin-mediated activation of EGFR. *J Cell Sci.* 2015.128:4366-79.
191. Abdouh M, Zhou S, Arena V, Arena M, Lazaris A, Onerheim R*, et al.* Transfer of malignant trait to immortalized human cells following exposure to human cancer serum. *J Exp Clin Cancer Res.* 2014.33:86.
192. Camerlingo R, Miceli R, Marra L, Rea G, D'Agnano I, Nardella M*, et al.* Conditioned medium of primary lung cancer cells induces EMT in A549 lung cancer cell line by TGF-ss1 and miRNA21 cooperation. *PLoS One.* 2019.14:e0219597.
193. Christofides A, Strauss L, Yeo A, Cao C, Charest A, Boussiotis VA. The complex role of tumor-infiltrating macrophages. *Nat Immunol.* 2022.23:1148-56.
194. Li J, Sun J, Zeng Z, Liu Z, Ma M, Zheng Z*, et al.* Tumour-associated macrophages in gastric cancer: From function and mechanism to application. *Clin Transl Med.* 2023.13:e1386.
195. Xiao P, Long X, Zhang L, Ye Y, Guo J, Liu P*, et al.* Neurotensin/IL-8 pathway orchestrates local inflammatory response and tumor invasion by inducing M2 polarization of Tumor-Associated macrophages and epithelial-mesenchymal transition of hepatocellular carcinoma cells. *Oncoimmunology.* 2018.7:e1440166.
196. Zhao Y, Sun J, Li Y, Zhou X, Zhai W, Wu Y*, et al.* Tryptophan 2,3-dioxygenase 2 controls M2 macrophages polarization to promote esophageal squamous cell carcinoma progression via AKT/GSK3beta/IL-8 signaling pathway. *Acta Pharm Sin B.* 2021.11:2835-49.
197. Li W, Zhang X, Wu F, Zhou Y, Bao Z, Li H*, et al.* Gastric cancer-derived mesenchymal stromal cells trigger M2 macrophage polarization that promotes metastasis and EMT in gastric cancer. *Cell Death Dis.* 2019.10:918.
198. Aldinucci D, Colombatti A. The inflammatory chemokine CCL5 and cancer progression. *Mediators Inflamm.* 2014.2014:292376.
199. Zeng Z, Bao X, Lei S, Tang W, Tai H, Wang L*, et al.* MRO/HNRNPU/CCL5 feedback loop amplifies M2 macrophage and breast cancer cell crosstalk to drive progression. *J Transl Med.* 2025.23:920.
200. Murray PJ. Macrophage Polarization. *Annu Rev Physiol.* 2017.79:541-66.
201. Arroyo E, Laudato JA, Gibson BM, Dulaney CS, Vaughan JA, Followay BN*, et al.* Tumor necrosis factor-alpha, TNF receptor, and soluble TNF receptor responses to aerobic exercise in the heat. *Cytokine X.* 2020.2:100033.
202. Huang Y, Du KL, Guo PY, Zhao RM, Wang B, Zhao XL*, et al.* IL-16 regulates macrophage polarization as a target gene of mir-145-3p. *Mol Immunol.* 2019.107:1-9.
203. Becker A, Thakur BK, Weiss JM, Kim HS, Peinado H, Lyden D. Extracellular Vesicles in Cancer: Cell-to-Cell Mediators of Metastasis. *Cancer Cell.* 2016.30:836-48.
204. Welsh JA, Goberdhan DCI, O'Driscoll L, Buzas EI, Blenkiron C, Bussolati B*, et al.* Minimal information for studies of extracellular vesicles (MISEV2023): From basic to advanced approaches. *J Extracell Vesicles.* 2024.13:e12404.
205. Lane RE, Korbie D, Khanna KK, Mohamed A, Hill MM, Trau M. Defining the relationship between cellular and extracellular vesicle (EV) content in breast cancer via an integrative multi-omic analysis. *Proteomics.* 2024.24:e2300089.
206. Garcia-Martin R, Brandao BB, Thomou T, Altindis E, Kahn CR. Tissue differences in the exosomal/small extracellular vesicle proteome and their potential as indicators of altered tissue metabolism. *Cell Rep.* 2022.38:110277.
207. Igami K, Uchiumi T, Shiota M, Ueda S, Tsukahara S, Akimoto M*, et al.* Extracellular vesicles expressing CEACAM proteins in the urine of bladder cancer patients. *Cancer Sci.* 2022.113:3120-33.
208. Towbin H, Staehelin T, Gordon J. Electrophoretic transfer of proteins from polyacrylamide gels to nitrocellulose sheets: procedure and some applications. *Proc Natl Acad Sci U S A.* 1979.76:4350-4.
209. Schindelin J, Arganda-Carreras I, Frise E, Kaynig V, Longair M, Pietzsch T*, et al.* Fiji: an open-source platform for biological-image analysis. *Nat Methods.* 2012.9:676-82.
210. Dixit P, Kokate SB, Poirah I, Chakraborty D, Smoot DT, Ashktorab H*, et al.* Helicobacter pylori-induced gastric cancer is orchestrated by MRCKbeta-mediated Siah2 phosphorylation. *J Biomed Sci.* 2021.28:12.

## APPENDIX I
## LIST OF PLASMIDS USED

| Antibody | Source |
|---|---|
| pcDNA3.1$^{+}$ | Cat. No. V79020, Thermo Fisher Scientific |
| CEACAM6-pdKCR-neo | Gift from Prof. Bernhard B. Singer, University of Essen, Germany |

## APPENDIX II

## LIST OF PRIMARY ANTIBODIES USED

| Antibody | Dilution | Source |
|---|---|---|
| GAPDH | 1:5000 (WB) | Cat. No. 10-10011, ABGENEX Pvt. Ltd., India |
| CEACAM1 | 5 µg/mL (WB)<br>2 µg/mL (IF)<br>2 µg/mL (Flow) | Gift from Prof. Bernhard B. Singer |
| CEACAM5 | 5 µg/mL (WB)<br>2 µg/mL (IF)<br>2 µg/mL (Flow) | Gift from Prof. Bernhard B. Singer |
| CEACAM6 | 5 µg/mL (WB)<br>2 µg/mL (IF)<br>2 µg/mL (Flow) | Gift from Prof. Bernhard B. Singer |
| CEACAM6 | 1:1000 (WB) | Cat. No. NBP2-54626, |

| | | |
|---|---|---|
| | | Novus Biologicals, USA |
| CEACAM6 | 1:100 (IF) | Cat. No. ab134074, Abcam, USA |
| CD68 | 1:50 (IF) | Cat. No. ab955, Abcam |
| Arginase1 | 1:200 (IF) | Cat. No. NB100-59740, Novus Biologicals |
| iNOS | 1:500 (IF) | Cat. No. PA303A, Thermo Fisher Scientific |
| Alix | 1:200 (WB) | Cat. No. sc-53540, Santa Cruz Biotechnology, USA |
| CD63 | 1:200 (WB) | Cat. No. sc-5275, Santa Cruz Biotechnology |
| GM130 | 1:1000 (WB) | Cat. No. NBP2-53420, Novus Biologicals |
| HSPA8 | 1:1000 (WB) | Cat. No. 8444, Cell Signaling Technology (CST), USA |
| CD40-APC | 5 µL (0.06 µg)/test (Flow) | Cat. No. 17-0409-42, Thermo Fisher Scientific |
| CD64-PE | 5 µL (0.125 µg)/test (Flow) | Cat. No. 12-0649-42, Thermo Fisher Scientific |
| CD68-FITC | 5 µL (0.125 µg)/test (Flow) | Cat. No. 11-0689-42, Thermo Fisher Scientific |
| CD206-APC | 5 µL (0.06 µg)/test (Flow) | Cat. No. 17-2069-42, Thermo Fisher Scientific |

## APPENDIX III

## LIST OF SECONDARY ANTIBODIES USED

| Antibody | Dilution | Source |
|---|---|---|
| Anti-mouse HRP-conjugated | 1:2000 (WB) | Cat. No. 7076S, CST |
| Anti-rabbit HRP-conjugated | 1:2000 (WB) | Cat. No. 7074S, CST |
| Anti-mouse Alexa fluor 488 | 1:500 (IF), 1:200 (Flow) | Cat. No. A-11001, Thermo Fisher Scientific |
| Anti-rabbit Alexa fluor 488 | 1:500 (IF) | Cat. No. A-21206, Thermo Fisher Scientific |
| Anti-rabbit Alexa fluor 595 | 1:500 (IF) | Cat. No. A-21206, Thermo Fisher Scientific |
| Anti-goat Alexa fluor 488 | 1:500 (IF) | Cat. No. A-11055, Thermo Fisher Scientific |
| Anti-goat Alexa fluor 595 | 1:500 (IF) | Cat. No. A-11058, Thermo Fisher Scientific |

WB- Western blotting, IF- Immunofluorescence, Flow- Flow cytometry